

Long-term survival of halophilic microorganisms entombed in fluid inclusions of halite



Maria Magliulo

A thesis submitted for the degree of Doctor of Philosophy

In Microbiology

School of Life Sciences

University of Essex

October 2022

Acknowledgements

I would like to begin by thanking my supervisor Professor Terry McGenity, who gifted me invaluable knowledge and for the trust I was given. His genuine scientific curiosity has inspired me, nourishing my passion for science, especially during hard times. I will keep the knowledge I received from him as inestimable worth.

A special thanks to the SALTGIANT team for the once-in-a-lifetime experience they gifted me with this project. I am grateful for these four years, for the support and the precious memories I will keep in my heart for ever.

I would also like to thank Dr James Bradley, Dr Petra Rettberg and Dr Kristina Beblo-Vranesevic, for their continued support, their suggestions, and inspiring discussions during this project.

Special thanks also go to Farid Benyahia for his support, especially in the lab. I was lucky to have had such a great lab group, which made lighter even the toughest day in the lab, especially during the pandemic.

I would also like to thank all my colleagues and friends at the University of Essex with whom I have shared every aspect of this Ph.D. during the last four years, great companions of a great adventure, I will never forget. To the fantastic women in the School of Life Sciences that have supported me through a delicate moment.

To my flatmates, for the feeling of family we created in Colchester and in Tooting Bec.

To my closest friends, a tailwind when I run out of breath.

To my family, the Northern Star during the darkest nights, the sunlight during the coldest days. Simply thinking of you have always put a smile on my face.

To my dog, I wish you could live for ever.

To Andrea, my other half. Thank you for all the warm cups of tea, for all the songs sang to me, for all the times you pushed me to win my limits. I am one; with you I am half of something bigger.

I am grateful.

Abstract

Hypersaline environments are subjected to dynamic environmental conditions which can result in the precipitation of salts, including halite. Microbial communities can get trapped inside fluid inclusions of halite, primarily haloarchaea. The entombment can be an advantage, including the protection afforded by halite to shield against intense radiation, which complements the inherent radiation resistance of many haloarchaea. We tested the capacity of the haloarchaeal species, *Halobacterium salinarum* NRC-1 and *Halobacterium noricense* A1, and the halophilic bacterial species, *Salinibacter ruber* M13, to tolerate UV and ionising radiation when in halite crystals. All species survived UV irradiation when in halite crystals and, with different lag phases, they even survived an ionising radiation dose of 5 kGy.

Halobacterium salinarum NRC1 was entombed in halite crystals, and its proteome examined at 42 days of entombment compared with growth prior to entombment. This strain down-regulated proteins involved in transcription and translation, suggesting that its energy is primarily devoted to maintenance. In contrast to all other ribosomal proteins detected, ribosomal protein L13 had an elevated abundance at day 42, suggesting that it has a role connected with long-term survival. We also found the up-regulation of several proteins, highlighting the existence of on-going anaerobic metabolic activities.

We explored the biodiversity of the Dead Sea entrapped in halite deposited from 1980 to present, and to this end, in November 2021, we collected samples of water and halite and the DNA was extracted. Archaeal and bacterial 16S rRNA genes were amplified from these halite crystals and water samples. Overall, we have gained insights into the radiation resistance of entombed halophiles, started to understand the mechanisms by which Haloarchaea survive inside halite, and indication about which Haloarchaea preferentially survive in halite in the environment. The findings of this study have implications about the survival of life on Earth, and opens the possibility of life elsewhere.

Contents

Acknowledgements	i
Abstract	ii
Abbreviations	vii
Declaration.....	viii
Chapter 1: General introduction.....	1
1.1 Microbial longevity: the case of Halophiles	1
1.2 Hypersaline environment and life associated with it.....	4
1.3 Halite as a protective environment.....	6
1.4 Halophiles' abilities enabling long-term survival	8
1.5 Longevity in halite: a model system to investigate extraterrestrial life	9
1.6 The geological context of Mars.....	11
1.7 Detection of life on Mars: first attempt	13
1.8 References	13
Chapter 2: Long-term survival of halophiles in laboratory-made halite and characteristics of halite precipitation	19
Abstract	19
2.1 Introduction	20
2.1.1 Halophiles in fluid inclusions of halite	20
2.1.2 The fluid inclusions microenvironment	20
2.1.3 Aim of the study	22
2.2 Methodology	22
2.2.1 Growth of strains	22
2.2.2 Entombment of halophilic microorganisms	23
2.2.3 Recovery of cells from laboratory-made halite	24
2.2.4 Cell visualization inside fluid inclusions.....	25
2.2.5 Influence of abiotic and biotic factors on the precipitation of lab-made halite.....	25
2.2.6 Sorting crystals by dimension and microscope analysis	27
2.3 Results.....	27
2.3.1 Recovery of cells from salt crystals	27
2.3.2 Cell visualization inside fluid inclusions.....	29
2.3.3 Influence of biotic and abiotic factors on the formation of lab-made halite	31
2.4 Discussion	32
2.6 References	35

2.7 Supplementary info	38
Chapter 3: Exposure of entombed halophiles to different doses of UV and ionizing radiation	43
Abstract	43
3.1 Introduction	43
3.1.2 Martian salts and radiation	45
3.1.3 The ability of halophiles to withstand high doses of radiation	46
3.1.4 Photoprotection in halophiles	47
3.1.5 Genomic signatures of halophiles offering resistance to radiation	48
3.1.6 Terrestrial life exposed under simulated Martian conditions	49
3.1.7 Aims and objectives	52
3.2 Methodology	52
3.2.1 Growth of halophiles	52
3.2.2 Exposure to increasing doses of polychromatic UV radiation of cells immersed in liquid ..	52
3.2.3 Exposure to increasing doses of polychromatic UV radiation of halophiles in lab-made halite	54
3.2.4 Lab-made halite exposure to different types of radiation	56
3.2.5 Comparison between freshly grown cells of <i>Hbt. salinarum</i> NRC-1 and starved cells	57
3.2.6 Downstream analysis for lab-made halite samples	58
3.3 Results	58
3.3.1 Exposure of cells immersed in liquid and entombed in halite on quartz discs	59
3.3.2 Lab-made halite exposure to different types of radiation	59
3.3.3 Comparison between starved cells and freshly grown cells of <i>Hbt. salinarum</i> NRC-1	61
3.4 Discussion	63
3.4.1 Exposure of cells immersed in liquid and entombed in halite on quartz discs	63
3.4.2 Lab-made halite exposure to different types of radiation	64
3.4.3 Comparison between freshly grown and starved cells of <i>Hbt. salinarum</i> NRC-1	65
3.5 Conclusions	66
3.6 References	68
3.7 Supplementary info	72
Chapter 4: Differential protein expression in <i>Halobacterium salinarum</i> NRC-1 during entombment in lab-made halite	76
Abstract	76
4.1 Introduction	76
4.2 Phenotypical and genotypical signature of halophiles	77
4.3 Aims and objectives	78
4.2 Methodology	79

4.2.1 Microbial culture	79
4.2.2 Entombment of <i>Halobacterium salinarum</i>	79
4.2.3 Protein extraction	80
4.2.4 Protein analysis.....	81
4.2.5 Statistical analysis	83
4.3 Results.....	84
4.3.1 Visualisation of proteins on SDS-PAGE precast gels.....	84
4.3.2 LC-MS/MS Shotgun Proteomic Analysis	84
4.3.3 Comparison of the proteome of <i>Hbt. salinarum</i> NRC-1between T-0 and T-1.....	85
4.3.4 Comparison of the proteome between T-1 and T-2	86
4.3.5 Comparison of the proteome between T-0 and T-2	87
4.3.5.1 Differentially abundant ribosomal proteins	89
4.3.5.2 Differentially abundant proteins involved in the biosynthesis of new proteins	90
4.3.5.3 Up-regulation of enzymes involved in the fermentative arginine degradation	92
4.3.5.4 Use of alternative electron acceptors	93
4.3.5.5 Other proteins significantly differentially abundant after 42 days of entombment.....	94
4.3.6 Contamination by <i>Natrinema</i> sp.....	96
4.4 Discussion	97
4.4.1 Differentially abundant proteins involved in the biosynthesis of new proteins.....	97
4.4.2 Up-regulation of enzymes involved in the fermentative arginine degradation	101
4.4.3 Use of alternative electron acceptors.....	103
4.4.4 Other proteins significantly differentially expressed during the entombment	104
4.5 Conclusions.....	105
4.6 References	110
Chapter 5: Investigation into the microbial communities associated with Dead-Sea halite.....	117
Abstract	117
5.1 Introduction	118
5.1.1 Stratigraphy of halite section in Ein Gedi, Dead Sea.....	119
5.1.2 Diversity of microorganisms inhabiting the Dead Sea waters	121
5.1.3 Aim of the study	123
5.2 Methodology	123
5.2.1 Samples and sampling sites.....	123
5.2.2 Halite sampling.....	127
5.2.3 Halite surface sterilization.....	127
5.2.4 Halite dissolution and filtration.....	127

5.2.5 DNA extraction from halite samples.....	128
5.2.6 Water sampling.....	128
5.2.7 DNA extraction from water samples.....	129
5.2.8 PCR amplification	129
5.2.9 Sequencing and bioinformatic analysis	130
5.3 Results.....	131
5.3.1 Amplification 16S rRNA genes for detection of archaeal and bacterial DNA	131
5.3.2 Preliminary analysis	132
5.3.3 Identification of Archaea in different sample types.	135
5.4 Discussion	139
5.5 Conclusion.....	141
5.6 References	143
5.7 Supplementary info	147
Chapter 6: General discussion.....	148
6.2 References	152

Abbreviations

NaCl	Sodium chloride
Kyr	1000 years
MgCl ₂ ·6H ₂ O	Magnesium chloride hexahydrate
KCl	Potassium chloride
MgSO ₄ ·7H ₂ O	Magnesium sulphate heptahydrate
Rpm	Rotation per minute
kGy	1000 Gray (unit measure)
Myr	Million years
GCR	Galactic Cosmic Rays
ROS	Reactive oxygen species
CHAPS	3-cholamidopropyl dimethylammonio 1-propanesulfonate
SDS	Sodium dodecyl sulfate
TRIS-HCl	Tris(hydroxymethyl)aminomethane hydrochloride
e/aIF2	Translation initiation factor 2
<i>SUI2</i>	Gene coding for the subunit alpha of the e/aIF2
<i>SUI3</i>	Gene coding for the subunit beta of the e/aIF2
<i>GCD11</i>	Gene coding for the subunit gamma of the e/aIF2
GTP	Guanosine tri phosphate
<i>GCD11</i>	(GCD: general control depressed)
<i>GCN4</i>	(GCN: general control non-inducible)
AUG	Codon of start

Declaration

This thesis is submitted to the University of Essex in support of my application for the degree of Doctor of Philosophy. I declare that the work presented in this thesis was conducted by me, under the supervision of Professor Terry McGenity, with the exception of those instances where the contribution of others has been specifically acknowledged.

The work presented, including data generated and data analysis, was carried out by the author except in the cases outlined below:

- An in-gel trypsin digest was performed on extracted proteins and the resulting peptide fragments prepared for LC-MS/MS analysis (Chapter 4) by Dr Gergana Metodieva (University of Essex).
- Initial peptide data analysis in MaxQuant and protein identification and validation (Chapter 4) were performed by Dr Metodi Metodiev (University of Essex).
- The exposure to polychromatic UV, UV-C and ionizing radiation of halite samples of the experiment D and E (Chapter 3) was performed by Dr Kristina Beblo-Vranesevic and Dr Petra Rettberg.
- The samples collected on the Dead Sea during the SALTGIANT field trip (Chapter 5), were collected by the author, Prof Terry McGenity and Dr James Bradley. DNA sequencing were performed at Novogene. Initial analyses were performed by the author under the scrutiny of Prof Terry McGenity.

Chapter 1: General introduction

1.1 Microbial longevity: the case of Halophiles

1.2 Hypersaline environment and life associated with it

1.3 Halite as a protective environment

1.5 Longevity in halite: a model system to investigate extraterrestrial life

1.6 The geological context of Mars

1.7 Detection of life on Mars: first attempt

1.1 Microbial longevity: the case of Halophiles

Among the first documents reporting the discovery of living microorganisms in ancient samples, the one from Lipman (1931), led the research to focus on the longevity of microorganisms. The author pointed out the need to investigate the long-term survival of microorganisms entrapped in different chemical compounds, in the case of his study, the anthracite coal. The scientific community at that time was skeptical about any possible positive results resulting from such studies for many reasons. The first and obvious one, was regarding the isolation techniques in order to prevent contamination; a concern that is still present nowadays. Since then, it was just in the 1960s that the first cultivations of halophiles have been reported (Dombrowski, 1963; Reiser and Tasch, 1960). Indeed, there is still no availability of a unique method that will permit to isolate microorganisms from ancient samples, in addition to this, determining the age of the living microorganism found inside (and so, determining if it is not the result of contaminations) is still a big challenge.

Fish et al., (2002) detected 16S ribosomal RNA gene fragments from halite samples ranging in age from 11 to 425 Myr, but it was difficult to assess whether the DNA originated from intact microorganisms or whether it was free DNA from lysed cells. However, a conclusion has been that DNA entrapped in halite can survive over geological timescales. Proof that Haloarchaea have remained viable in the subsurface of different hypersaline environments have been reported in several

studies; there is evidence of isolation of archaea from samples older than 100,000 years, albeit the most ancient samples are controversial and the reproducibility is very low (Mormile et al., 2003; Schubert et al., 2010a). Although viable prokaryotes have been reported from fluid inclusions in ancient halite, discussions have arisen about their longevity, possible damage of the DNA, and the conditions required for long-term survival (Hebsgaard et al., 2005). However, evidence is accumulating, and new and independent methodology have been used, and many studies have now reported the isolation of viable cells from old and ancient halite (summarized in Table 1.1). The great question is how they have been surviving or even thriving in such a closed, low-nutrient, salty environment. To this end different explanations have been proposed. On one side, salt is known to preserve to some extent macromolecules, and this has been extensively reviewed (Grant et al., 1998). On the other side, the idea of simple food chains and mutual interactions that may occur between microorganisms in fluid inclusions in salt may provide an answer to the energetic demands, yet, considering the potential, this has been poorly explored. It has been reported in different studies that co-cultures of halophiles could enhance the longevity of specific strains. Gramain *et al.* (2011) found, for example, that co-cultures of *Salinibacter* and *Haloquadratum* survive for longer and with more rapid growth in the recovery media than when grown alone, remaining viable for the 26 months duration of the experiment. The same study also reported specialists, *e.g.* *Halobacterium* sp., at long-term survival in halite, and it has been estimated that haloarchaea could survive by feeding on co-entombed microorganisms for millions of years (McGenity et al., 2008). In this perspective, it is worth mentioning the role of *Dunaliella salina*, a halophilic green micro-algae that is entombed with halophilic microbes as brines evaporate: the glycerol it produces, which serves as an osmolyte, along with all components of dead cells, can serve as carbon and energy source for a certain period of time (Lowenstein et al., 2011; Schubert et al., 2010b)

Table 1.1. Papers reporting both isolation of organisms and detection of genetic material. The main concern about papers reporting very old samples is about the sterilization procedures they have been used and laboratory contaminations. Although it is reported that salt is widely known as good milieu for preserving biological molecules, great care should be taken in assuming that it is the only best preserving milieu. This table is not exhaustive.

Age of the sample (My)	Organism	Reference	Evidence
0.022 – 0.034	Haloarchaea	Schubert et al. 2010	16S and isolates
0.022 – 0.034	Haloarchaea	Sankaranarayanan et al. 2014	16S
0.0096 and 0.097	<i>Halobacterium salinarum</i>	Mormile et al. 2003	16S and isolates
5.3 – 1.8	<i>Halobacterium</i> spp.	Gramain et al. 2011	16S and isolates
11 – 16	<i>Halobacterium noricense</i>	Fish et al. 2002	16S
23	Haloarchaea including <i>Halorubrum</i> spp.	Park et al. 2009	16S
38 – 41	<i>Halobacterium</i> and <i>Halolamina</i>	Jaakkola et al. 2014	isolates
112 – 121	Haloarchaea	Vreeland et al. 2007	isolates
123	<i>Halobacterium hubeiense</i>	Jaakkola et al. 2016	isolates
121 and 419	<i>Halobacterium</i>	Park et al. 2009	16S

Demonstration of whether intact microbial cells remain viable for longer than thousands of years has remarkable implications regarding the resilience of these microorganisms, and this raises questions about the physiological mechanisms about their survival, metabolism and DNA preservation (Grant et al., 1998; McGenity *et al.* 2000; Vreeland et al., 2000).

1.2 Hypersaline environment and life associated with it

Halobacterium salinarum is a model organism for Haloarchaea and is able to live at 5 M NaCl, thriving in environments close to saturation with salt, hypersaline environments. Generally, halophiles have two strategies to cope with high levels of salt; in the first one, the halophilic organism accumulates organic compatible solutes, in order to balance the osmotic pressure (Figure 1.1). One of the most studied halophiles adopting this strategy is *Dunaliella salina*, known to accumulate glycerol according to the salinity of the environment. This strategy, however, does not allow this species to survive for long time in waters nearly saturated with salt, in fact, the maximum salinity *Dunaliella salina* is able to withstand is 3.5 M (Oren, 2008). The second strategy is called “Salt-in”, and is a strategy adopted by the extreme halophiles, like *Halobacterium salinarum*. With this strategy, the halophile accumulates KCl to counteract the osmotic pressure of the surrounding salty waters.

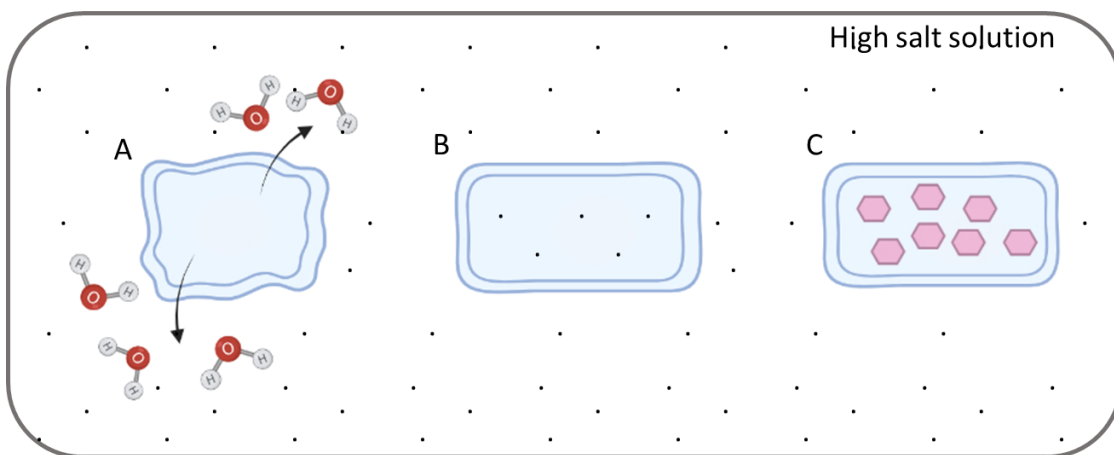


Figure 1.1. Schematic view of the three different possibilities of cells immersed in high salt solution. A: Non-halophilic cell. B: Salt-in strategy, adopted by extreme halophiles. C: Accumulation of organic compatible solutes to counteract the osmotic pressure.

The strategy adopted by extreme halophiles results in them having a proteome with an excess ratio of acidic to basic amino acids. To avoid problems such as unfolding and instability, proteins of *Halobacterium salinarum*, and Haloarchaea in general, are overall relatively negatively charged. This feature has been extensively studied (Oren, 2013; Soppa, 2006) but it is not the only adaptation to high salt environments; different works have investigated the stability of proteins with low hydrophobicity in halophiles, and proposed this as an additional molecular signature of life in hypersaline environments (Hutcheon et al., 2005; Lanyi, 1974). In another work, the authors

investigate the physical and chemical principles sustaining the stability of proteins in high salt milieu, and found that proteins that form coils in their secondary structure rather than alpha helices are preferred in halophiles more than non-halophiles (Paul et al., 2008). In the same study, they also investigate the physical and chemical structure of the DNA of halophiles for signatures of adaptation to high salt. They found evidence in favour of specific selection on dinucleotide and synonymous codon usage that are preferred in halophiles, and how this is a salt-specific signature: in fact, the higher frequency of GA, AC and GT, reflect without doubts the preference of Asp, Glu, Thr and Val typical of halophiles proteome (Paul et al., 2008).

It is known that halophiles tend to have a higher abundance of GC, and it is believed to be an adaptation to intense UV radiation, and that *Haloquadratum walsbyi* compensate the lower GC-content with more photolyases genes devoted to repairing UV damages (Jones and Baxter, 2016). Paul and colleagues, in their study, suggest an additional explanation to the high GC-content of halophiles: that high salt concentrations can result in the modification of the three-dimensional structure of the DNA, enhancing the transition from B-DNA to Z-DNA.

The discovery of alternative three-dimensional structures of DNA brought about the possibility that different formations might be at the basis of the regulation of transcription of specific genes, that are more or less exposed according to the conformation of the DNA. At a physiological level (especially of non-halophiles) the B-DNA is the most thermodynamically favourable as it corresponds to the minimum of free energy and therefore is the more stable. The bases of B-DNA are found towards the inside of the molecule and the phosphates towards the outside, with the deoxyriboses bridging the two, the hydrophobic bases in the inside and the hydrophilic phosphates on the outside. A-DNA exhibits a similar structure and contains molecules of water inside the DNA: this scenario can occur when there is a lower amount of water in the milieu, compared to optimal physiological conditions. The various structures resulting from different physical and chemical properties of the intracellular milieu influence transcription: sequences can be differentially exposed and different protein-regulators can differentially interact, according to the conformation of the sequences. This holds true especially with the Z-DNA, an alternative structure that was first discovered in 1971 by Pohl and Jovin (Pohl and Jovin, 1972). The authors synthesised a double-stranded oligomeric poly(dG-dC)·poly(dG-dC), that in high salt concentration resulted in a left-handed with the G in “anti-” and the C in “syn-” (for reference: B-DNA and A-DNA are right-handed and the bases are all in “anti-”), a substantially different three-dimensional form of the more stable B-DNA (David and Cox, 2017). Although this finding referred to a synthetic DNA in non-physiological high salt conditions, it has been proposed that in physiological conditions, when there is energy to dissipate (for example in points where the DNA is supercoiled) the transition from B-DNA to Z-DNA can occur (Drew et al.,

1980; Pohl and Jovin, 1972). In the Z-DNA the major groove is less exposed whereas the minor groove is more exposed: this has been proposed as a signal, as it exposes different sequences that can interact with different proteins. Paul and colleagues suggest that the high GC-content in halophiles might be a genomic signature of halophiles, as short d(GC)_n sequences adopt the Z-conformation (Paul et al., 2008), especially considering the “salt-in” strategy, that results in an intracellular milieu to be high in salt concentration. Based on this, it is possible to speculate a possible role of regulation of the transcription associated with alternative DNA structures.

1.3 Halite as a protective environment

Hypersaline environments are subjected to dynamic environmental conditions which can result in precipitation of salt crystals, generally defined halite. Microbial communities living in those environments can get entrapped in halite as a survival strategy and the work from Crits-Cristoph and colleagues showed that inside nodules of halite the community is metabolically active, dominated by Archaea (71%) of which the majority represented by the Halobacteria, Bacteria (27%) mainly belonging to the *Salinibacter* genera and Eukarya (1%) (Crits-Christoph et al., 2016). Although such microbial communities depend on the presence of moisture, halite can provide home for microbial consortia constituted of members from the three domains of life, thriving in this extreme environment (Figure 1.2).

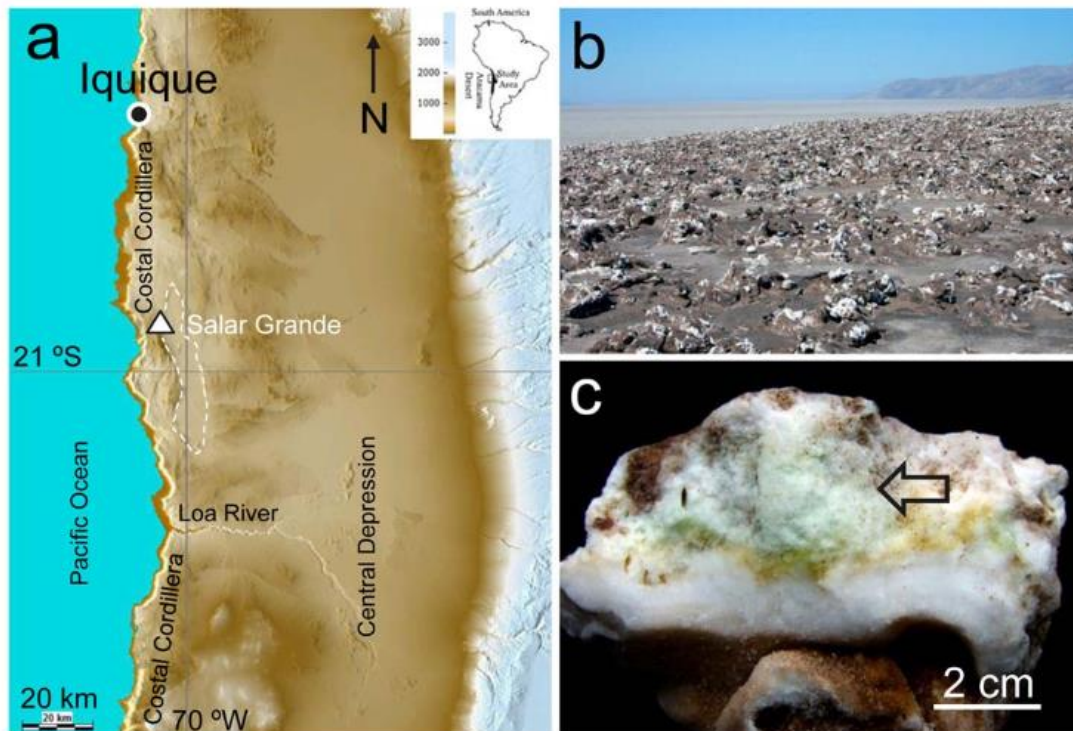


Figure 1.2 Map of the northern Atacama Desert, Chile, showing the location of the study from Crits-Cristoph and colleagues. B. Salar Grande halite field. C. Detail of halite with arrow indicating colonizing microbial communities. It is also possible to notice different metabolisms according to the different zones of the halite. From: Crits-Christoph *et al.* 2016.

In another study on the same location, Uritskiy and colleagues found that the community composition of microbes inhabiting the halite can change according to major episodes of rain, in which the community enters an unstable intermediate state, resulting also in a change in protein contents due to a higher availability of water. As such, these highly specialized communities are more vulnerable to change compared with generalist communities; this makes halite microbiomes ideal for studying temporal dynamics of microbial communities (Uritskiy *et al.*, 2019). Such studies could potentially help addressing the huge deposition of halite during the Messinian Salinity Crisis (see section 3). Fendrihan *et al.*, (2009) explored the role of halite as a shield against radiation: in this study, they found that the survival of Haloarchaea inside fluid inclusions of laboratory-made halite when exposed to simulated Martian UV-radiation was 2 order of magnitude higher than when exposed in liquid culture (dose of 37% survival) (Fendrihan *et al.*, 2009). The same study concludes with the hypothesis that potential life on Mars could survive damages by UV-radiation.

1.4 Halophiles' abilities enabling long-term survival

Halophiles, when entombed in fluid inclusions of halite crystals, face changes in many environmental parameters such as those of space restriction, variations in extracellular salt composition and concentration, pH and availability of oxygen. Therefore, they would have special adaptations to all these changes in order to survive for long periods of time entombed in salt crystals. The most relevant adaptation enabling those halophilic microbes to live in salt-saturated environment is a great excess of acidic amino acids composition in the proteins, required to withstand the high salt concentration. The acidic proteins found in most of the halophilic microorganisms, go together with high concentration of KCl, in order to provide osmotic balance of the cells. The osmotic adaptation and the properties of proteins of Haloarchaea has been extensively reviewed by Oren (2013), as well as what is known about other halophilic microorganisms from the domain of Bacteria, such as *Salinibacter ruber*, an aerobic heterotrophic bacterium isolated from Spanish salterns (Antón et al., 2002). The acidic nature of its proteins has been confirmed by analysis of its genome and the author suggest this adaptation as an extensive exchange of genes with Haloarchaea found in the same environment. Besides the acidic nature of the proteins, most halophilic microorganisms can also accumulate compatible solutes, uncharged and usually zwitterionic molecules, of which the concentration can rapidly be adjusted according to a wide range of salinity (Oren, 2013). A clear example of halophilic microorganisms using this strategy is given by *Dunaliella salina*, which accumulates large quantity of glycerol for osmotic stabilization (Oren, 2014). This large amount of organic carbon can be used as a source of carbon and energy for microbes entombed in fluid inclusions when halite precipitate: remains of the microalgae have been found in ancient halite in a core from Death Valley, CA (Lowenstein, et al. 2011). The presence of dead cells of *D. salina* can, in part, explain the long-term survival of Halophiles in fluid inclusions of halite.

Hypersaline environments are generally colored in red: halophilic microorganisms are indeed equipped with red pigments that give this coloration to the environment. The evolution of this feature is mainly due to the fact that hypersaline environments, beside salt, are subjected to high doses of UV-radiation, so the presence of carotenoids and derivatives help mitigating UV-radiation damages (Shahmohammadi et al., 1998). However, Haloarchaea have also important adaptations helping them contrasting the damaging effect of UV-radiation, as well as ionising radiation. It has been hypothesized that, besides the presence of carotenoids and genes involved in DNA repair, the high content in G + C in the genome of Haloarchaea can be attributed in part to a genomic strategy, which reduces the genomic photoreactivity (Jones and Baxter, 2016). In this study, the only outlier of this hypothesis is *Haloquadratum walsbyi*, having only 48% G + C content compared to the 63.09%

(mean) found in Haloarchaea. However, this halophilic archaeon has a higher number of photolyase genes, which can explain its ability to counteract solar DNA damage. The correlation between a higher content in G + C and reduced DNA damages caused by UV-radiation is due to the fact that it reduces the number of thymines present, which in turn, reduces the number of TT lesions in the DNA (Jones and Baxter, 2016). Haloarchaea have also specific strategies to cope against ionising radiation and IR-induced oxidation: it has been established that a high intracellular Mn increases the tolerance of the organism to ionising radiation (IR) (Daly et al., 2004; Webb et al., 2013). The accumulation of antioxidant Mn-complexes can confer radioprotection to the cell, and Mn can also enhance oxidative stress resistance by substituting as a cofactor for iron in certain enzymes susceptible to oxidative attack, however, this alone cannot explain the resistance showed by radiation-resistant microorganisms. Indeed, as concluded by Webb and colleagues (2013), the increased tolerance of *Hbt. salinarum* is a result of metabolic regulatory adjustments and the accumulation of Mn-antioxidant complexes.

All the strategies listed so far, increase the chance of long-term survival of Haloarchaea in fluid inclusions, however, further research is needed to investigate which mechanisms enable specific species of *Halobacteriaceae* to be found alive in ancient halite. In a first attempt to determine whether a metabolic change can be responsible of such ability, Gramain (2009) extracted proteins from laboratory-grown halite with entombed microbes. As observed by A. Gramain (2009), in response to the process of being entombed *Hbt. salinarum* NRC-1 accumulates fumarate. Three different explanations have been given: Marwan and colleagues (1990) indicated the fumarate as a player in the rotation of the flagella, however, an increase in motility would bring also an increase in energy consumption. Oren (1991) investigated its role as a terminal electron acceptor in anaerobic conditions; it might be that the fumarate could be actively produced by microorganisms entombed in order to deal with the change in oxygen content and so the consequent change in their metabolism. Further analysis is needed to confirm this hypothesis.

1.5 Longevity in halite: a model system to investigate extraterrestrial life

The question on how life originated remain unanswered, and different theories have been proposed during the years to explain the origin of life on Earth. Among three main views, the theory of Panspermia supports the idea that life did not originate on Earth, but was brought here from elsewhere in space by meteorites, asteroids or comets. This theory though only moves the question further, on

how life began elsewhere in the space. One of the rationales behind this theory is related to the origin of water present on Earth, and as a consequence of this, and other geological and geochemical features, the presence of life. Morbidelli et al., (2000), summarized different phases of accretion of water on Earth throughout its formation. According to astronomical models, at the beginning of Earth formation, when the planet was still embedded in the solar nebula, it was water-depleted. Later, hydrated 10 km asteroids came from the outer, bringing, potentially, the amount of water presently existing on our planet. However, because of the small mass of the Earth at that time, very little of it should have been retained during the collisions that completed the Earth's formation. When Jupiter accreted up to its current mass, a rapid depletion of the asteroid belt occurred and the forming Earth, experienced a shower of asteroids. The scientific group found that in their simulations, towards the end of its formation, the Earth accreted few planetary embryos coming from the asteroid belt, which were heavily hydrated (Morbidelli et al., 2000). In the Solar System, Mars and Earth are neighbors, and are therefore most likely to share certain early geological processes (Figure 1.3).

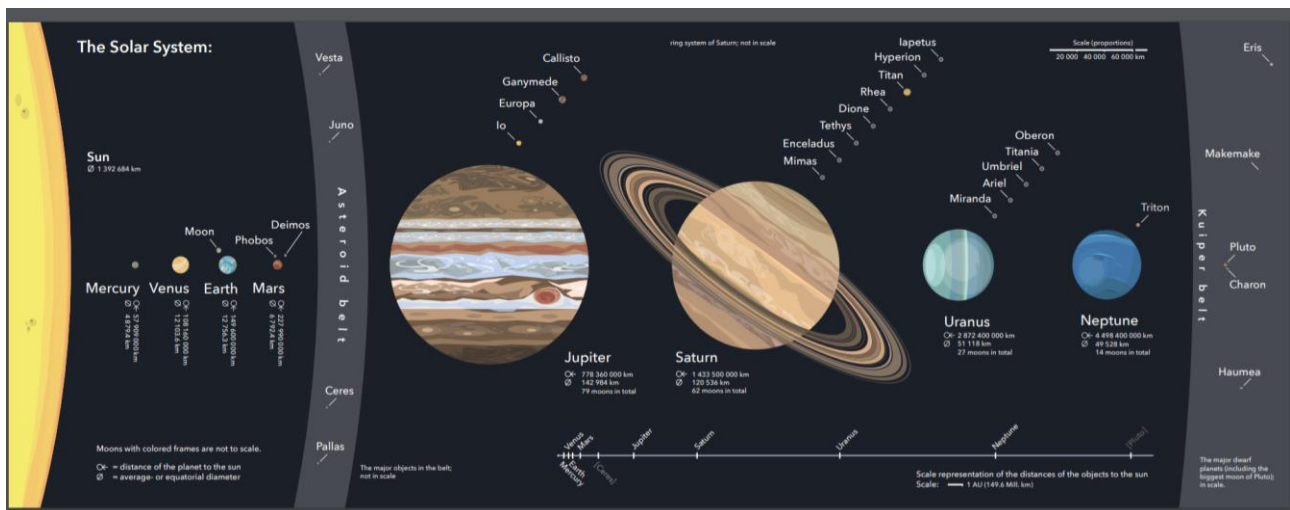


Figure 1.3. Schematic representation of the present Solar System. The asteroid belt is located between the four terrestrial planets most close to the Sun and the two gas giants Jupiter and Saturn. The geological history of Mercury, Venus, Earth and Mars is most likely to be common, whereas Jupiter and Saturn, due to their gaseous nature evolved independently. Credit: Wikipedia.

However, sharing certain early geological processes is not enough: indeed, the distance from the star is key to have liquid water on the surface. A “habitable zone” is defined by the right distance from the star to have liquid water on the surface, and Mars is very close to this boundary. However, the absence of a thick atmosphere makes Martian surface exposed to the radiation coming from the Sun and outer space, that strip away gaseous and liquid molecules from its thin atmosphere.

The isolation of viable extremely Haloarchaea from ancient rock salt suggests the possibility of their long-term survival. Since halite has been found on Mars (Rieder *et al.* 2004; Squyres *et al.* 2006) and in meteorites (Gooding, 1992; Treiman *et al.*, 2000; Zolensky *et al.*, 1999), the potential to find surviving life-forms or any sign of past life on Martian surface or subsurface is intriguing. Halophilic microorganisms are a good model to investigate putative signs of past or present life on Mars, based on at least three counts: 1) they are able to live and thrive at high levels of salinity, 2: evidence that haloarchaea survive entombed in salt crystals for millions of years, 3) evidence that they can recover from radiation damages (Baliga *et al.*, 2004). There is increasing evidence that in the early history of Mars there would have been liquid salty water on the surfaces that now is dried out (Carr 1996; Gendrin 2005). Images have been taken of more than 200 places where thick salt layers exist (Osterloo *et al.* 2008); these ancient salt deposits could be spots we might look at for the signs of past life. It could be plausible that life has survived during the period of time when Mars could have been habitable and the present day. Any salts crystals could preserve or record the existence of life on Mars and to support this theory, investigation of Mars analogues on Earth would be pertinent to this important Mars question.

1.6 The geological context of Mars

It is well-known that hypersaline brines can extend the range and stability of liquid water on Earth such as Deep Lake Antarctica, where Haloarchaea have been isolated. When looking for possible habitable exoplanets in respect to Haloarchaea, such a planet would have to have two major environmental factors present: water and salt. Characterization of Martian surface has yielded evidence of hypersaline ancient lakes on early Mars and were widely distributed in space and likely an order of magnitude more saline than terrestrial seawater (Ojha *et al.*, 2015; Tosca *et al.*, 2008).

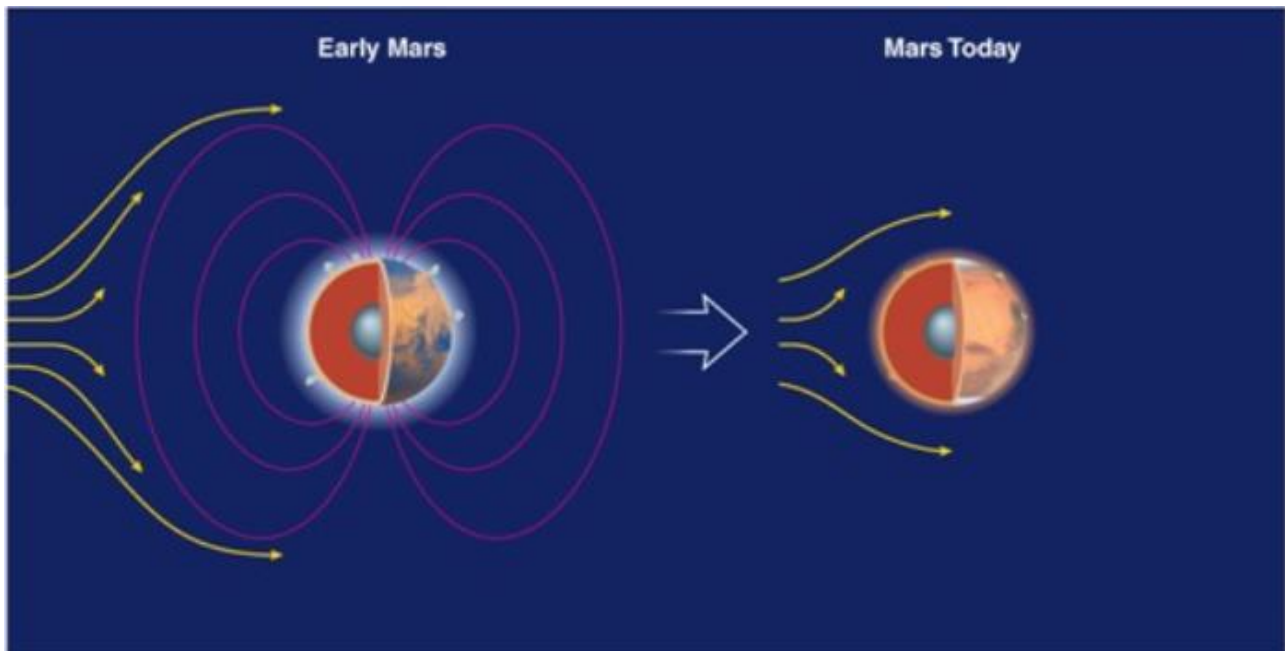


Figure 1.4. From “Pearson education (2012)”. Schematic illustration comparing early Mars and present Mars. Early Mars was warmer, and the core generated a stronger magnetic field, protecting the atmosphere from solar radiation. Present Mars lacks core convection, resulting in the absence of a global magnetic field. This causes the solar wind to be strong on the surface, stripping away the thin atmosphere, which results in a colder environment.

Many previous studies draw a picture of early Mars as being a warmer and wetter planet with a substantial amount of water earlier in its history, indicating the possibility of hypersaline brines on early Mars. More recently, evidence for water vapor in excess of saturation in the atmosphere has been shown, and it has also been highlighted that Mars is a salt rich environment. It is therefore intriguing to postulate that although Mars today is an inhospitable planet for life, Haloarchaea may have been enclosed in one of those brines and lying dormant over geological time there ever since. Although life on these planets and moons would be possible under certain circumstances, no trace of life has yet been found on either of them. However, further explorations and refined techniques for the detection of life may alter that. The most important challenge life on Mars has to face is protection against solar and cosmic radiations: the ability of Haloarchaea at long-term survival and strategies against radiations, coupled with the shielding properties of halite, makes them an interesting model to address the question of present or past life on Mars.

1.7 Detection of life on Mars: first attempt

Historically speaking, the first attempt to look for life on Mars were the Viking lander mission (Klein, 1978). The Viking landers were launched with the purposes of finding evidence of microbial life on the planet. The entire experiment comprised three sub-set of experiments:

- Labeled release experiment – Here the nutrients were tagged with radio-labeled carbon, subsequently released in the soil. The basic idea was that nutrients would have been used by microbes and, in turn, released radioactive CO₂ as a byproduct. The latter could have been picked up by the instrument as a demonstration that there were metabolically active microbes in Martian soil. The result of this was indeed gas, but such a result has never been obtained again (Oyama *et al.* 1976).

- Gas exchange experiment – The instrument released nutrients into the soil. If microbes were there, the instrument would have recorded any gases, namely methane, hydrogen, oxygen, that might be the products of biological activity. Here, the instrument was able to detect oxygen, but they found out that oxygen was also produced in the negative control (Klein, 1978).

- Pyrolytic release experiment – The idea was that the carbon dioxide would have been taken up by any microorganisms able to use it as a carbon source, so the instrument released into the soil radio-labeled carbon dioxide. As a result, radioactive carbon was found both in the experiment and in the negative control (Hubbard 1976).

Although it is difficult to see any possibility for Martian metabolism in these experiments, the results were overall not negative, so the author claimed that there must be something else reacting with the Martian soil.

1.8 References

- Antón, J., Oren, A., Benlloch, S., Rodríguez-Valera, F., Amann, R., Rosselló-Mora, R., 2002. *Salinibacter ruber* gen. nov., sp. nov., a novel, extremely halophilic member of the Bacteria from saltern crystallizer ponds. *International Journal of Systematic and Evolutionary Microbiology* 52, 485–491. <https://doi.org/10.1099/00207713-52-2-485>
- Baliga, N.S., Bjork, S.J., Bonneau, R., Pan, M., Iloanusi, C., Kottemann, M.C.H., Hood, L., DiRuggiero, J., 2004. Systems Level Insights Into the Stress Response to UV Radiation in the Halophilic Archaeon *Halobacterium* NRC-1. *Genome Res* 14, 1025–1035. <https://doi.org/10.1101/gr.1993504>
- Crits-Christoph, A., Gelsinger, D.R., Ma, B., Wierzchos, J., Ravel, J., Davila, A., Casero, M.C., DiRuggiero, J., 2016. Functional interactions of archaea, bacteria and viruses in a hypersaline endolithic community. *Environmental Microbiology* 18, 2064–2077. <https://doi.org/10.1111/1462-2920.13259>
- Daly, M.J., Gaidamakova, E.K., Matrosova, V.Y., Vasilenko, A., Zhai, M., Venkateswaran, A., Hess, M., Omelchenko, M.V., Kostandarithes, H.M., Makarova, K.S., Wackett, L.P., Fredrickson, J.K., Ghosal, D., 2004. Accumulation of Mn(II) in *Deinococcus radiodurans* Facilitates Gamma-Radiation Resistance. *Science* 306, 1025–1028. <https://doi.org/10.1126/science.1103185>
- Dombrowski, H., 1963. Bacteria from Paleozoic salt deposits. *Ann N Y Acad Sci* 108, 453–460. <https://doi.org/10.1111/j.1749-6632.1963.tb13400.x>
- Drew, H., Takano, T., Tanaka, S., Itakura, K., Dickerson, R.E., 1980. High-salt d(CpGpCpG), a left-handed Z' DNA double helix. *Nature* 286, 567–573. <https://doi.org/10.1038/286567a0>
- Fendrihan, S., Bérces, A., Lammer, H., Musso, M., Rontó, G., K Polacsek, T., Holzinger, A., Kolb, C., Stan-Lotter, H., 2009. Investigating the Effects of Simulated Martian Ultraviolet Radiation on *Halococcus dombrowskii* and Other Extremely Halophilic Archaeobacteria. *Astrobiology* 9, 104–12. <https://doi.org/10.1089/ast.2007.0234>
- Fish, S.A., Shepherd, T.J., McGenity, T.J., Grant, W.D., 2002. Recovery of 16S ribosomal RNA gene fragments from ancient halite. *Nature* 417, 432–436. <https://doi.org/10.1038/417432a>
- Gooding, J.L., 1992. Soil mineralogy and chemistry on Mars: Possible clues from salts and clays in SNC meteorites. *Icarus* 99, 28–41. [https://doi.org/10.1016/0019-1035\(92\)90168-7](https://doi.org/10.1016/0019-1035(92)90168-7)
- Gramain, A., Díaz, G.C., Demergasso, C., Lowenstein, T.K., McGenity, T.J., 2011. Archaeal diversity along a subterranean salt core from the Salar Grande (Chile). *Environ. Microbiol.* 13, 2105–2121. <https://doi.org/10.1111/j.1462-2920.2011.02435.x>

Grant, W.D., Gemmell, R.T., McGenity, T.J., 1998. Halobacteria: the evidence for longevity. *Extremophiles* 2, 279–287. <https://doi.org/10.1007/s007920050070>

Hebsgaard, M.B., Phillips, M.J., Willerslev, E., 2005. Geologically ancient DNA: fact or artefact? *Trends Microbiol* 13, 212–220. <https://doi.org/10.1016/j.tim.2005.03.010>

Hutcheon, G.W., Vasisht, N., Bolhuis, A., 2005. Characterisation of a highly stable alpha-amylase from the halophilic archaeon *Haloarcula hispanica*. *Extremophiles* 9, 487–495. <https://doi.org/10.1007/s00792-005-0471-2>

Jones, D.L., Baxter, B.K., 2016. Bipyrimidine Signatures as a Photoprotective Genome Strategy in G + C-rich Halophilic Archaea. *Life (Basel)* 6. <https://doi.org/10.3390/life6030037>

Lanyi, J.K., 1974. Salt-dependent properties of proteins from extremely halophilic bacteria. *Bacteriol Rev* 38, 272–290.

Lowenstein, T., Schubert, B., Timofeeff, M., 2011. Microbial communities in fluid inclusions and long-term survival in halite. *GSA Today* 21. <https://doi.org/10.1130/GSATG81A.1>

McGenity, T.J., Hallsworth, J.E., Timmis, K.N., 2008. Connectivity between “ancient” and “modern” hypersaline environments, and the salinity limits of life, in: Briand, F. (Ed.), . *CIESM*, pp. 115–120.

Morbidelli, A., Chambers, J., Lunine, J.I., Petit, J.M., Robert, F., Valsecchi, G.B., Cyr, K.E., 2000. Source regions and timescales for the delivery of water to the Earth. *Meteoritics & Planetary Science* 35, 1309–1320. <https://doi.org/10.1111/j.1945-5100.2000.tb01518.x>

Mormile, M.R., Biesen, M.A., Gutierrez, M.C., Ventosa, A., Pavlovich, J.B., Onstott, T.C., Fredrickson, J.K., 2003. Isolation of *Halobacterium salinarum* retrieved directly from halite brine inclusions. *Environmental Microbiology* 5, 1094–1102. <https://doi.org/10.1046/j.1462-2920.2003.00509.x>

Ojha, L., Wilhelm, M.B., Murchie, S.L., McEwen, A.S., Wray, J.J., Hanley, J., Massé, M., Chojnacki, M., 2015. Spectral evidence for hydrated salts in recurring slope lineae on Mars. *Nature Geoscience* 8, 829–832. <https://doi.org/10.1038/ngeo2546>

Oren, A., 2014. The ecology of *Dunaliella* in high-salt environments. *J Biol Res (Thessalon)* 21. <https://doi.org/10.1186/s40709-014-0023-y>

Oren, A., 2013. Life at high salt concentrations, intracellular KCl concentrations, and acidic proteomes. *Frontiers in microbiology* 4, 315. <https://doi.org/10.3389/fmicb.2013.00315>

Oren, A., 2008. Microbial life at high salt concentrations: phylogenetic and metabolic diversity. *Aquat. Biosyst.* 4, 2. <https://doi.org/10.1186/1746-1448-4-2>

Paul, S., Bag, S.K., Das, S., Harvill, E.T., Dutta, C., 2008. Molecular signature of hypersaline adaptation: insights from genome and proteome composition of halophilic prokaryotes. *Genome Biology* 9, R70. <https://doi.org/10.1186/gb-2008-9-4-r70>

Pohl, F.M., Jovin, T.M., 1972. Salt-induced co-operative conformational change of a synthetic DNA: equilibrium and kinetic studies with poly (dG-dC). *J Mol Biol* 67, 375–396. [https://doi.org/10.1016/0022-2836\(72\)90457-3](https://doi.org/10.1016/0022-2836(72)90457-3)

Reiser, R., Tasch, P., 1960. Investigation of the Viability of Osmophile Bacteria of Great Geological Age. *Transactions of the Kansas Academy of Science (1903-)* 63, 31–34. <https://doi.org/10.2307/3626919>

Rieder, R., Gellert, R., Anderson, R.C., Brückner, J., Clark, B.C., Dreibus, G., Economou, T., Klingelhöfer, G., Lugmair, G.W., Ming, D.W., Squyres, S.W., d'Uston, C., Wänke, H., Yen, A., Zipfel, J., 2004. Chemistry of Rocks and Soils at Meridiani Planum from the Alpha Particle X-ray Spectrometer. *Science* 306, 1746–1749. <https://doi.org/10.1126/science.1104358>

Schubert, B.A., Lowenstein, T.K., Timofeeff, M.N., Parker, M.A., 2010a. Halophilic Archaea cultured from ancient halite, Death Valley, California. *Environmental Microbiology* 12, 440–454. <https://doi.org/10.1111/j.1462-2920.2009.02086.x>

Schubert, B.A., Timofeeff, M.N., Lowenstein, T.K., Polle, J.E.W., 2010b. *Dunaliella* Cells in Fluid Inclusions in Halite: Significance for Long-term Survival of Prokaryotes. *Geomicrobiology Journal* 27, 61–75. <https://doi.org/10.1080/01490450903232207>

Shahmohammadi, H.R., Asgarani, E., Terato, H., Saito, T., Ohyama, Y., Gekko, K., Yamamoto, O., Ide, H., 1998. Protective roles of bacterioruberin and intracellular KCl in the resistance of *Halobacterium salinarum* against DNA-damaging agents. *J. Radiat. Res.* 39, 251–262. <https://doi.org/10.1269/jrr.39.251>

Soppa, J., 2006. From genomes to function: haloarchaea as model organisms. *Microbiology* 152, 585–590. <https://doi.org/10.1099/mic.0.28504-0>

Squyres, S.W., Knoll, A.H., Arvidson, R.E., Clark, B.C., Grotzinger, J.P., Jolliff, B.L., McLennan, S.M., Tosca, N., Bell, J.F., Calvin, W.M., Farrand, W.H., Glotch, T.D., Golombek, M.P., Herkenhoff, K.E., Johnson, J.R., Klingelhöfer, G., McSween, H.Y., Yen, A.S., 2006. Two Years at Meridiani Planum: Results from the Opportunity Rover. *Science* 313, 1403–1407. <https://doi.org/10.1126/science.1130890>

Tosca, N.J., Knoll, A.H., McLennan, S.M., 2008. Water Activity and the Challenge for Life on Early Mars. *Science* 320, 1204–1207. <https://doi.org/10.1126/science.1155432>

Treiman, A.H., Gleason, J.D., Bogard, D.D., 2000. The SNC meteorites are from Mars. *Planetary and Space Science, Mars Exploration Program* 48, 1213–1230. [https://doi.org/10.1016/S0032-0633\(00\)00105-7](https://doi.org/10.1016/S0032-0633(00)00105-7)

Uritskiy, G., Getsin, S., Munn, A., Gomez-Silva, B., Davila, A., Glass, B., Taylor, J., DiRuggiero, J., 2019. Halophilic microbial community compositional shift after a rare rainfall in the Atacama Desert. *The ISME Journal* 13, 2737–2749. <https://doi.org/10.1038/s41396-019-0468-y>

Webb, K.M., Yu, J., Robinson, C.K., Noboru, T., Lee, Y.C., DiRuggiero, J., 2013. Effects of intracellular Mn on the radiation resistance of the halophilic archaeon *Halobacterium salinarum*. *Extremophiles* 17, 485–497. <https://doi.org/10.1007/s00792-013-0533-9>

Zolensky, M.E., Bodnar, R.J., Gibson, E.K., Nyquist, L.E., Reese, Y., Shih, C.-Y., Wiesmann, H., 1999. Asteroidal Water Within Fluid Inclusion-Bearing Halite in an H5 Chondrite, Monahans (1998). *Science* 285, 1377–1379. <https://doi.org/10.1126/science.285.5432.1377>

Lipman, Chas B. “Living microorganisms in ancient rocks”. *Journal of Bacteriology* 22, no.3 (1931):183.

Nelson, David L., and Michael M. Cox. 2017. *Lehninger Principles of Biochemistry*. 7th ed. New York, NY: W.H. Freeman.

Chapter 2: Long-term survival of halophiles in laboratory-made halite and characteristics of halite precipitation

Abstract

2.1 Introduction

2.1.1 Halophiles in fluid inclusions of halite

2.1.2 The fluid inclusions microenvironment

2.1.3 Aim of the study

2.2 Methodology

2.2.1 Growth of strains

2.2.2 Entombment of halophilic microorganisms

2.2.3 Recovery of cells from laboratory-made halite

2.2.4 Cell visualization inside fluid inclusions

2.2.5 Influence of abiotic and biotic factors on the precipitation of lab-made halite

2.2.6 Sort of crystals by dimension and microscope analysis

2.3 Results

2.3.1 Recovery of cells from salt crystals

2.3.2 Cell visualization inside fluid inclusions

2.3.3 Influence of biotic and abiotic factors on the formation of lab-made halite

2.4 Discussion

2.5 Conclusions

2.6 References

2.7 Supplementary info

Chapter 2: Long-term survival of halophiles in laboratory-made halite and characteristics of halite precipitation

Abstract

Several reviews have provided a description of parameters that limit life (*i.e.*, temperature, pH, pressure, salinity, and radiation); interestingly, time has rarely been considered as such. Hypersaline environments, home for halophilic microbes, are subjected to occasional periods of evaporation from which salt crystals of halite can result. Many fluid inclusions can be found embedded in halite, and in those fluid inclusions, halophilic microbes can get entrapped. Evidence that specific microbes can survive over a geological time scale is accumulating and has remarkable implications about the longevity of life on Earth and opens to the possibility of life elsewhere. *Halobacterium* spp., for instance, are considered specialists in long-term survival.

This chapter attempts to address whether the chlorophyte, *Dunaliella salina* can survive inside fluid inclusions, and whether it enhances survival of *Halobacterium* spp. by experimentally entombing them individually and together. *Halobacterium* species are able to survive over 35 weeks in fluid inclusions of lab-made halite, with no nutrients. *Dunaliella salina* was able to survive the process of entombment, however, it did not survive beyond 2 days. Interestingly, the co-presence of *Halobacterium* 91-R6 had a significant positive effect on the speed of recovery of *Dunaliella* in the first days of entombment. Additionally, dynamics between the precipitation of halite and the life evolved in association with it may exist.

2.1 Introduction

2.1.1 Halophiles in fluid inclusions of halite

Hypersaline environments are very dynamic, subjected to period of desiccation and periodic rain that dissolves salt crystals. As reported in the main introduction (Chapter 1), evidence from several studies adds to the proof that Haloarchaea have remained viable in the subsurface of different hypersaline environments. These studies together increase the evidence base that Haloarchaea are able to survive over geological time scale (Gramain *et al.*, 2011; Jaakkola *et al.*, 2016a, 2014; Mormile *et al.*, 2003; Schubert *et al.*, 2010a). Many of these studies reported the isolation of halophilic microorganisms representing the species of *Halobacterium*, among others, from the class Halobacteria. Gramain *et al.* (2011) concluded that Haloarchaea are specialists in long-term survival, opening to the possibility that there could be specific mechanisms enabling the longevity of *Halobacterium* species in fluid inclusions over geological time scale. In the same study, the authors investigated the hypothesis that co-entombment of different species might benefit the survival, and their results support this hypothesis: they found that co-entombment of *Haloquadratum walsbyi* and *Salinibacter ruber* enhanced survival of both species in laboratory-made halite crystals (Gramain *et al.*, 2011).

2.1.2 The fluid inclusions microenvironment

The brine of fluid inclusions is composed of high levels of dissolved salt. Salt is known to preserve to some extent macromolecules, and this has been extensively reviewed (Grant *et al.*, 1998). In addition to this, the idea of simple food chains and mutual interactions that may occur between microorganisms in fluid inclusions in salt may provide an answer to the energetic demands. It has been estimated that haloarchaea could survive by feeding on co-entombed microorganisms for millions of years (McGenity *et al.*, 2008). In this perspective, it is worth mentioning the role of *Dunaliella salina*, the halophilic chlorophyte that can get entombed with halophilic microbes as brines evaporate. The glycerol it produces, which serves as an osmolyte, along with all components of dead cells, can potentially serve as carbon and energy source for a certain period of time. Evidence of remains of large carotenoid-rich cells resembling *D. salina* were observed within 10-34 kyr and

100 kyr old halite crystals from Death Valley, CA (Lowenstein *et al.*, 2011; Orellana *et al.*, 2013; Schubert *et al.*, 2010a). There is a crucial feature to take into consideration when documenting prokaryotes in ancient halite: as pointed by Schreder-Gomes *et al.* (2022), it is important to look at the petrographic context, in order to prove that the identified prokaryotes are the same age as the host halite. When salt minerals precipitate, fluid inclusions are encased in the crystal lattice. Primary fluid inclusions are created alongside the precipitation of the crystal a form characteristic structures called “chevron bands”, whereas secondary fluid inclusions are the result of a second precipitation, and are not considered representative of evaporative parent waters (Benison and Goldstein, 1999). Fluid inclusions in halite may be altered even by moderate heat, however, methods exist to evaluate whether fluid inclusions have been altered since entrapment, allowing the study of them to be considered representative; a good representative of these methods is reported in Benison and Goldstein (1999). In the same study, the researchers also described primary and secondary fluid inclusions, using photomicrograph images. The alteration of the halite structure has effect on the biology relative to the halite: levels of relative humidity may also alter halite structure. According to Crist-Cristoph *et al.*, (2016), deliquescence of halite can provide sufficient moisture to sustain a wide microbial community constituted of members from the three domains of life (Crist-Christoph *et al.*, 2016).

During previous experiments where laboratory-made halite crystals were created, we observed that, although the chemical composition of the salt solution was always the same, crystals precipitated differently in each new experiment. As crystals made in June and in October showed a different rate of precipitation, the seasonal conditions in the lab were offered as a possible explanation. Additionally, a somewhat diversity in the shape and size of the crystals was also observed. Norton and Grant (1988) performed experiments aiming to understand the extent of microbial entrapment in fluid inclusions, and its possible role in promoting halobacterial survival in salt, as well as a potential influence of microbes on the precipitation of halite. Their findings suggest that lab-made halite crystals forming from solutions heavily loaded with microbial cells contained more and larger inclusions than crystals formed from sterile solutions, as well as reporting the survival of strains of Haloarchaea within salt crystals, thus suggesting that biotic factors can influence the shape and the size of the precipitating halite crystals.

2.1.3 Aim of the study

The aim was to study the survival in lab-made halite crystals of three extreme halophiles, the Archaea, *Halobacterium salinarum* 91-R6, *Halobacterium noricense* A1, and the Bacterium, *Salinibacter ruber* M13, as well as the halotolerant green microalgae *Dunaliella salina* 19/18, individually and in a combination of them, in order to explore:

- 1) the ability of *Dunaliella salina* to get entombed inside fluid inclusions of halite,
- 2) the ability of the individual species to survive the entombment,
- 3) the potential benefit of combining *Dunaliella salina* with *Halobacterium salinarum* 91-R6 on the survival of each strain

In order to study the influence of different factors influencing the precipitation of halite, in collaboration with Nora Georgiev, we explored:

- 4) the possible influence of different temperature, the presence of high humidity, and the presence of microbes on the precipitation of lab-made halite crystals.

2.2 Methodology

2.2.1 Growth of strains

Halobacterium salinarum 91-R6 and *Halobacterium noricense* A1 were grown individually in 500 ml flasks with 350 ml of Payne 20% NaCl growth medium (Payne 1960) (Table S2.1), at 30°C on a shaker at 100 rpm. *Salinibacter ruber* DSMZ 13855 was grown in 500 ml flasks with 350 ml of *Salinibacter* 936 medium (Table S2.3) at 30°C on a shaker 100 rpm. *Dunaliella salina* CCAP 19/18 (Borowitzka and Siva, 2007) was grown in the medium (50 ml) for *Dunaliella*, developed by Hard and Gilmour (1996) (Table S2.2), in 300 ml flasks with a breathable cap, at 26°C with a 12:12 hour light:dark cycle (intensity 141 $\mu\text{mol m}^{-2} \text{s}^{-1}$). Previous experiments in the laboratory showed that species of *Halobacterium* reach the late exponential phase after seven days when grown in Payne medium 20% NaCl (Figure S2.1).

2.2.2 Entombment of halophilic microorganisms

The salt solution was prepared according to what has been published by Dyall-Smith (2009), modified with a higher concentration of total salt (Table 2.1). Each organism to be entombed individually was grown in 350 ml of growth media. When the late exponential phase was reached, 30 ml of cell culture was centrifuged (8500 g, 4°C, 20 min) and the cell pellets were washed in 25 ml of 25% NaCl; 2.5% MgSO₄·7H₂O. Cells were resuspended in 100 ml of salt solution (Table 2.1) and cell concentrations were determined by using a counting chamber. Where cell count was lower than 10⁸ cell/ml, additional 100 ml of cell culture was centrifuged, washed in salt solution, and the cell pellet dissolved with the previous suspension. Each suspension was then poured into sterile 145 mm diameter Petri dish was left, with lids off, on a disinfected, unused laboratory bench. The target cell concentration for both single and co-entombment, as reported also in previous experiments, is in the order of 10⁸ cell/ml. In the co-entombment experiments the final cell number was the same, as multiple strains were added equally up to a total of the order of 10⁸ cell/ml (Figure 2.1). The complete precipitation of lab-made halite took approximately eleven days.

Table 2.1. Salt solution formulation to mimic the concentrated brines where halophiles are found (Dyall-Smith, 2009).

Salt	Concentration (g/L)
NaCl	240
MgSO ₄ ·7H ₂ O	35
MgCl ₂ ·6H ₂ O	30
KCl	7

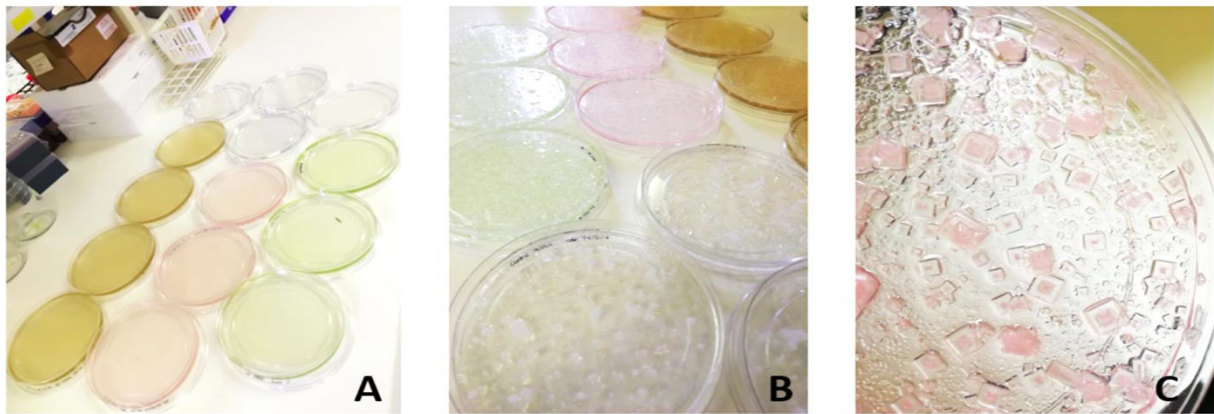


Figure 2. 1. (A) Petri dishes with salt solution (described in Table 2.1) and cells of *Halobacterium salinarum* NRC-1 (pinkish), *D. salina* 19/18 (green), and a mix of the two (brownish). (B) Early crystals forming after three days. (C) Detail of single entombed of *Halobacterium salinarum*. Plates were left with lids open until complete crystallisation and then stored with lids on.

2.2.3 Recovery of cells from laboratory-made halite

A mass equal to 0.3 g of salt crystals from each sample was aseptically placed into 15 ml of fresh medium using sterilized forceps and incubated. Specifically, in the case of *Halobacterium* spp., salt crystals were placed into 50 ml Falcon tubes with 15 ml of 20% NaCl Payne medium and placed on a shaker (100 rpm), in the dark, at 30°C until first sign of growth was visible. In the case of *D. salina* 19/18, salt crystals were placed into 50 ml cell culture flasks, with breathable cap, with 15 ml of *Dunaliella* growth medium, at 26°C ($141 \mu\text{mol m}^{-2} \text{s}^{-1}$, on a 12:12 light:dark cycle). In the case of multiple entombment, crystals were dissolved both in liquid media for *Halobacterium* spp. and in liquid media for *D. salina* and kept at the respective conditions as mentioned above. The falcon tubes and flasks were checked regularly until clear signs of growth were detectable by eye. The interval of time between the dissolution of the crystal and the first sign of growth detectable by naked eye, was defined as the time required by entombed cells to recover.

2.2.4 Cell visualization inside fluid inclusions

In order to stain cells and visualize them, new salt crystals were prepared. As the dye is light sensitive, the entire process was done in dark conditions. Cells of *Halobacterium salinarum* 91-R6 and *Dunaliella salina* 19/18 were stained adding the MitoTracker to the growth medium at a 1:1000 dilution (to a final concentration of 1 μ M) (as described in Maslov *et al.*, 2018). Previous trials of this experiment showed that better microscopic images were obtained when the stained cells were then washed with the salt solution, in order to get rid of the excess of stain. Subsequently, 500 μ l of salt solution with stained microbes were poured on ethanol-cleaned microscope slides and kept in dark conditions until crystallisation was completed. The microscope observations were performed with the supervision of Dr. Philippe Laissue (University of Essex). Samples were observed under the fluorescence inverted microscope using a Nikon Eclipse Ti-E main body and NIS-Elements (version 3.21.03, build 705 LO) for image acquisition (as described in Laissue *et al.*, 2020).

2.2.5 Influence of abiotic and biotic factors on the precipitation of lab-made halite

In this experiment, performed in collaboration with Nora Georgiev, two Haloarchaea *Halobacterium salinarum* NRC-1, *Halobacterium noricense* A1, the microalga *Dunaliella salina* 19/18 and the bacterium *Salinibacter ruber* M31 were grown in their respective medium (Section 2.2.1) and entombed individually in laboratory-made halite, in replicates. Two types of brine were tested: the first one had the composition of brine more closely mimicking the natural chemical condition of hypersaline environments (as described in Dyall-Smith, 2009) (Table 2.1), the second brine tested was only composed by 25% NaCl. Cells were collected by centrifugation (8500 g, 4°C, 20 min) and, half were washed with salt solution (Table 2.1) and resuspended in this brine, the other half were washed with 25% NaCl and resuspended in salt solution made only of 25% NaCl. Serial dilution of each sample followed, and cell concentration was defined (Table S2.4), before pouring the cell suspension in Petri dishes. In order to constrain information about the precipitation of laboratory-made halite, we designed three setups with fixed environmental conditions, summarized in Figure 2.2. In Room 1, the Petri dishes with precipitating halite were left on the shelf, with lid open, in the

incubator at 30.5°C (mean value). In Room 2, the only difference with Room 1, was the temperature of 19.8°C (mean value). In Room 3, Petri dishes with the lid open were kept in an open plastic box during the dry cycle. The temperature in Room 3 was the same as in Room 1 (30.5°C). To expose the halite crystals of Room 3 to high levels of humidity, a cool mist air humidifier was inserted in the plastic box, closed, for two hours. Levels of humidity and temperature were checked in all rooms with a digital thermometer hygrometer, every day at the same time for 20 days. Specifically, Nora Georgiev worked on the pair-wise comparison between Room 1 and Room 2 of halite precipitated from brine mimicking the natural composition of hypersaline environments and halite precipitated from the 25% NaCl solution, whereas I focussed on the comparison among Room 1, 2 and 3 of halite precipitated from the brines mimicking hypersaline environments.

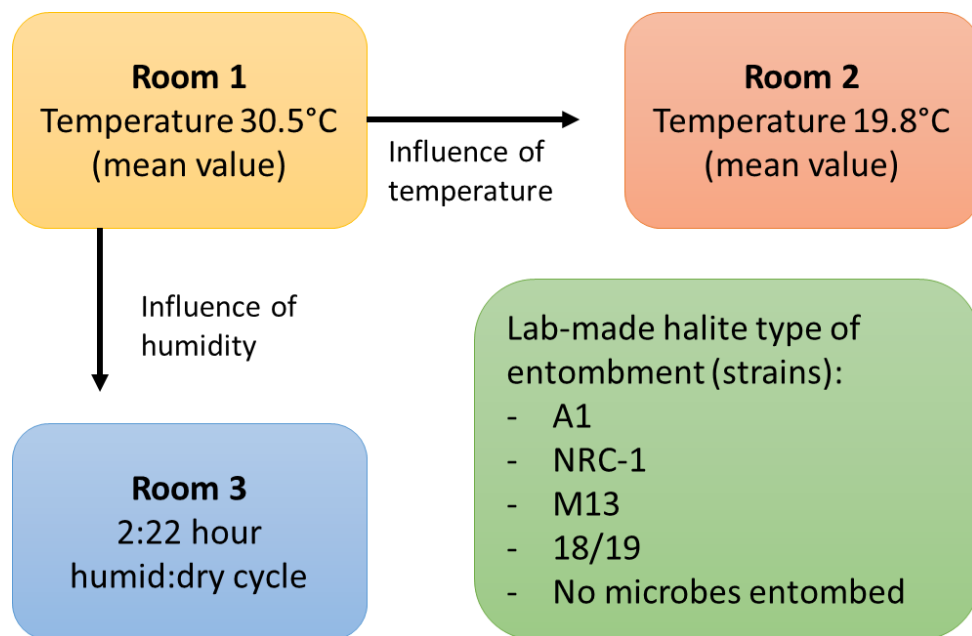


Figure 2. 2. General scheme of the experiment where the influence of biotic and/or abiotic factors on the precipitation of lab-made halite was investigated. Room 1 was used as a reference to investigate the effect of lower temperature (Room 2) and the effect of higher humidity (Room 3). Five different types of entombment were tested (green box), respectively, single entombment of *Halobacterium noricense* A1, *Halobacterium salinarum* NRC-1, *Salinibacter uber* M13 and *Dunaliella salina* 19/18, additionally, lab-made halite with no microbes entombed were also included. This scheme was the same for both halite made of brine mimicking the natural environment and brine composed only of 25% NaCl. The mean temperature was calculated using the values measured every day at the same time for the entire duration of the experiment (about 20 days). Values of humidity changed trough time, however, never exceeding 33% in Room 1 and 2, whereas in Room 3, during the 2 hours of humidification, levels of humidity always reached values higher than 85%.

2.2.6 *Sorting crystals by dimension and microscope analysis*

Once the precipitation of lab-made halite was completed, individual crystals were sampled and analysed under the microscope in order to visualize the fluid inclusions. Subsequently, all the crystals were quickly washed with saturated NaCl solution and then immediately sieved; this step was necessary to obtain separated crystals to be sieved by size. Four sieves with different diameters were placed one on the top of each other and the crystals were sorted in five different measures, respectively 1-3 mm, 3-4 mm, 4-9 mm and >9 mm. The last measure is indicated as <1 mm, and it is calculated by the total mass of crystals before sieving them, minus the total mass of crystals after sieving them, and it comprises smaller crystals, as well as fragile structures that were lost during the washing in saturated NaCl solution. The sieves were shaken by hands to sort them, and the total mass obtained from each sieve was measured.

2.3 Results

2.3.1 *Recovery of cells from salt crystals*

The results of the experiment aiming at understanding the survival in fluid inclusions of lab-made halite are reported in Figure 2.3. *Halobacterium salinarum* 91-R6 is able to survive fluid inclusions over 35 weeks. In the first five weeks the lag-phase was 4 days in all replicates, while after 20 weeks, the recovery was slower, with a lag of 10 days (after > 20 weeks) and 15 days (after 35 weeks). Until 35 weeks, the recovery of *Hbt. salinarum* 91-R6 entombed together with *D. salina* 19/18 was the same as when grown alone, but at 35 days there was the lag phase was 14 days when co-entombed and 15 days when grown alone, however, this difference is not significant (p-value > 0.05; t-test). Over a period of 35 weeks, Nora Georgiev (2020) found that *Hbt. salinarum* A1 was the best survivor, being able to recover after four days in all replicates, except in the last recovery, where for two replicates out of four, it took five days to show first sign of growth.

Dunaliella salina 19/18 was a poor survivor, being able to survive only the process of entombment, which lasted 11 days: at time 0 (reported in Figure 2.3), after the lag phase was 27 days. Interestingly, when *Dunaliella salina* 19/18 was entombed together with *Halobacterium salinarum* 91-R6, after the lag phase was 7 days, significantly faster (t-test; p-value < 0.05) than in the single entombment. To the best of my knowledge, this is the first time the recovery in fluid inclusions of *Dunaliella salina* 19/18 was tested.

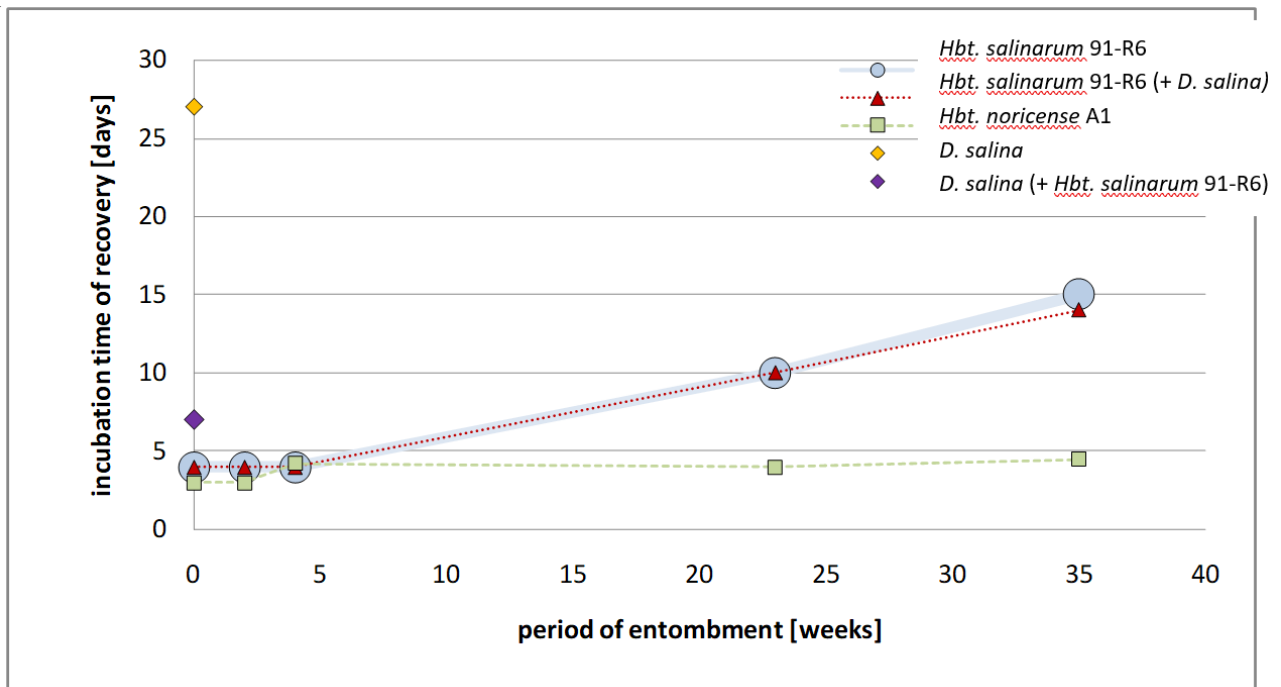


Figure 2. 3. Results from the recovery of the strains involved in this experiment. Each single crystal was dissolved in liquid medium every two weeks and the lag phase (expressed in days on the y-axis) shows how many days passed before any sign of growth was detected by eye. In this figure, the time point 0 on the x-axis represents the first day at which the precipitated halite was dissolved in liquid media and does not include the eleven days passed to have complete precipitation of halite in the Petri dishes. Crystals from the co-entombment experiment were dissolved both in 20% NaCl Payne to allow the growth of *Halobacterium salinarum* 91-R6, and *Dunaliella* medium in the case of the microalgae, and incubated at their respective optimum growth conditions. The experiment was carried out in four replicates and there was no difference among the replicates (hence no error bars). Data regarding *Halobacterium noricense* A1 are taken from the work of the master thesis of Nora Georgiev (2020).

2.3.2 Cell visualization inside fluid inclusions

The organisms stained using the MitoTracker Orange CMTMRos were *Halobacterium salinarum* 91-R6 and *Dunaliella salina* 19/18, for an individual entombment and co-entombment of both. The images confirmed that these halophilic microorganisms were entombed in fluid inclusions of the precipitated halite, and it is clear also that intact cells of *Dunaliella salina* 19/18 can get entombed together with *Halobacterium salinarum* 91-R6 (Figure 2.4).

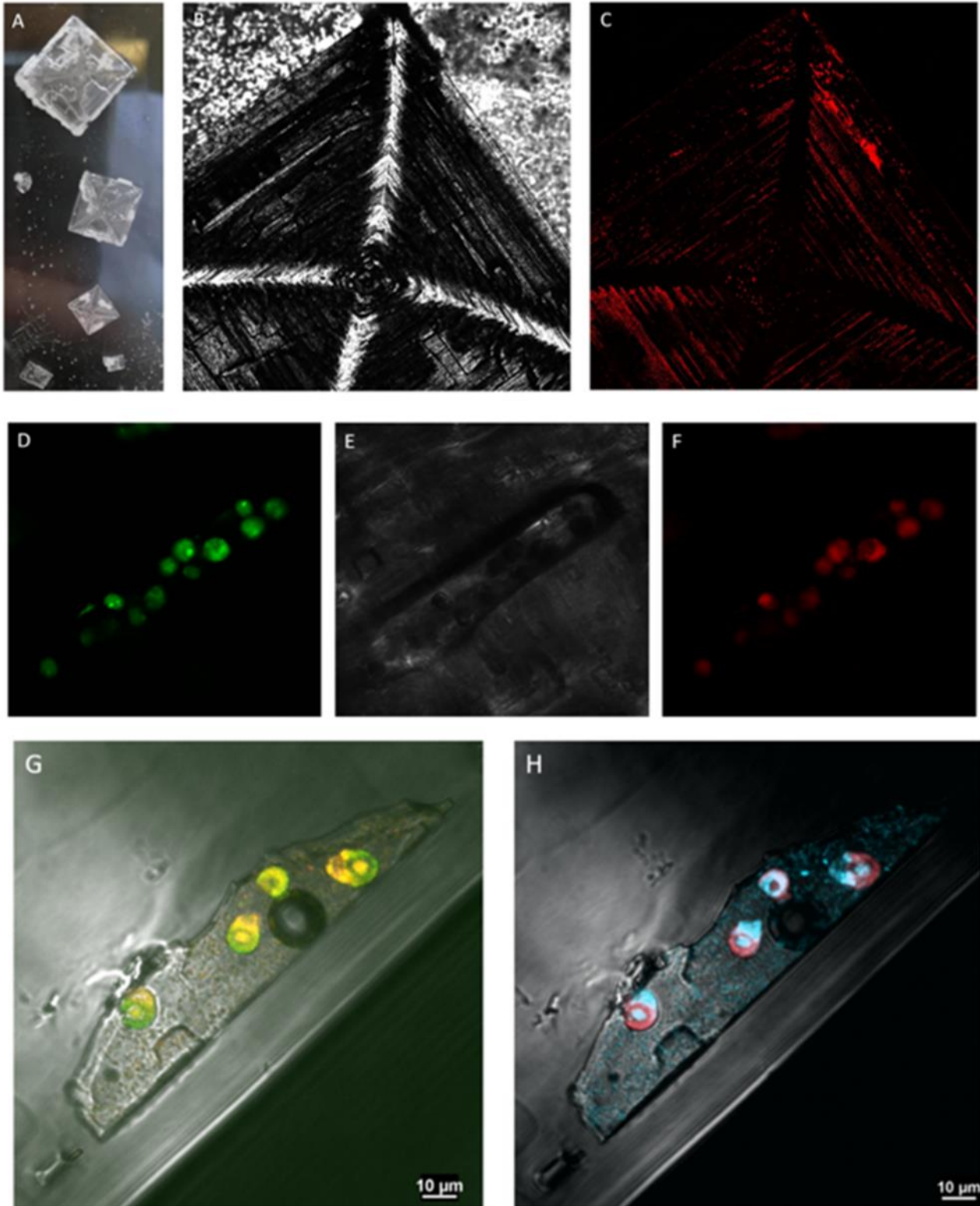


Figure 2.4 Detail of lab-made halite crystals precipitated on microscope slides (A); details of the halite seen under the microscope (4×) (B); single entombment of *Halobacterium salinarum* 91-R6 shown in red inside fluid inclusions (C); single entombment of *Dunaliella salina* shown inside the fluid inclusion (D – E – F) where the photosynthetic pigment of the microalgae is auto fluorescing in red (F) and the MitoTracker in green (D); co-entombment of *Dunaliella salina* and *Halobacterium salinarum* 91-R6 (G – H) where it is possible to see the dimension of the microalgae compared to the haloarchaea. In (H) blue represents MitoTracker staining and red indicates chlorophyll.

2.3.3 Influence of biotic and abiotic factors on the formation of lab-made halite

The halite crystals precipitated from the brine mimicking the composition of hypersaline environments were sieved in order to sort crystals based on size. It is important to note that, as mentioned in the Methodology section, in order to obtain individual crystals, those were washed in saturated NaCl solution, in order to carefully separate agglomerated crystals without dissolving them. When compared only the physical parameters, *e.g.*, temperature and humidity, the results showed that the total mass calculated after the sieving, in Room 1 (30.5°C) was the highest, while in Room 3 (30.5°C and 2:22 hour humid:dry cycle) was the lowest, respectively 65.31 g versus 53.41 g. The size of crystals in Room 1 was similarly distributed, with crystals of 1-3 mm that were the most abundant, 42.42% of the total. The majority of crystals precipitated in Room 2 (19.8°C) had a dimension ranging between 3 and 4 mm, and only in Room 2, there were crystals as big as 9 mm, although they were a small part of the total. In Room 3 (19.8°C), 86.21% of the crystals were 3 mm in size, the highest percentages registered. Georgiev (2020) observed that crystals made from 25% NaCl precipitated in Room 2 took 14 days, versus the seven days needed in Room 1 to have complete precipitation from the same brine composition. She also observed a different precipitation of rate between crystals made from brine mimicking the composition of hypersaline environments and brine composed of 25% NaCl: the evaporation rate for NaCl solution was faster than the other (data not shown here, available in Grogiev (2020)). In this chapter, the differences of crystals precipitated only from brine mimicking the composition of hypersaline environments in Room 1 and Room 3 are discussed. The complete precipitation of crystals in Room 3 (humid:dry cycle) was never achieved, as the cycles of high humidity kept the crystals moist for the entire duration of the experiment (20 days). After 20 days, all the crystals, except those in Room 3 for the reason mentioned above, were fully precipitated. Crystals were then sieved according to their size, and sorted in four different measures, respectively, < 1, 3, 4 and 9 mm (Figure 2.5). In Room 1 and Room 3, the crystals precipitated in the presence of microbes were overall significant bigger than the sterile brine solution, used as a control, in the respective Rooms. There were some pairwise significant differences observed in the comparison between Rooms, however those differences were inconsistent and do not allow a clear distinction between the influences biotic and abiotic parameters have had on the precipitation of halite crystals.

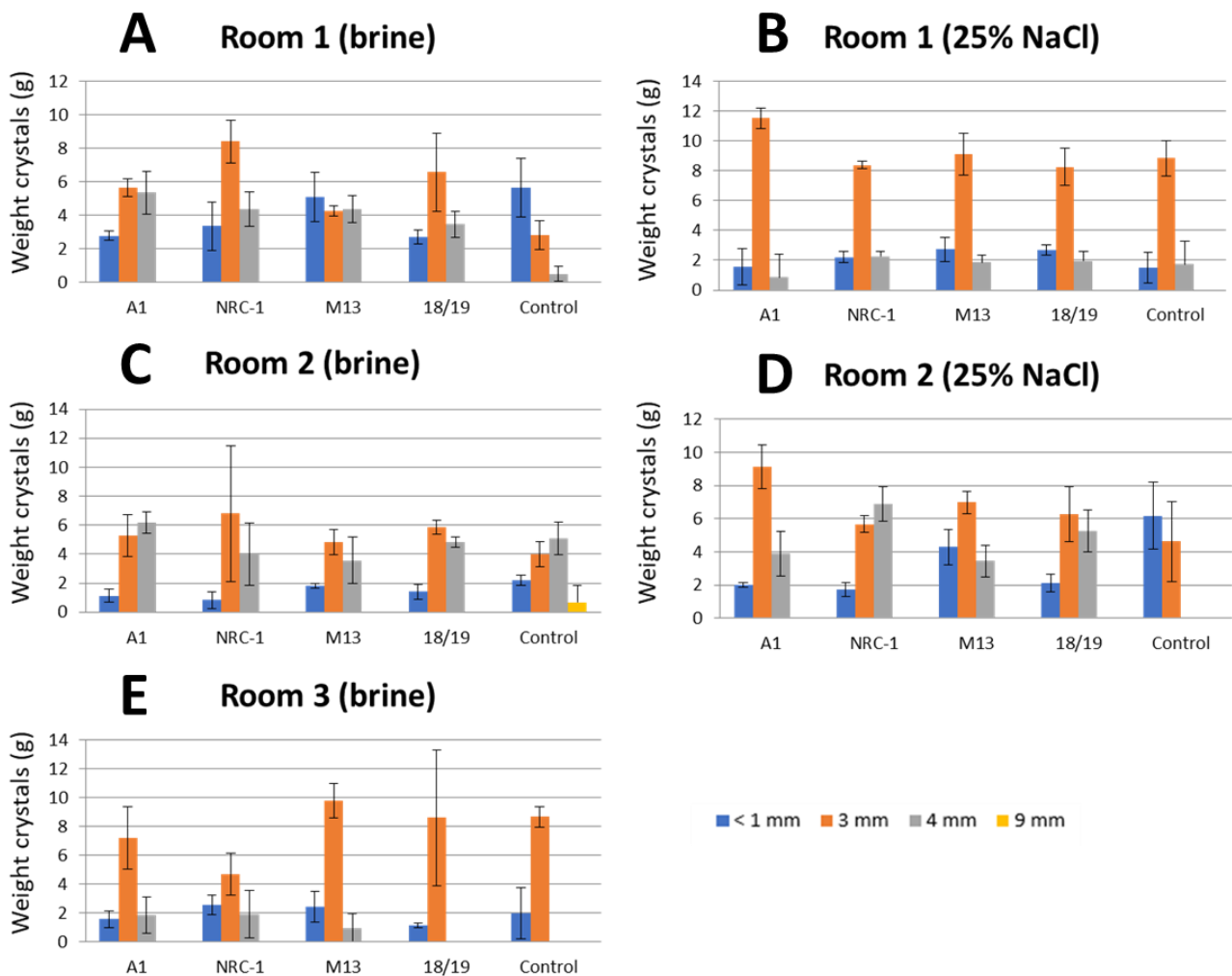


Figure 2.5. Comparison between the results obtained from the experiment about the factors influencing the precipitation of lab-made halite. The comparison between halite crystals precipitated from brines versus 25% NaCl solution (A versus B and C versus D) are discussed in the Master Thesis of Nora Georgiev (2020).

2.4 Discussion

In this chapter I explored the ability of haloarchaeal species *Halobacterium salinarum* 91-R6, *Halobacterium noricense* A1 and the green microalgae *Dunaliella salina* 19/18 individually entombed in lab-made halite and found that haloarchaeal species are better survivor compared to *D. salina*, which was a poor survivor, unable to recover weeks after the entombment. This is probably due to the different strategies these halophiles have, as the “salt-in” strategy of Haloarchaea allows them to survive in saturated brines, whereas the accumulation of compatible solutes, the strategy used by *D. salina*, does not allow it to survive in brine higher than 3.5 M salt, as reported by Oren (2013).

Halobacterium noricense A1 was a better survivor than *Halobacterium salinarum* NRC-1: in the first six weeks of entombment, there was no significant difference between the two species, however, after ten weeks, *Hbt. noricense* A1 recovered faster than *Hbt. salinarum* 91-R6. The available data collected in this experiment could not explain that, however, these results are in line with the results published by Gramain *et al.* (2011). The authors found that haloarchaeal species are specialists in long-term survival (except for *Haloquadratum walsbyi*, which was affected by the entombment over 27 months, showing a slower recover), and also in their experiments *Hbt. noricense* A1 was a better survivor compared to *Hbt. salinarum* NRC-1. The authors also found that *Salinibacter ruber* and *Haloquadratum walsbyi*, when entombed together, showed enhanced survival to the entombment, with both cell types being visible by microscopy after 26 months (Gramain *et al.*, 2011). Similarly, also in the experiment reported in this chapter there seems to be an advantage to *Dunaliella salina* from co-entombment: *Dunaliella salina* recovered faster in the first time point when it was entombed together with *Halobacterium salinarum* 91-R6. However, there was no significant positive effect on *Halobacterium salinarum* 91-R6. This was counter to expectation, because *Dunaliella* species produce glycerol as compatible solute, and at high salinity levels, cells might lyse, releasing intracellular content, that has been proposed to be part of the organic carbon supporting the metabolism of *Halobacterium salinarum* in fluid inclusions over geological time scale (Jaakkola *et al.*, 2016b; Lowenstein *et al.*, 2011; Orellana *et al.*, 2013; Oren, 1995; Schubert *et al.*, 2010b). Orellana *et al.* (2013) also suggested that there might be symbiotic relationships between some Haloarchaea and species of *D. salina*, with the Haloarchaea providing nutrients to stimulate the growth of *D. salina*, which in turn, might sustain the metabolism of some Haloarchaea. This supports the results of the first experiment presented in this chapter.

In previous studies, the influence of microbes on the precipitation of halite has been investigated. In the study published by Norton and Grant (1988), the presence of microbes speeded up the precipitation of lab-made halite, compared to sterile solution. The explanation given by the authors is related to the influence of microbes in creating a “seed” promoting the initial crystal formation. Similar explanations were given by Lopez-Cortes *et al.* (1994), who observed that the presence of Haloarchaea yielded bigger halite crystals compared to sterile brines. Castanier *et al.* (1999) found similar results, supporting the interpretation that microbes are influencing the precipitation of halite; according to their results, the presence of microbes induces the precipitation of halite and the orientation of the growing crystals. In a short-course on the Pre-history and History of salt organized by the ETN Saltgiant, Jules Vleugels reported that it is common use to add drops of beer on the surface of evaporating brines for salt production at the “God-given salina”, a structure composed of a 300-meter-long graduation tower and a salt house (Germany, Westphalia region), suggesting that

the creation of bubbles on the surface induces the crystallisation of halite (personal communication). The results of this experiment support the hypothesis that the presence of microbes influences the halite precipitation, by increasing the rate of precipitation. A possible explanation might be that, as previously suggested, the presence of microbes induces the formation of crystals on the surface, along which the rest of the structure grows. Although microbes living in hypersaline environment have no choice but to get trapped inside fluid inclusions of halite, the entombment seems to be an advantage, as the remaining brines after the precipitation of halite are mainly composed of $MgCl_2$ -rich water bodies, which appear to be sterile (Javor, 1989), because of its chaotropicity (Hallsworth *et al.*, 2007). Therefore, the putative role/influence of microbes on the process of precipitation, might result in an advantage for the microbes entombed in the halite. *Dunaliella salina*, an important primary producer in hypersaline environments (Oren, 2014), is not as good as a survivor: in this experiment *Dunaliella salina* survived the process of entombed, but did not recover from further on. To the best of my knowledge, it is the first time the survival in fluid inclusions of halite of *Dunaliella salina* was tested. It can be concluded that *Dunaliella salina* gets trapped in halite fluid inclusions but does not survive beyond the initial entombment. Although it appears to not influence the survival of *Halobacterium salinarum* over the short time frame of this experiment, it remains to be tested whether it can enhance its survival over the longer term.

2.6 References

Benison, K.C., Goldstein, R.H., 1999. Permian paleoclimate data from fluid inclusions in halite. *Chemical Geology* 154, 113–132. [https://doi.org/10.1016/S0009-2541\(98\)00127-2](https://doi.org/10.1016/S0009-2541(98)00127-2)

Borowitzka, M.A., Siva, C.J., 2007. The taxonomy of the genus *Dunaliella* (Chlorophyta, Dunaliellales) with emphasis on the marine and halophilic species. *J Appl Phycol* 19, 567–590. <https://doi.org/10.1007/s10811-007-9171-x>

Castanier, S., Perthuisot, J.-P., Matrat, M., Morvan, J.-Y., 1999. The salt ooids of Berre salt works (Bouches du Rhône, France): the role of bacteria in salt crystallisation. *Sedimentary Geology* 125, 9–21. [https://doi.org/10.1016/S0037-0738\(98\)00144-4](https://doi.org/10.1016/S0037-0738(98)00144-4)

Crits-Christoph, A., Gelsinger, D.R., Ma, B., Wierzchos, J., Ravel, J., Davila, A., Casero, M.C., DiRuggiero, J., 2016. Functional interactions of archaea, bacteria and viruses in a hypersaline endolithic community. *Environmental Microbiology* 18, 2064–2077. <https://doi.org/10.1111/1462-2920.13259>

Gramain, A., Díaz, G.C., Demergasso, C., Lowenstein, T.K., McGenity, T.J., 2011. Archaeal diversity along a subterranean salt core from the Salar Grande (Chile). *Environ. Microbiol.* 13, 2105–2121. <https://doi.org/10.1111/j.1462-2920.2011.02435.x>

Hallsworth, J.E., Yakimov, M.M., Golyshin, P.N., Gillion, J.L.M., D’Auria, G., De Lima Alves, F., La Cono, V., Genovese, M., McKew, B.A., Hayes, S.L., Harris, G., Giuliano, L., Timmis, K.N., McGenity, T.J., 2007. Limits of life in MgCl₂-containing environments: chaotropicity defines the window. *Environmental Microbiology* 9, 801–813. <https://doi.org/10.1111/j.1462-2920.2006.01212.x>

Jaakkola, S.T., Pfeiffer, F., Ravantti, J.J., Guo, Q., Liu, Y., Chen, X., Ma, H., Yang, C., Oksanen, H.M., Bamford, D.H., 2016a. The complete genome of a viable archaeum isolated from 123-million-year-old rock salt. *Environmental Microbiology* 18, 565–579. <https://doi.org/10.1111/1462-2920.13130>

Jaakkola, S.T., Ravantti, J.J., Oksanen, H.M., Bamford, D.H., 2016b. Buried Alive: Microbes from Ancient Halite. *Trends Microbiol.* 24, 148–160. <https://doi.org/10.1016/j.tim.2015.12.002>

Jaakkola, S.T., Zerulla, K., Guo, Q., Liu, Y., Ma, H., Yang, C., Bamford, D.H., Chen, X., Soppa, J., Oksanen, H.M., 2014. Halophilic Archaea Cultivated from Surface Sterilized Middle-Late Eocene Rock Salt Are Polyploid. *PLoS One* 9. <https://doi.org/10.1371/journal.pone.0110533>

Javor, B., 1989. *Hypersaline Environments*, Brock/Springer Series in Contemporary Bioscience. Springer, Berlin, Heidelberg. <https://doi.org/10.1007/978-3-642-74370-2>

Laissue, P.P., Roberson, L., Gu, Y., Qian, C., Smith, D.J., 2020. Long-term imaging of the photosensitive, reef-building coral *Acropora muricata* using light-sheet illumination. *Sci Rep* 10, 10369. <https://doi.org/10.1038/s41598-020-67144-w>

Lopez-Cortes, A., Ochoa, J., Vazquez-Duhalt, R., 1994. Participation of halobacteria in crystal formation and the crystallization rate of NaCl. *Geomicrobiology Journal* 12, 69–80. <https://doi.org/10.1080/01490459409377973>

Lowenstein, T.K., Schubert, B.A., Timofeeff, M.N., 2011. Microbial communities in fluid inclusions and long-term survival in halite. *GSAT* 21, 4–9. <https://doi.org/10.1130/GSATG81A.1>

Maslov, I., Bogorodskiy, A., Mishin, A., Okhrimenko, I., Gushchin, I., Kalenov, S., Dencher, N., Fahlke, C., Büldt, G., Gordeliy, V., Gensch, T., Borshchevskiy, V., 2018. Efficient non-cytotoxic fluorescent staining of halophiles. *Scientific Reports* 8. <https://doi.org/10.1038/s41598-018-20839-7>

Mormile, M.R., Biesen, M.A., Gutierrez, M.C., Ventosa, A., Pavlovich, J.B., Onstott, T.C., Fredrickson, J.K., 2003. Isolation of *Halobacterium salinarum* retrieved directly from halite brine inclusions. *Environmental Microbiology* 5, 1094–1102. <https://doi.org/10.1046/j.1462-2920.2003.00509.x>

Norton, C.F., Grant, W.D., 1988. Survival of Halobacteria Within Fluid Inclusions in Salt Crystals. *Microbiology* 134, 1365–1373. <https://doi.org/10.1099/00221287-134-5-1365>

Orellana, M.V., Pang, W.L., Durand, P.M., Whitehead, K., Baliga, N.S., 2013. A Role for Programmed Cell Death in the Microbial Loop. *PLOS ONE* 8, e62595. <https://doi.org/10.1371/journal.pone.0062595>

Oren, A., 2014. The ecology of *Dunaliella* in high-salt environments. *J Biol Res (Thessalon)* 21. <https://doi.org/10.1186/s40709-014-0023-y>

Oren, A., 2013. Life at high salt concentrations, intracellular KCl concentrations, and acidic proteomes. *Frontiers in microbiology* 4, 315. <https://doi.org/10.3389/fmicb.2013.00315>

Oren, A., 1995. The role of glycerol in the nutrition of halophilic archaeal communities: a study of respiratory electron transport. *FEMS Microbiology Ecology* 16, 281–290. <https://doi.org/10.1111/j.1574-6941.1995.tb00292.x>

Schreder-Gomes, S.I., Benison, K.C., Bernau, J.A., 2022. 830-million-year-old microorganisms in primary fluid inclusions in halite. *Geology* 50, 918–922. <https://doi.org/10.1130/G49957.1>

Schubert, B.A., Lowenstein, T.K., Timofeeff, M.N., Parker, M.A., 2010a. Halophilic Archaea cultured from ancient halite, Death Valley, California. *Environmental Microbiology* 12, 440–454. <https://doi.org/10.1111/j.1462-2920.2009.02086.x>

Schubert, B.A., Timofeeff, M.N., Lowenstein, T.K., Polle, J.E.W., 2010b. *Dunaliella* Cells in Fluid Inclusions in Halite: Significance for Long-term Survival of Prokaryotes. *Geomicrobiology Journal* 27, 61–75. <https://doi.org/10.1080/01490450903232207>

Georgiev, N. 2020. Understanding how halophiles survive in evaporites. Master Thesis. University of Essex

2.7 Supplementary info

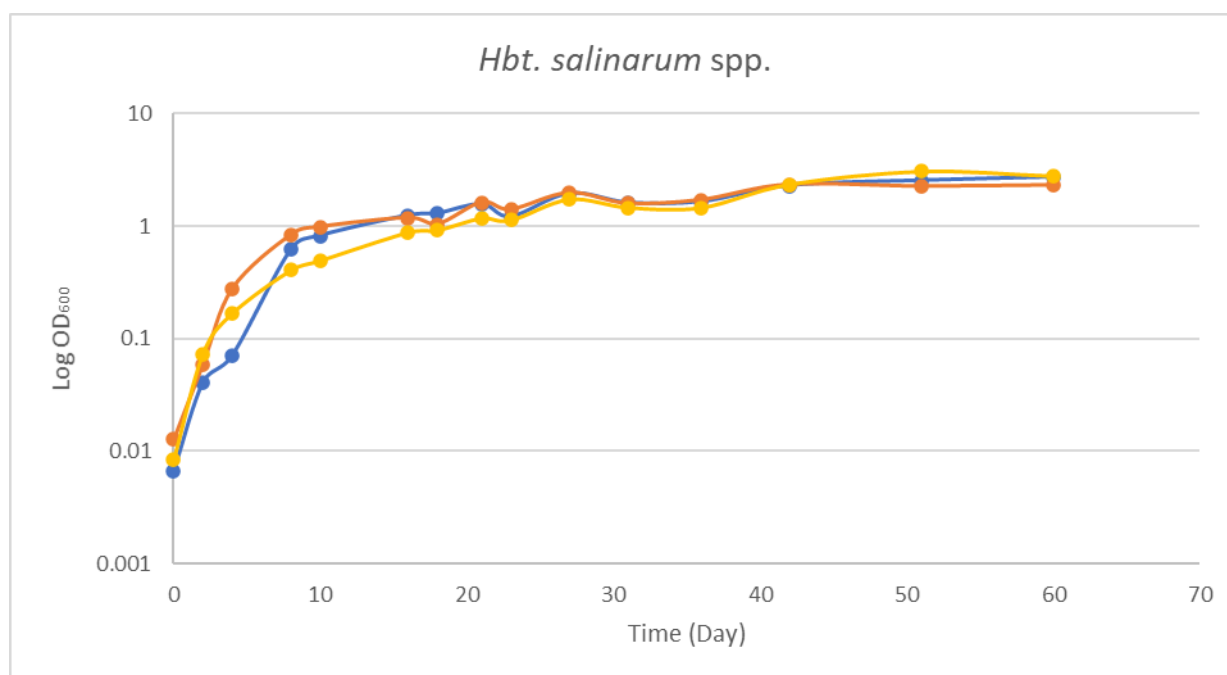


Figure S2.1. Growth curve of *Halobacterium salinarum* NRC-1 (yellow), *Halobacterium noricense* A1 (blue) and *Halobacterium salinarum* 91-R6 (orange).

Table S2.1. Modified 20% NaCl Payne media to grow *Halobacterium* species.

Chemical	Quantity
NaCl	200 (3.42 M)
MgSO ₄ ·7H ₂ O	20 (0.08 M)
KCl	2g/L
TriNaCitrate	3g/L
Yeast extract	10g/L
Casamino acids	7.5g/L
FeCl ₂ ·4H ₂ O	1 ml
MnCl ₂ ·4H ₂ O	1 ml

Thoma (Helber) counting cells chamber

In similar experiments Gramain *et al.* (2011) inoculated with cells at early exponential phase ($OD_{\lambda=600\text{nm}} \approx 0.200$) and a cell concentration of 2.3×10^8 cell ml^{-1} . Cell concentrations prior entombment were determined by using a counting chamber (Thoma, Helber). Cells were counted using as a reference the rectangle of 0.05 mm length, 0.025 mm and 0.02 mm depth.

In order to know the concentration of cells in 1ml I used the following formula:

$$0.05\text{mm} \cdot 0.025\text{mm} \cdot 0.02\text{mm} = 2.5 \cdot 10^{-5}\text{mm}^3$$

$$\frac{1000\text{mm}^3}{2.5 \cdot 10^{-5}\text{mm}^3} = 4 \cdot 10^7$$

Table S2.2. *Dunaliella* growth medium developed by Hard and Gilmour (1996). All the volumes of the stock solution are calculated for 1 litre. The pH is 7.5.

Stock Solution	Final concentration (mM)
Solid NaCl	1.5 M
2 M KCl	10
2 M MgCl ₂	20
1 M CaCl ₂	10
2.4 M MgSO ₄	24
4 M NaNO ₃	5
0.5 M Na ₂ SO ₄	24
100 mM NaH ₂ PO ₄	0.1
1.5 mM FeEDTA	0.0015
Trace elements	1 ml litre ⁻¹
1 M HEPES pH 7.6	20
NaHCO ₃ (solid)	1 g litre ⁻¹

Table S2.3. *Salinibacter ruber* medium. All the volumes of the stock solution are calculated for 1 litre. The final pH is 7.2.

Chemical	g/L
NaCl	195
MgCl ₂ · 6H ₂ O	34.6
MgSO ₄ · 7H ₂ O	49.5
CaCl ₂ · 2H ₂ O	1.25
KCl	5
NaHCO ₃	0.25
NaBr	0.625
Yeast extract	1

Table S2.4. Cell concentrations of microbial suspensions prior to crystallisation. This table is also reported in Georgiev (2020)).

<i>Hbt. noricense</i> A1		<i>Hbt. salinarum</i> NRC-1		<i>Sal. ruber</i> M31		<i>D. salina</i> CCAP 19/18	
NaCl	Sea salt	NaCl	Sea salt	NaCl	Sea salt	NaCl	Sea salt
7.2·10 ⁸	8.1·10 ⁸	5.5·10 ⁸	6.5·10 ⁸	5.2·10 ⁸	5.3·10 ⁸	1.5·10 ⁵	2.2·10 ⁵

Chapter 3: Exposure of entombed halophiles to different doses of UV and ionizing radiation

Abstract

3.1 Introduction

- 3.1.2 Martian salts and radiation
- 3.1.3 The ability of halophiles to withstand high doses of radiation
- 3.1.4 Photoprotection in halophiles
- 3.1.5 Genomic signatures of halophiles offering resistance to radiation
- 3.1.6 Terrestrial life exposed under simulated Martian conditions
- 3.1.7 Aims and objectives

3.2 Methodology

- 3.2.1 Growth of halophiles
- 3.2.2 Exposure to increasing doses of polychromatic UV radiation of cells immersed in liquid
- 3.2.3 Exposure to increasing doses of polychromatic UV radiation of halophiles in lab-made halite
- 3.2.4 Lab-made halite exposure to different types of radiation
- 3.2.5 Comparison between freshly grown cells of *Hbt. salinarum* NRC-1 and starved cells
- 3.2.6 Downstream analysis for lab-made halite samples

3.3 Results

- 3.3.1 Exposure of cells immersed in liquid and entombed in halite on quartz discs
- 3.3.2 Lab-made halite exposure to different types of radiation

3.3.3 Comparison between starved cells and freshly grown cells of *Hbt. salinarum* NRC-1

3.4 Discussion

3.4.1 Exposure of cells immersed in liquid and entombed in halite on quartz discs

3.4.2 Lab-made halite exposure to different types of radiation

3.4.3 Comparison between freshly grown and starved cells of *Hbt. salinarum* NRC-1

3.5 Conclusion

3.6 References

3.7 Supplementary info

Chapter 3: Exposure of entombed halophiles to different doses of UV and ionizing radiation

Abstract

Microbial communities living in salt-saturated environments get trapped inside fluid inclusions of halite when it precipitates. The entombment can be an advantage to avoid the harsh bittern brine that remains after halite precipitation, as well as shielding against intense radiation. The innate ability of Haloarchaea to withstand intense solar radiation and their capacity to become trapped inside halite allow them to tolerate high doses of different forms of radiations. This, coupled with their remarkable longevity, makes them an ideal model to investigate life, or signs of it, on Mars, where salt deposits have been found. Here, the capacity was tested of the haloarchaeal species, *Halobacterium salinarum* NRC-1 and *Halobacterium noricense* A1, and the halophilic bacterial species, *Salinibacter ruber* M13, to recover in liquid medium after doses of polychromatic UV, UV-C and ionizing radiation when in halite crystals. The chlorophyte, *Dunaliella salina* 18/19, was also tested with polychromatic UV, UV-C and ionizing radiation, but did not survive. The two archaeal and one bacterial species survived UV irradiation when in halite crystals, but the lag phase for recovery of *Salinibacter ruber* was significantly longer than haloarchaeal species, with different lag phases. They even survived an ionizing radiation dose of 5 kGy. *Halobacterium salinarum* NRC-1 even survived, in starved conditions, to high doses of polychromatic and UV-C radiation.

3.1 Introduction

Mars has caught the attention of astrobiologists, especially after the discovery of salt deposits buried under the Martian surface and the presence of ice at the poles. Recently, a review on the microbiological potential of lake on Mars reported a description of hundreds of ancient lake basins

detected on Mars that could preserve evidence of biogenesis on Mars (Michalski *et al.*, 2022). In 2004, a study reported the first direct observations of perennial water ice and carbon dioxide in the south polar regions on Mars (Bibring *et al.*, 2004). Head *et al.* (2003) showed evidence that dusty, water-ice-rich deposits exist in both hemispheres, from mid-latitudes to the poles. According to their studies, these deposits accumulated during a geologically recent ice age, occurred between 2.1 and 0.4 million years ago (Myr), as a result of variations in planetary orbit, which is significantly greater on Mars compared to Earth (Touma and Wisdom, 1993; Laskar *et al.*, 2002). The scientific objectives of the rover Curiosity, revolve around exploring and quantitatively assessing a local region on Mars' surface as a potential habitat for life, past or present. The rover continues to climb the surface of the mountain (informally named "Mount Sharp") inside Gale crater (Stern *et al.*, 2015). As the rover moves up the slopes, it has observed that the fine, layered clays are thinning compared to the foot of the mountain, and sand dunes and salt deposits (mainly sulphates) are appearing in their place (Franz *et al.*, 2017; Thomas *et al.*, 2019). These are the typical signs of the prolonged presence of a lake. Towards the top these become rarer, the lake deposits intersperse sand and salt; the remnants of a desiccating basin (Figure 3.1).

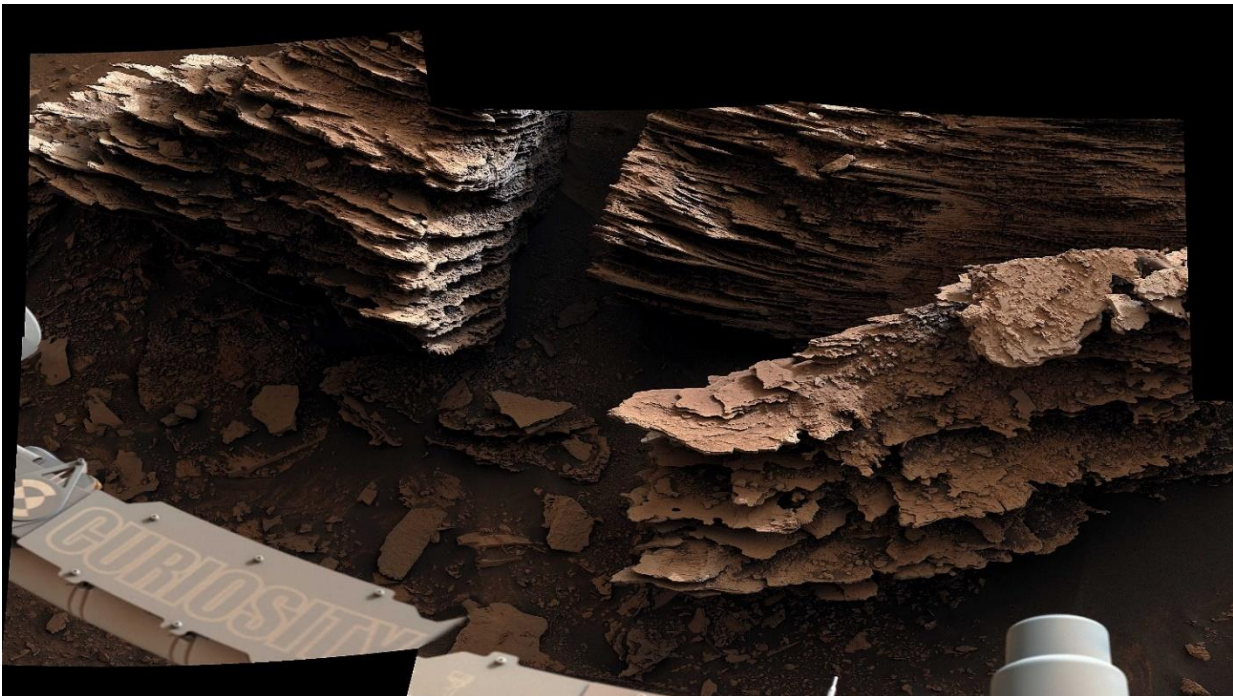


Figure 3.1. Image captured by Curiosity showing layered rocks believed to have formed in an ancient streambed. Credit: NASA/JPL-Caltech/MSSS.

The new rover, Perseverance is investigating the ancient river delta that fills part of the Jezero crater on Mars. The rover has collected pictures showing layers of sediments (Mangold *et al.*, 2021). In this study, Mangold *et al.* (2021), interpreted these strata as evidence of deltas that advanced into a lake, and suggested that the specific deposition in the uppermost fan strata was caused by high-energy flood episodes. These are several lines of evidence that clearly show that Mars was warmer and wetter in the past. It has been suggested that this era ended between 4 and 3.5 billion years ago (Pollack *et al.*, 1987; Carr and Wänke, 1992; Ramirez and Craddock, 2018). The main reason for the desertification of Mars, giving the planet the present-day appearance, is that the electromagnetic field started to weaken. Mars is smaller than planet Earth, about 1/3 the mass of our planet, and as they share similar geological history, the central core of Mars started to cool down quicker. This resulted in much less geologically activity compared to Earth (Clark and Van Hart, 1981; Gooding, 1992; Ojha *et al.*, 2015). Geological activity still exists on Mars, as evidenced by the detection of 174 seismic events in ten months of geophysical observations by Insight (Banerdt *et al.*, 2020). These events included over 10% of seismic events of magnitude $M_w = 3-4$ (Banerdt *et al.*, 2020). The geological activity of a planet is tightly connected to the existence of an electromagnetic field, shielding a planet from intense solar and cosmic radiation. Once weakened, the intense radiation led to the evaporation of the majority of the water once present on Mars (Fang *et al.*, 2010). Lisse *et al.* (2020) proposed an observational strategy to detect Earth-like biosignature and pointed to planets that would have subaerial weathering of rocks, implying that geochemical cycles could occur. Mars is a good candidate to look for signs of past or present life: the liquid water on the surface might have sustained microbial activity when the red planet was geologically active, resembling early Earth conditions (Falkowski *et al.*, 2008).

3.1.2 Martian salts and radiation

The observation of ice water, different salts, brine aquifers and methane (Formisano *et al.*, 2004), and the geological history of the red planet, led to speculations of the possibility of halophilic life on the surface in the past or currently buried in salt deposits or putative brine aquifers. If life was present in the past, and could have evolved adopting a halophilic lifestyle, areas where salts are present on the surface could have the potential to record signs of past (or even present) life. These salts have the ability to absorb water vapor and make liquid water locally and sporadically available on present-day

Mars (Zorzano *et al.*, 2009). The main salts detected on Mars surface include sulphates, chlorides, bromides, carbonates, and nitrates, based upon Viking measurements (Clark and Van Hart, 1981, and references therein). In fact, NaCl has not been detected widely, but has been seen in Mars-derived meteorites (Kounaves *et al.*, 2014) and it is likely to have been missed due to weak spectral signatures (Benison and LaClair, 2003). NaCl is not the only salt present on Mars, among others, there is evidence that perchlorate is also present (Chevrier *et al.*, 2009; Hecht *et al.*, 2009). Perchlorate is known to be highly oxidizing and toxic (depending on the dose), and its presence on Mars gave rise to questions about how putative halophilic life could survive in its presence. To address this, Oren *et al.* (2014) tested members of the family *Halobacteria* and the bacterium *Halomonas elongata* and showed that these halophiles grew well in NaCl-based media containing 0.4 M of perchlorate, and growth was limited by a concentration of 0.6 M of perchlorate, except for *Haloferax mediterranei* that, although significantly affected, was able to grow. Oren *et al.* (2014) demonstrated that the perchlorate could even be used as an alternative electron acceptor for respiratory activity. The lack of a magnetic field and the thin atmosphere of Mars, which is <1% of the Earth (REF), results in a desert-like planet with intense radiation on the surface. On the surface of Mars the daily Galactic Cosmic Rays (GCR) dose rate, measured by Mars Science Laboratory's Radiation Assessment Detector (RAD), was 0.210 mGy/day (Hassler *et al.*, 2014). The unit used to define the absorbed dose of ionizing radiation is gray (Gy) and is defined as the absorption of one joule of radiation energy per kilogram of matter, according to the International System (IS). As a comparison, in humans, gamma radiation at doses of 2 Gy results in varying degrees of acute radiation sickness, and doses of 10 Gy are lethal (Mettler, 2012). Different forms of radiation can damage biomolecules directly (see Section 3.3), and indirectly by forming reactive oxygen species (ROS), *e.g.* through the radiolysis of water producing peroxides, superoxide and hydroxyl radicals (David and Cox, 2017). A number of studies have reported an enhanced protection offered by the salt environment to radiation-resistant halophiles, especially Haloarchaea, which includes the protection offered by the halite as well as the Na⁺ and Cl⁻ ions (Fendrihan *et al.*, 2009; Kish *et al.*, 2009; Webb *et al.*, 2013; Arun *et al.*, 2017).

3.1.3 The ability of halophiles to withstand high doses of radiation

The striking ability of Haloarchaea to survive over geological timescale (see Chapter 1, section 1.5), coupled with their ability to withstand intense UV radiation (see Chapter 1, section 1.2), opens the discussion about where to look for signs of past or present life buried in salt deposits on other celestial

bodies. On Earth, salt and soda lakes, salterns and other brines on the surface are naturally subjected to cycles of desiccation and intense UV radiation, therefore, halophilic microorganisms living there must be equipped with special adaptations enabling them to survive (see Chapter 1, section 1.5).

3.1.4 Photoprotection in halophiles

Haloarchaea have evolved a number of strategies to avoid DNA damage caused by radiation, which can be grouped in two main mechanisms: DNA repair and photoprotection. Photoprotection is a first line defense and includes pigmentation by carotenoids and mechanisms of oxidative damage avoidance as immediate defense. Haloarchaea possess a protein called bacteriorhodopsin, that acts as a light-activated proton pump that generates ATP for the cell (Bickel-Sandkötter, *et al.*, 1996). When light hits the cell, photons get absorbed by the bacteriorhodopsin, which then undergoes conformational changes (David and Cox, 2017). While bacteriorhodopsin allows some Haloarchaea to make use of light energy, pigmentation by carotenoids offers photoprotection. The two major carotenoids present in Haloarchaea are bacterioruberin and β -carotene, both of them able to offer photoprotection as well as fluidity to the membrane subjected to different osmotic conditions (D'Souza *et al.*, 1997; Jones and Baxter, 2017). Menaquinones (MK), have been proposed as an additional photoprotective strategy (Kellermann *et al.*, 2016). The aromatic ring of menaquinone reacts with and destroys the most reactive forms of oxygen radicals (reactive oxygen species, ROS) and other free radicals, protecting unsaturated fatty acids from oxidation and preventing oxidative damage to membrane lipids (David and Cox, 2017). Carotenoids in general are able to expand the spectrum of absorbed light in photosynthetic organism, and thanks to their alternating single and double carbon-carbon bonds, they offer protection from ROS, formed by intense light exceeding the system's capacity to accept electrons (David and Cox, 2017). Menaquinones and carotenoids are highly abundant in Haloarchaea, and are related to the ability of these organisms to withstand oxidative stress damage, generated by high radiation experienced in hypersaline environments (Stan-Lotter and Fendrihan, 2015; Kellermann *et al.*, 2016; Jones and Baxter, 2017). Another characteristic of Haloarchaea that provide photoprotection of proteins and DNA is the high intracellular concentration of ions, that act as scavengers for reactive oxygen species (ROS), generated from the aerobic metabolism in normal cases, but which can also result from irradiation. This was suggested by Kish and colleagues (2009), who found that intracellular halides (chloride and bromide) in *Halobacterium salinarum* NRC-1 scavenge ROS through electron transfer, producing the less

reactive chloride and bromide radicals, and this helps to protect bases in the DNA, as well as the structure of proteins.

A high Mn/Fe ratio has also been proposed as a signature of radioresistant microbes. In fact, it is present in one of the most radio-resistant bacteria *Deinococcus radiodurans* (Daly *et al.*, 2004), and a high Mn/Fe ratio has been also found in *Halobacterium salinarum* (Kish *et al.*, 2009). Proteins containing iron-sulfur groups are susceptible to irradiation, as this can cause the release of ferrous iron (Fe^{2+}) that then gets oxidized by hydrogen peroxide, producing ferric ion (Fe^{3+}) and the hydroxyl radical (HO) and hydroxide ion (OH^-) as byproducts (Kish *et al.*, 2009). The ferric ion can be reduced back to the ferrous iron with the hydrogen peroxide, creating a loop (David and Cox, 2017). Manganese can offer protection to protein by creating Mn-peptide complexes and may also substitute Fe in the Fe-S cluster of enzymes, affecting positively the effect of the oxidative stress (Daly *et al.*, 2007; Kish *et al.*, 2009; Robinson *et al.*, 2011; Webb *et al.*, 2013). The location of Mn and Fe in *Halobacterium salinarum* have not been elucidated and it is not known what is the cycle of Mn in hypersaline environments. Kish *et al.* (2009) suggested that it is a combination of metabolic regulatory adjustment and the accumulation of Mn-antioxidant complexes to explain the increased tolerance to radiation in *Halobacterium salinarum*.

3.1.5 Genomic signatures of halophiles offering resistance to radiation

Other adaptations to radiation damage are intrinsic in the DNA and are referred to as genomic signatures, making the DNA less susceptible to photodamage. One of the main forms of UV-induced DNA damage is the condensation of two ethylene groups to form a cyclobutane ring, referred to as cyclobutane pyrimidine dimers (CPDs). This happens most frequently between adjacent thymidine residues on the same DNA strand. Bipyrimidine photoreactivity is in descending order of: (5' to 3') TC > TT > CT > CC. Jones and Baxter (2016) proposed that a reduction in number of the most photoreactive sequences should reduce overall genomic photoreactivity, and found that there is a strong negative correlation between the genomic photoreactivity (P_g) and G+C content. Ionizing radiation (x-rays and γ -rays) can cause ring opening and fragmentation of bases as well as breaks in the covalent backbone of nucleic acids. DNA repair instead, consists in photoreactivation, nucleotide excision repair, base excision repair and homologous recombination (reviewed in Jones and Baxter 2017). Polyploidy, where the cell has multiple copies of a presumably identical chromosome, is a

typical feature of Haloarchaea and provides a copy so that any damaged chromosome can be faithfully repaired through homologous recombination (Soppa *et al.*, 2014). Additional copies of chromosomes can also serve as a storage for phosphate, especially in extreme conditions (Soppa, 2014; Zerulla and Soppa, 2014). Enzymes provide another line of defense by deactivating of ROS, like the superoxide dismutase and the catalase.

3.1.6 Terrestrial life exposed under simulated Martian conditions

There have been many studies reporting the ability of Haloarchaea to withstand intense radiation as recently summarised by Wu *et al.* (2022). Table 3.1 highlights a subset of these studies, largely focussing on *Halobacterium salinarum*. Baliga *et al.* (2004) analysed the stress response to UV radiation in *Halobacterium salinarum* NRC-1 and found that there were 2400 mRNA changes during the recovery. They also found a UV-induced down-regulation of many metabolic functions during the recovery, which has been observed in all three domains of life. According to their results, the recovery after a dose of 200 J/m² was 16-fold higher in light conditions, indicating that photoreactivation is a preferred pathway for UV lesion repair (Baliga *et al.*, 2004). McCready *et al.* (2005) found that homologous recombination plays an important role in the repair of UV-induced damages in *Halobacterium salinarum* NRC-1, and that proteins involved in DNA metabolism were significantly induced after the irradiation. Fendrihan *et al.* (2009) calculated the potential survival of *Halococcus dombrowskii* in halite is at least 3000 kJ/m² and that the protection afforded by the halite resulted in survival two orders of magnitude higher compared to when in liquid. The same study reported similar values for *Halobacterium salinarum* NRC-1 and *Haloarcula japonica*, used as a comparison with other Haloarchaea. Karan *et al.* (2014) used RAD mutants of the strain NRC-1 to investigate the genetic basis of the RAD phenotype, displaying higher transcription levels of the *rfa3* operon, coding for three genes involved in the increased radiation resistance of the RAD phenotype, and found that these mutants are more resistant by order of magnitude than the strain NRC-1; both species survived an irradiation dose of 3 kGy. Leuko *et al.* (2015) tested three Haloarchaea and found that *Halococcus hamelinensis* accumulates compatible solutes such as trehalose that improved survivability following exposure, while cells of *Halococcus morrhuae* form cell clusters improving resistance to radiation. Overall, their results indicate that the survival of these two species, and *Halobacterium salinarum* NRC-1, is significantly increased when in halite compared to liquid medium. Leuko and Rettberg (2017), based on the measurements provided by Hassler *et al.* (2014),

calculated that on Mars it would take 65,231 years to accumulate 5 kGy of ionizing radiation dose, a dose that *Halobacterium salinarum* NRC-1, *Halococcus hamelinensis* and *Halococcus morrhuae* were able to survive.

Halite is an interesting mineral in terms of colour modifications. It can be naturally transparent, but can turn blue or brown when exposed to ionizing radiation, as a result of stress and a modification in the crystal lattice (Arun *et al.*, 2017). This characteristic of halite makes it a good model to be used for the radiation monitoring. The protection offered by halite, together with the natural ability of Haloarchaea to survive the process of entombment and withstand intense irradiation (Table 3.1), open to the possibility of looking for traces of past or present life entrapped in halite on other celestial bodies in the Solar System. To the best of my knowledge, *Salinibacter ruber* and *Dunaliella salina*, which are halophiles from the bacterial and eukaryote domains of life respectively, and are common in hypersaline environments, have not been tested before for survival under intense radiation.

Table 3.1. Selected studies where the ability of Haloarchaea to withstand radiation was tested. Time of irradiation varies according to the instrument used. Time of irradiation in this table is assumed to be continuous until the aimed radiation dose was reached, as reported in most of the cited papers. The mutants (IR⁺) and (RAD) are strains of *Halobacterium salinarum* with enhanced radiation resistance.

Organism	Radiation	Dose (time of irradiation)	Condition	Response	Author
<i>Hbt. salinarum</i> NRC-1	UV-C	110-280 J/m ²	In liquid	No loss of viability up to 110 J/m ² and 37% survival at 280 J/m ²	Baliga <i>et al.</i> (2004)
<i>Hbt. salinarum</i> NRC-1	UV-C	30-70 J/m ²	In liquid growth medium	Resulting DNA damage largely repaired within 3 hours in the dark	McCready <i>et al.</i> (2005)
<i>Hcc. hamelinensis</i>	UV-C	up to 500 J/m ²	In liquid	Able to survive. The photolyase <i>phr2</i> 20-fold higher in light conditions	Leuko <i>et al.</i> (2011)
<i>Hcc. dombrowskii</i>	UV-C	148 kJ/m ²	In halite	75% survival	Fendrihan <i>et al.</i> (2009)
<i>Hcc. dombrowskii</i>	UV-C	0.41 kJ/m ²	In liquid	No loss up to this dose	Fendrihan <i>et al.</i> (2009)
<i>Hbt. salinarum</i> (IR ⁺)*	⁶⁰ Co gamma source	up to 23 kGy	In liquid growth medium	0.0035-0.1% survival	Webb <i>et al.</i> (2013)
<i>Hbt. salinarum</i> NRC-1	⁶⁰ Co gamma source	0, 2.5, 5 or 7.5 kGy	In liquid	Modified DNA bases were repaired in 2 h post irradiation	Kish <i>et al.</i> (2009)
<i>Hbt. salinarum</i> NRC-1, <i>Hbt. salinarum</i> (RAD)*	X-ray	3 kGy	In liquid	The mutant showed a survival one order of magnitude higher than NRC1. All species survived	Karan <i>et al.</i> (2014)
<i>Hbt. salinarum</i> NRC-1, <i>Hcc. morrhuae</i> , <i>Hcc. hamelinensis</i>	UV	87.446 W/m ²	In liquid, in halite	Significantly higher survival in halite	Leuko <i>et al.</i> (2015)
<i>Hbt. salinarum</i> NRC-1	UV-B, UV-C	UV-B at doses equivalent to 30 J/m ² and 5 J/m ² of UVC	In liquid growth medium	Four genes were up-regulated	Boubriak <i>et al.</i> (2008)
<i>Hbt. salinarum</i> NRC 34001, <i>Hbt. salinarum</i> R-1, <i>Hfx. volcanii</i>	UV-C	50, 150 J/m ²	In liquid	Found photoproducts repaired in dark and light conditions	McCready <i>et al.</i> (1996)
<i>Hbt. salinarum</i> NRC-1, <i>Hcc. hamelinensis</i> , <i>Hcc. morrhuae</i>	⁶⁰ Co gamma source, X-ray	Gamma radiation dose of 6 kGy	In liquid	<i>Hcc. morrhuae</i> and <i>Hcc. hamelinensis</i> able to recover with growth delayed. <i>Hbt. salinarum</i> unable to recover	Leuko and Rettberg (2017)
<i>Hbt. salinarum</i>	⁶⁰ Co gamma source, UV	Gamma radiation dose of 3 kGy	In liquid	Survival. Bacterioruberin involved in scavenging of ROS	Shahmohammadi <i>et al.</i> (1997)
<i>Hbt. salinarum</i>	⁶⁰ Co gamma source, UV-C	Gamma radiation dose of 3 kGy	In liquid	Deficiency in Bacterioruberin corresponds to higher sensitivity to radiation damages	Shahmohammadi <i>et al.</i> (1998)
<i>Hbt. salinarum</i> NRC-1	⁶⁰ Co gamma source	0.5-5 kGy	Desiccated	DNA breaks were repaired within several hours of incubation under optimal conditions	Kottemann <i>et al.</i> (2005)

3.1.7 Aims and objectives

The aim of this chapter is to understand the extent to which halophiles tolerate different forms of radiation, and thus give insights into their potential to survive in different locations on Earth and on Mars, whether they were/are part of a habitable Mars or may be inadvertently transported there. Specifically, the aim is to test resistance to a range of doses of UV-C, polychromatic UV and ionizing radiation on halophilic species. The specific objectives of this study are:

- 1) Compare the survival of the halophilic species (haloarchaeal species *Halobacterium salinarum* NRC-1, *Halobacterium noricense* A1, the halophilic bacterium *Salinibacter ruber* M13 and the halotolerant green microalgae *Dunaliella salina* 18/19) when dissolved in liquid brines to their survival when entombed in laboratory-made halite, after the exposure to increasing doses of polychromatic UV, UV-C, and ionizing radiation,
- 2) Compare the tolerance to UV and ionizing radiation of the individual species in halite compared to mixture of species,
- 3) Test the response of starved cells versus freshly grown cells of *Halobacterium salinarum* NRC-1 to increasing doses of polychromatic UV, UV-C and ionizing radiation.

3.2 Methodology

3.2.1 Growth of halophiles

The strains tested in this experiment were *Halobacterium noricense* A1, *Halobacterium salinarum* NRC-1 and *Salinibacter ruber* M13 (see Chapter 2 for details of their source). *Halobacterium* spp. were grown in 50 ml Falcon tubes in 15 ml of Payne 20% NaCl, on a shaker (100 rpm) at 30°C in dark, and *S. ruber* and *D. salina* which were grown in their own media (see Chapter 2, Methodology, for details of media), until the late exponential phase was reached (OD₆₀₀ of 0.6 – 0.7).

3.2.2 Exposure to increasing doses of polychromatic UV radiation of cells immersed in liquid

The halophiles tested were *Halobacterium salinarum* NRC-1, *Halobacterium noricense* A1, and *Salinibacter ruber* M13 individually, and NRC-1 together with M13 (Figure 3.2 A). When the late-exponential phase was reached, 1 ml of liquid culture, from the three replicates, was collected and diluted in 9 ml phosphate-buffered saline (PBS) 20% NaCl. The resulting volume was equally divided into quartz cuvettes (0.5 cm Hellma GmbH & Co. KG, Muelheim, Germany) at 1.5 ml capacity. Each quartz cuvette had a small magnet that, once placed on a magnetic stirrer, guaranteed homogeneous distribution and thus irradiation of the cell suspension. The magnetic stirrer was placed at a distance of 86.6 cm from the source and exposed to polychromatic UV light (200 – 400 nm) (Figure 3.3). Every 1.08 min, 200 μ l from each replicate was collected with a sterile syringe four times, representing different doses of radiation, respectively, 3, 6, 9 and 12 kJ/m². Subsequently, 30 μ l was diluted in 270 μ l of PBS 20% NaCl, and the serial dilution was continued down to 10⁻⁵, in triplicates. In order to count colony forming units (CFUs), 25 μ l was plated onto solid media specific to each halophile, and after incubation at 30°C colonies were counted in order to define the survival in accordance with the radiation dose, as previously published (Beblo-Vranesevic *et al.*, 2017). Samples with co-culture of NRC-1 and M13 were plated both on *Salinibacter* medium and 20% NaCl Payne medium, in triplicates, for both species. No-radiation controls (biological replicates) were prepared following the same procedure, but instead of being exposed to radiation, they were kept at room temperature.

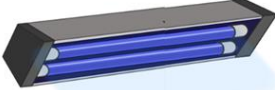
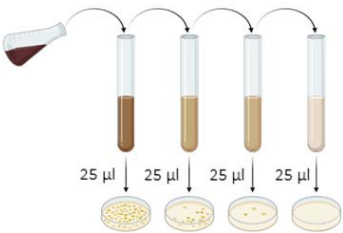
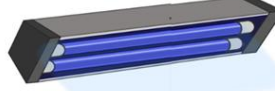
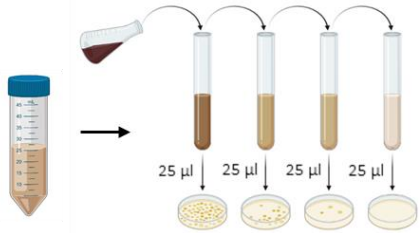
Experiment	Medium	Polychromatic UV rad. (kJ/m ²)	Downstream analysis
A		 3, 6, 9, 12	
A1			
NRC-1			
M13			
NRC-1 : M13			
B		 2.5, 5, 10, 15	
A1			
NRC-1			
M13			
NRC-1 : M13			

Figure 3.2. Schematic view of the steps of the experiment where halophiles were exposed to increasing doses of polychromatic UV radiation, in liquid (A) or laboratory-made halite (B).

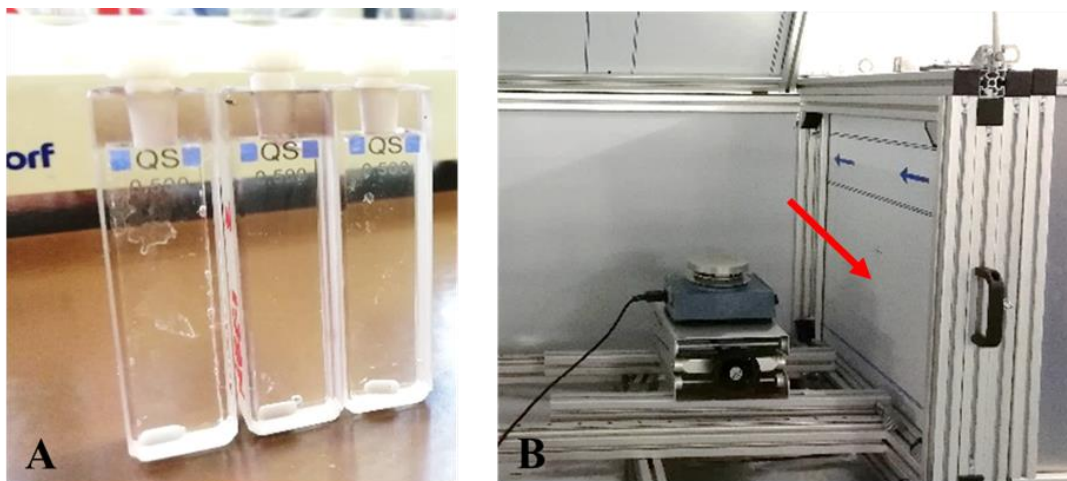


Figure 3.3. (A) Quartz cuvettes used for the exposure to polychromatic UV light, containing cells resuspended in PBS 20% NaCl and a small magnet. (B) Magnetic stirrer placed in front of the source of radiation (indicated by the red arrow). The base was adjustable in order to have the defined dose of radiation. Once the quartz cuvette was placed on the magnetic stirrer, the protection panel on the top was closed and the protection panel on the right was removed to allow the irradiation.

3.2.3 Exposure to increasing doses of polychromatic UV radiation of halophiles in lab-made halite

The strains tested were the haloarchaea *Halobacterium noricense* A1, *Halobacterium salinarum* NRC-1 and the bacterium *Salinibacter ruber* M13 (Figure 3.2 B). After the late exponential phase was reached, 2 ml of liquid culture was collected and centrifuged 15 minutes at 8500 g and washed twice in 1.5 ml of salt solution (Table 3.2).

Table 3.2. Salt solution formulation to mimic the concentrated brines where halophiles are found (Dyall-Smith, 2009).

Salt	Concentration (g/L)
NaCl	240
MgSO ₄ ·7H ₂ O	35
MgCl ₂ ·6H ₂ O	30
KCl	7

Cell pellets were collected, and 1.5 ml of salt solution was added. In order to know how many cells were alive prior to entombment, a serial dilution was done to 10^{-5} , and 25 μl was plated onto solid media specific to each halophile, and colonies were counted. In the case of the co-entombment of strains NRC-1 and M13, 1 ml from each culture was collected and the pellet washed twice in 0.5 ml of salt solution. After the second wash, cells were pelleted, resuspended and mixed together in salt solution to a final volume of 2 ml. Negative controls were prepared following the same procedure and instead of being exposed to radiation, these were kept on an unused bench, at room temperature. For the initial serial dilution, in the case of co-entombment of *Halobacterium salinarum* NRC-1 and *Salinibacter ruber* M13, the same volume was plated both on plates with 20% NaCl Payne medium for growth of the archaeon, and *Salinibacter* solid media for the growth of the bacterium. Subsequently, 250 μl was poured on a quartz disc of 11 mm diameter (Aachener Quarzglas Technologie, Aachen, Germany) and left to dry so that they became entombed in halite (Figure 3.4). For each strain, 15 quartz discs were prepared in order to have triplicates to test under 4 different radiation doses, respectively 2.5, 5, 10, 15 kJ/m^2 . Two months after the exposure to polychromatic UV light (200 – 400 nm), crystals were dissolved in salt solution (Table 3.2), and a ten-fold serial dilution for each sample up to 10^{-5} was performed. Subsequently, 25 μl was plated, and colonies counted.

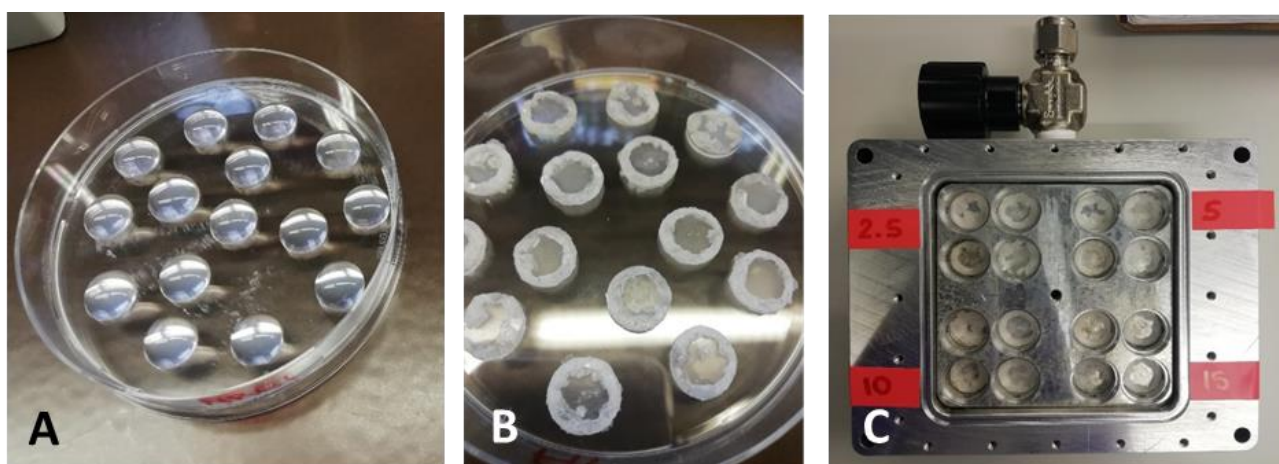
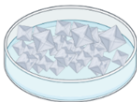


Figure 3.4. Illustration of the experiment B using quartz discs. (A) 250 μl of cell suspension was poured onto quartz glass discs. (B). discs were left to dry until the halite crystals formed (C) The halite crystals precipitated on quartz glass discs were positioned in the Trex-box (Beblo-Vranesevic *et al.*, 2017) and then exposed to the polychromatic UV radiation.

3.2.4 Lab-made halite exposure to different types of radiation

In a first attempt to test the limit of radiation damage halophilic microorganisms can handle when entombed in halite, salt crystals previously prepared (as described in Chapter 2), were exposed to three different types of radiations, respectively polychromatic UV (200 – 400 nm), UV-C (254 nm) and ionizing radiation. The conditions used for the polychromatic UV light were as described in section 3.2.2. UV-C exposure was performed with a low-pressure mercury lamp (Model NN 8/15 Heraeus, Berlin, Germany) with a major emission line at 254 nm (fluence rate 1.80 W/m²). The fluence was controlled by a regularly calibrated UVX radiometer with an UV sensor (UV-25) for 254 nm (both UVP Ultra-Violet Products, Cambridge, UK). The output of the lamp was determined by UVX radiometer measurements before and after each exposure experiment. Exposure to ionizing radiation was performed with using an X-ray source Müller Typ MG 150 (MCN 165, Philipps, Hamburg, Germany) and exposed to X-ray (150 kV, 16 mA) at a dose rate of 200 Gy/min using the X-ray source. In this first attempt, halophiles tested were *Hbt. salinarum* NRC-1, *Hbt. noricense* A1, *S. ruber* M13, and co-entombments of respectively, *Hbt. salinarum* NRC-1 with *S. ruber* M13, *Hbt. salinarum*. NRC-1 and *D. salina* 18/19, and lastly, *Hbt. salinarum* NRC-1 with both *S. ruber* M13 and *D. salina* 18/19. The chosen doses were 5 kGy for the ionizing radiation, 20 kJ/m² for the polychromatic UV radiation and 5 kJ/m² for the UV-C radiation (Figure 3.5 C).

Following the results of the first experiment, the experiment was repeated, increasing the doses of radiation, and focusing on the response of *Hbt. salinarum* NRC-1 and *S. ruber* M13 (Figure 3.5 D). Cells of *Hbt. salinarum* NRC-1 were tested both as freshly grown and as >100 days starved cells (see next section for more details). The radiation sources and the respective doses were respectively polychromatic UV radiation (40 kJ/m²), UV-C radiation (10 kJ/m²) and ionizing radiation (10 kGy).

Experiment	Medium	Source of radiation and dose	Downstream analysis
C		Polychromatic UV (200 – 400 nm), 20 kJ/m ²	
A1			
NRC-1			
NRC-1 : 18/19		UV-C (254 nm), 5 kJ/m ²	
M13			
NRC-1 : M13		Ionising (X-ray), 5 kGy	
M13 : 18/19			
NRC-1 : M13 : 18/19			

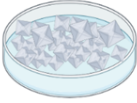
Experiment	Medium	Source of radiation and dose	Downstream analysis
D		Polychromatic UV (200 – 400 nm), 40 kJ/m ²	
NRC-1			
NRC-1 (starved)		UV-C (254 nm), 10 kJ/m ²	
M13			
		Ionising (X-ray), 10 kGy	

Figure 3.5. Schematic view of the steps of the experiment where halophiles were exposed to different types of radiation. In the second part of the experiment (D), radiation doses were increased, and species tested were *Hbt. salinarum* NRC-1 and *S. ruber* M13, additionally, samples of NRC-1 in starving conditions for >100 days were also included to compare the recovery rate after the exposure with freshly grown cells.

3.2.5 Comparison between freshly grown cells of *Hbt. salinarum* NRC-1 and starved cells

In order to investigate different responses in survival between freshly grown cells and starved cells, cells of *Halobacterium salinarum* NRC-1, kept resuspended in salt solution in sealed glass tubes (simulated fluid inclusions) with no nutrients for >100 days, were entombed in lab-made halite and exposed to high doses of radiation. In order to have quantitative data about the survival of *Halobacterium salinarum* NRC-1, and the comparison between freshly grown cells and starved cells,

lab-made halite (with entombed halophiles) was exposed to increasing doses of polychromatic UV light, respectively, 10, 20, 30, 40, 50 kJ/m² (Figure 3.6). Negative controls were prepared following the same procedure and were kept at room temperature.

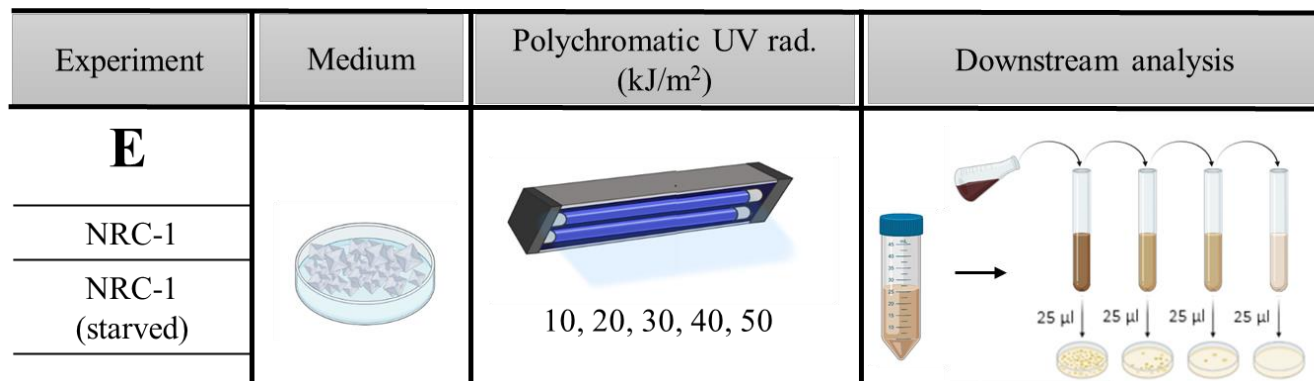


Figure 3.6. Schematic view of the steps of the experiment where NRC-1 in different conditions was exposed to increasing doses of polychromatic UV radiation.

3.2.6 Downstream analysis for lab-made halite samples

The samples were kept in the dark at room temperature, and two months after the exposure, 0.35 g of salt crystals were aseptically placed into 15 ml of liquid culture, specific for each strain, into 50 ml falcon tubes, then placed on a shaker (100 rpm) and left at room temperature until complete dissolution. For the experiments A and B, a serial dilution was carried out from 10⁻¹ to 10⁻⁵, and 5 µl were plated on solid media, specific for each strain. Both the liquid media and the solid media were incubated in the dark at 30°C for a maximum of four months for CFUs counting. In order to study the survival of the tested strains to high radiation doses, the days between the dissolution of the crystals in liquid medium and the first sign of growth have been used to assess the time the species required to recover.

3.3 Results

3.3.1 Exposure of cells immersed in liquid and entombed in halite on quartz discs

The samples used in the experiment A and B (Figure 3.4) revealed contamination in the downstream analysis, which was subsequently identified as a strain with 100% 16S rRNA identity to the type of strain of *Natrinema pallidum*, a haloarchaea from the order *Halobacteriales*. This contamination was likely present already in the starter cultures, as it was detected also in the samples that served to count initial CFUs, immediately before the exposure. However, due to the time required for growth, the contamination was not detected before two weeks. Due to the contamination, it was not possible to assess quantitatively CFUs, however, due to a distinct colony morphology, it was possible to qualitatively distinguish between the two haloarchaea (Figure 3.7). *D. salina* showed no growth in the experiments conducted in this chapter.

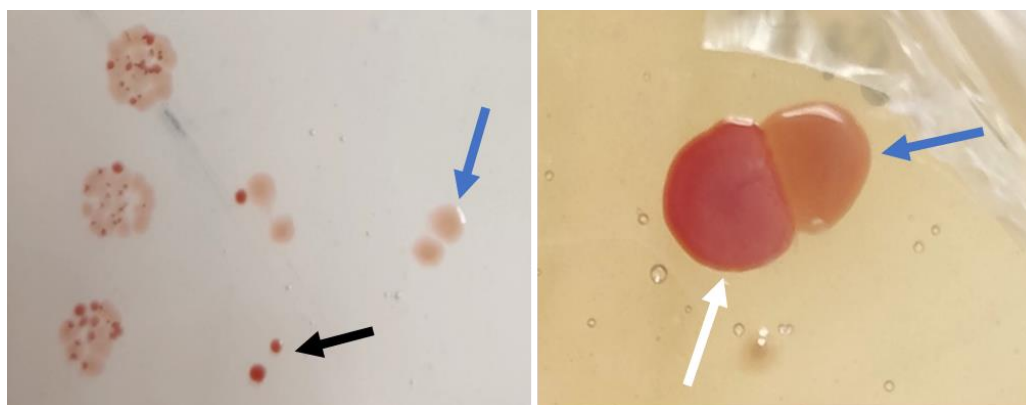


Figure 3.7. (Left) Colonies of *Salinibacter ruber* M13 (black arrow) and *Natrinema pallidum* (blue arrow) growing on *Salinibacter* solid medium. (Right) Colonies of *Halobacterium salinarum* NRC-1 (white arrow) and *Natrinema pallidum* (blue arrow) growing on Payne 20% NaCl solid media.

The clear morphological difference allowed the identification of cells on agar plates, and although it was not possible to quantify the survival, the strains tested, namely *Hbt. salinarum* NRC-1, *Hbt. noricense* A1 and *S. ruber* M13 all survived the maximum doses tested: 12 kJ/m² when in liquid media, and 15 kJ/m² when in halite. *Natrinema pallidum* was also found growing, after the exposure to radiation, hence, this Haloarchaea is also able to survive high doses of radiation.

3.3.2 Lab-made halite exposure to different types of radiation

Due mainly to shipment timings, samples in the experiment C (Figure 3.5) were kept in dark conditions at room temperature for two months before the downstream analysis. Additionally, also in the case of the experiment C, a contamination by *Natrinema pallidum* was found; for this reason, CFUs are not included. The results discussed here, *i.e.*, the time required for growth in liquid culture (expressed in days) refer to the respective discussed strain as colonies from the correspondent agar plate were visible (Figure S3.1 and S3.2) and the identity confirmed by 16S rRNA gene sequence. The recovery time (days needed to show first signs of growth) was different among species. *Halobacterium* spp. (both NRC-1 and A1) when entombed in halite, were not affected by UV radiation, and showed first signs of growth contemporaneously to the negative controls (6 days). These two species were also able to tolerate 5 kGy, showing first signs of growth after eight days (Figure 3.8). *Salinibacter ruber*, although clearly affected as only one replicate showed growth, was able to tolerate high doses of both UV radiation and ionizing radiation (Figure 3.9).

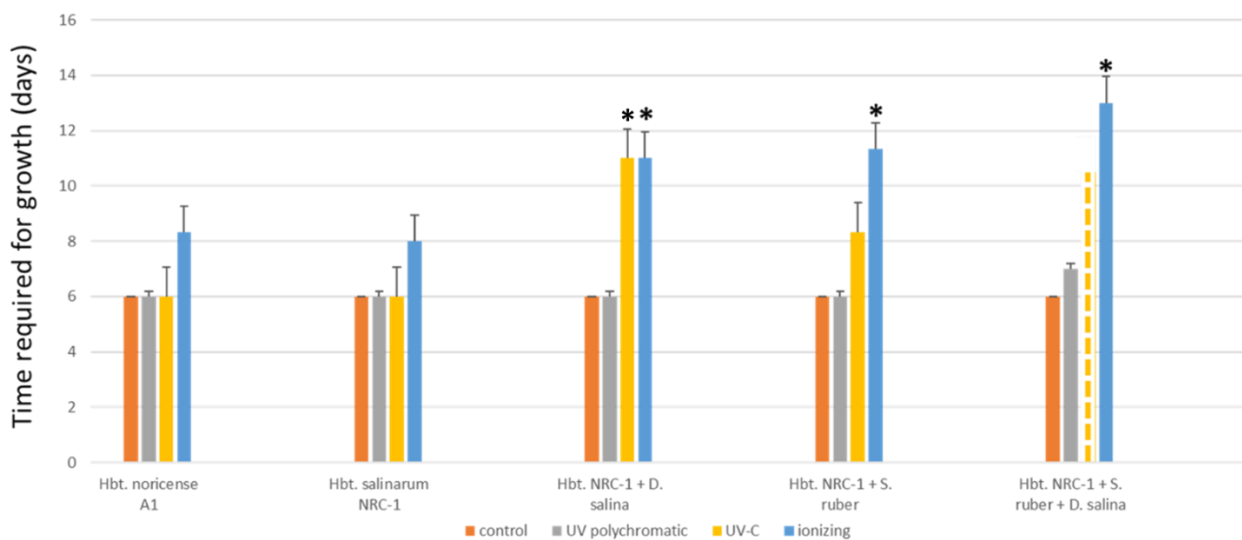


Figure 3.8. Overview of the survival of *Halobacterium* species after exposure to high doses (Polychromatic UV: 20 kJ/m², UV-C: 5 kJ/m², ionizing: 5 kGy) of different radiation sources, polychromatic UV (in grey), UV-C (in yellow) and ionizing (in blue), compared with the no-radiation control (in orange). The mean value of three replicates with standard error is shown. Dotted line indicates that only one out of three replicates grew for the specific treatment. * Indicates a significant difference between the value for the test versus the non-radiated control for the specific treatment (T-test; $p < 0.05$).

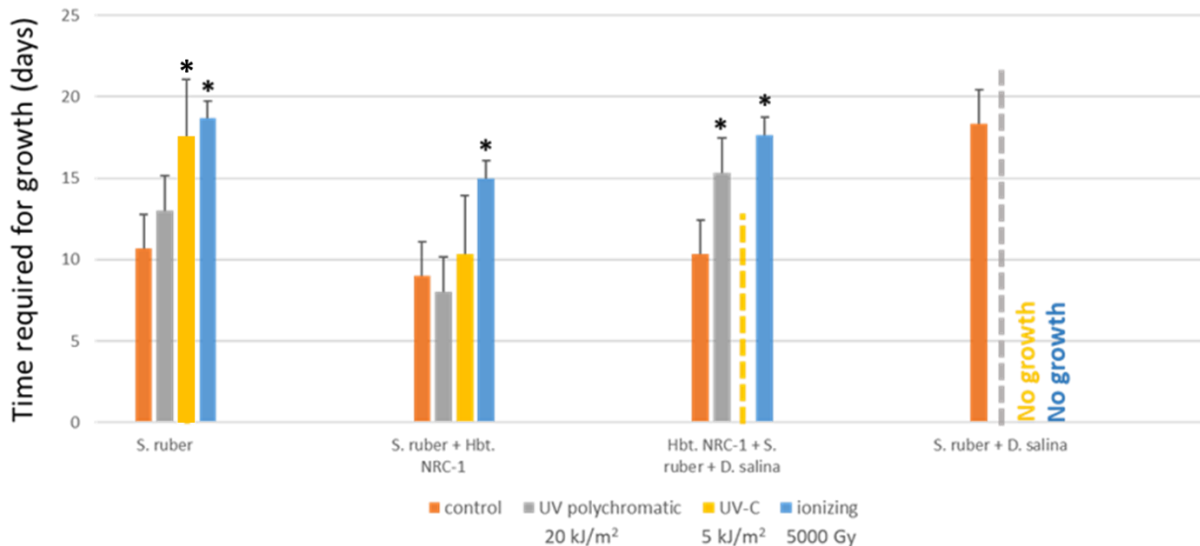


Figure 3.9. Overview of the survival of *Salinibacter ruber* M13 after exposure to high doses (Polychromatic UV: 20 kJ/m², UV-C: 5 kJ/m², ionizing: 5 kGy) of different radiation sources, polychromatic UV (in grey), UV-C (in yellow) and ionizing (in blue), compared with the no-radiation control (in orange). The mean value of three replicates with standard error is shown. Dotted line indicates that only one out of three replicates grew for the specific treatment. * Indicates a significant difference between the value for the test versus the non-radiated control for the specific treatment (T-test; $p < 0.05$).

3.3.3 Comparison between starved cells and freshly grown cells of *Hbt. salinarum* NRC-1

Samples in the experiment D and E (Figure 3.5 and 3.6) were kept in dark conditions at room temperature for ten days before the downstream analysis. The results in Figure 3.10 show that *Halobacterium salinarum* NRC-1 was not able to recover after the exposure to 10 kGy of ionizing radiation in halite (not included in the graph), but it was able to recover after the exposure to intense radiation, respectively polychromatic UV (40 kJ/m²), UV-C radiation (10 kJ/m²) with different responses (Figure 3.10). In particular, the starved cells grew faster than freshly grown cells (p -value 0.016; T-test) in samples not exposed to radiation (no-radiation control). On the contrary, freshly grown cells showed growth faster than starved cells, when exposed to polychromatic UV (p -value 0.013; T-test) and to UV-C (p -value 0.047; T-test) (Figure 3.10).

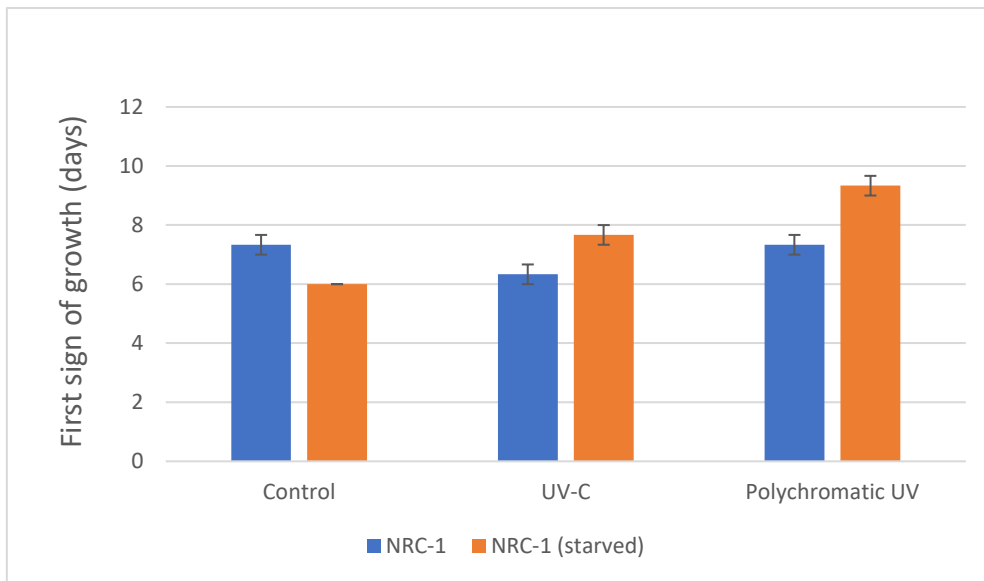


Figure 3.10. Overview of the survival of *Halobacterium salinarum* NRC-1 after exposure to high doses of different radiation sources, polychromatic UV (40 kJ/m²), UV-C (10 kJ/m²) and ionizing (10 kGy), compared with the no-radiation control. The mean value of three replicates with standard error is shown. The comparisons between freshly grown versus starved cells, in each treatment, have all statistical significance (T-test; $p < 0.05$).

In the case of the increasing doses of polychromatic UV radiation (Figure 3.11), *Halobacterium salinarum* NRC-1 was able to recover even after 50 kJ/m². In this case, the starved cells had the tendency to recover faster than the freshly grown cells, although this difference is not statistically significant. It is interesting to note that starvation, compared to freshly grown cells, resulted in better survival at 50 kJ/m², although not statistically significant (Figure 3.11). The results shown in Figure 3.11 show that starvation had no effect on tolerance over 10 and 20 kJ/m², while at 30 and 40 kJ/m² starvation had a positive effect. In the no-radiation controls, starved cells showed signs of growth significantly faster than the freshly grown ones (Figure 3.11).

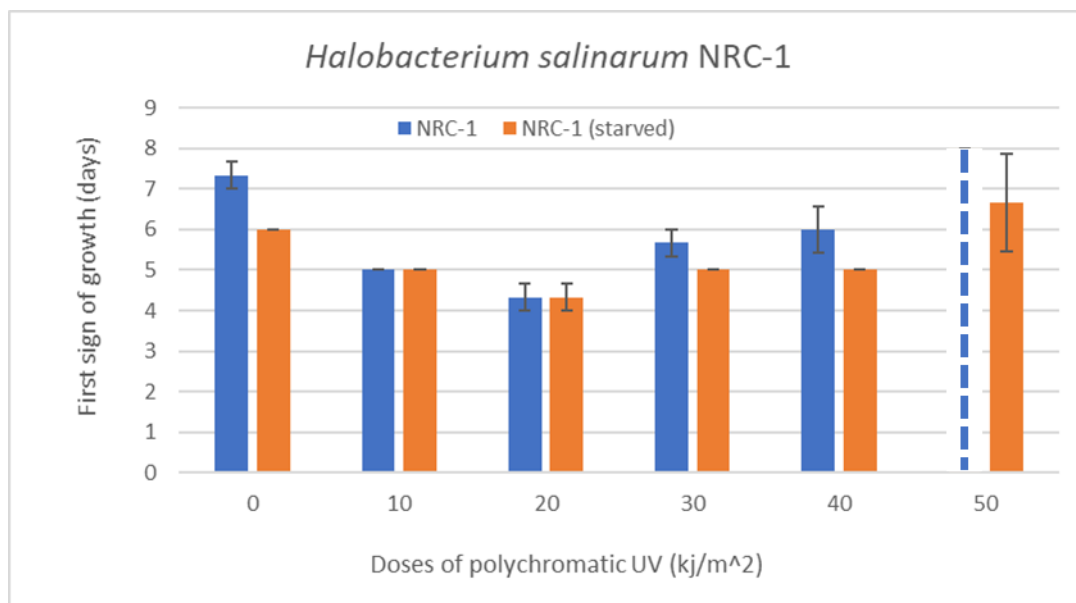


Figure 3.11. Overview of the survival of *Halobacterium salinarum* NRC-1 after exposure to increasing doses of polychromatic UV radiation. The mean value of three replicates with standard error is shown. Dotted line indicates that only one out of three replicates grew. * Indicates a significant difference between the value for the test versus the control (T-test; $p < 0.05$).

3.4 Discussion

3.4.1 Exposure of cells immersed in liquid and entombed in halite on quartz discs

In the experiment A and B, the results show that *Hbt.* spp., *S. ruber* M13 and *N. pallidum* are able to survive both entombed in halite crystals and in liquid medium (summarized in Figure 3.12). It was known from the literature that *Halobacterium* spp. were able to survive high doses of radiation (see Table 1), and, to the best of my knowledge, it is the first time that the survival of *Natrinema pallidum* and *Salinibacter ruber* M13 after the exposure to polychromatic UV radiation is reported. Due to the contamination and technical limitations, it was not possible to assess quantitatively the survival of the strains to the increasing doses of radiation, both in halite and in liquid. However, cells of all the tested strains were detected on the solid media by sequence identity (following the methods described in Section 4.3.6).

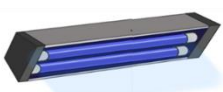
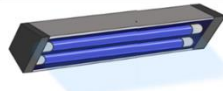
Sample	Medium	Polychromatic UV rad. (kJ/m ²)	Key results
A		 3, 6, 9, 12	- Contamination by <i>Natrinema pallidum</i>
A1			- All species survived
NRC-1			
M13			
NRC-1 : M13			
B		 2.5, 5, 10, 15	- Contamination by <i>Natrinema pallidum</i>
A1			- All species survived
NRC-1			
M13			
NRC-1 : M13			

Figure 3.12. Overview of the results of the experiment A and B.

3.4.2 Lab-made halite exposure to different types of radiation

In the experiment C, the results show that in the case of different types of radiation (polychromatic UV 20 kJ/m², UV-C 5 kJ/m² and ionizing radiation 5 kGy), the same species also survived, with different recovery time. *Dunaliella salina* did not survive. NRC-1 together with co-entombed species did worse than in the single entombment. One reason for that might be the cell abundance is half as abundant as in the single entombment. One of the hypotheses in this chapter was that the co-entombment could have a positive effect, by shielding cells during the exposure to radiation. Based on the results in the experiment C (summarized in Figure 3.13), the contrary is suggested: co-entombment has a negative effect, by significantly affect the recovery of all the tested strains. This might be related not to the co-entombment *per se*, but to the fact that in the co-entombment the cell concentration is half the abundance of the single entombment (one third in the multiple co-entombment). Ionizing radiation has negatively influenced the recovery of *Hbt.* species, however, in the comparison between the multiple co-entombment and single entombment of *Hbt. salinarum* NRC-1, the multiple co-entombment is a disadvantage, as there will be less chance of more resistant phenotypes.

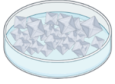
Sample	Medium	Source of radiation and dose	Results	
C		Polychromatic UV (200 – 400 nm), 20 kJ/m ²	- Contamination by <i>Natrinema pallidum</i>	
A1			- All <i>Hbt.</i> species survived all treatments	
NRC-1		UV-C (254 nm), 5 kJ/m ²	- Co-entombment had a negative effect	
NRC-1 : 18/19			Ionising (X-ray), 5 kGy	- <i>S. ruber</i> survived all treatments, although affected
M13				
NRC-1 : M13				
M13 : 18/19				
NRC-1 : M13 : 18/19				

Figure 3.13. Overview of the key results in the experiment C.

3.4.3 Comparison between freshly grown and starved cells of *Hbt. salinarum* NRC-1

In the experiment D and E, the results show that radiation had no significant effect on exposed cells (compared to the non-irradiated control), but high doses of UV-C (10 kJ/m²) and polychromatic UV (40-50 kJ/m²) did increase the time to start growing for starved cells significantly (p-value < 0.05; T-test). It has been reported in the literature that in the domain of Bacteria, starvation cross-protects against radiation (Mendonca *et al.*, 2004; Hong *et al.*, 2014), which seems the trend of *Hbt. salinarum* NRC-1 in starvation showed in the experiment E, however, this difference was not statistically significant. A different result came from the exposure of freshly grown and starved cells exposed to intense polychromatic UV, UV-C and ionizing, where freshly grown cells recovered significantly faster than starved cells. One explanation for this different response might be that increasing doses of polychromatic UV stimulates mechanisms involved in the protection from radiation. It should be considered that, as showed in Chapter 5, starved cells of *Halobacterium salinarum* NRC-1 initially decrease in cell abundance, hence, starvation, and then entombment, have concomitant effects on the survival of the cells. These cells, subsequently subjected to intense radiation (experiment D), are more affected than freshly grown cells. In the experiment E, instead, starved cells recovered faster than freshly grown. There might be protection mechanisms involved in the starvation that could help also in the protection from radiation at intermediate doses. Towards higher doses (40-50 kJ/m²) the cells (both starved and freshly grown) started to be affected.

3.5 Conclusions

The specific objectives of this study are: 1) Comparing the survival of the halophilic species when dissolved in liquid brines, to the survival when entombed in laboratory-made halite, after the exposure to increasing doses of UV radiation, 2) Comparing the survival of the individual species to high doses of UV and ionizing radiation to the survival when they are together, putatively offering mutual shielding effect (as in the case of *Hcc. morrhuae* where clusters of cells offer additive protection (Leuko *et al.*, 2015)), 3) Test the ability of these species to recover without relying on the presence of nutrients present in the media, assuming that, as showed in Chapter 4, the species focusses on survival rather than growth and reproduction during the first month in fluid inclusions.

Due to a contamination by *Natrinema pallidum* in the experiments A and B, it was not possible to assess quantitatively via CFUs the survival of the tested strains, hence it was not possible to fully address the first aim. Nevertheless, downstream analysis revealed that the strains *Hbt. salinarum* NRC-1, *Hbt. noricense* A1 and *S. ruber* were able to survive increasing doses of polychromatic UV light (up to 12 kJ/m² in liquid and up to 15 kJ/m² in halite). The contaminant was also found in the experiment C, therefore CFUs could not be counted, however, the results in Figure 3.8 and 3.9, showed that in the case of different types of radiation (polychromatic UV 20 kJ/m², UV-C 5 kJ/m² and ionizing radiation 5 kGy), the tested strains also survived, with different recovery time. *D. salina* 18/19 did not survive any radiation treatment: this was expected, as previous experiments (Chapter 2) showed that the survival of this green microalgae is limited to two weeks in fluid inclusions. Nevertheless, samples with co-entombment of *D. salina* were also tested to explore a putative role as shield protection against radiation. Indeed, the second objective of this study was to explore the putative protection offered by co-entombment of different species to radiation, and the results in the experiment C showed the opposite: co-entombment has a negative effect on the survival of *Hbt. salinarum* NRC-1 and *S. ruber* M13. As discussed in the previous section, this result might be because in the co-entombment the cells are half as abundant as in the single entombment (one third in the multiple co-entombment); according to this hypothesis, half the cell abundance, subjected to radiation (poly-UV, UV-C and ionizing), significantly affects recovery, affecting the probability of success. This, on one hand can explain why *Hbt. salinarum* NRC-1 was significantly affected in co-entombment compared to single entombment, on the other can lead to the conclusion that the survival of the single cell is positively affected by the number of cells of the same species, as higher the number of cells, higher the possibility to have more resistant phenotypes.

Interestingly, in the literature it has been reported that the bacterium *Listeria monocytogenes* showed the highest resistance to ionizing radiation after 8 days (on a total of 12 days) of starvation, and the study concluded that starvation in this species cross-protects against radiation (Mendonca *et al.*, 2004). In line with this conclusion, another study reported that the survival of the bacterium *E. coli* O157:H7 from ionizing radiation, is cross protected by starvation (Hong *et al.*, 2014).

Baliga *et al.* (2004) found that there were 2400 mRNA changes during the recovery after the exposure to UV radiation in *Hbt. salinarum* NRC-1. In the same study, the authors also found the down regulation of many metabolic functions during the recovery. In Chapter 4, it was clear that many metabolic pathways are either down or up regulated when NRC-1 is entombed in lab-made halite. It might be that among the differentially expressed proteins during entombment, some of them might also be involved in the protection to radiation, therefore offering recover faster than freshly grown cells at doses up to 30 kJ/m² of polychromatic UV light. At higher doses of polychromatic UV, both freshly grown cells and starved cells started to be affected. High doses of polychromatic UV (40-50 kJ/m²) and UV-C (10 kJ/m²) did not affect freshly grown cells, showing a recovery rate similar to the no-radiation control. In the comparison between freshly grown cells and starved cells exposed to high doses of polychromatic UV and UV-C, freshly grown cells recovered significantly faster than starved cells. These results are worth further investigations, as the present data are not sufficient to clearly understand what lies at the base of the different response of the starved cells and freshly grown.

There have been multiple technical issues with the experiments in this Chapter. The first part of the experiment was performed in November 2019 at the German Aerospace Centre (Germany) during a secondment. The contamination by *N. pallidum* was found at the end of the secondment, therefore it was decided to repeat the experiment in 2020. However, due to the COVID-19 pandemic, the experiment was post-poned, and samples were shipped in June 2021. The irradiation in the experiment D and E was entirely performed by Kristina Beblo-Vranesevic and colleagues at the German Aerospace Centre. Part of this new experiment aimed to explore the molecular mechanism involved in the survival response of the strain (by qPCR) however, due to shipment delays at the border control, the samples arrived at the University of Essex at room temperature and could have not been used.

3.6 References

- Arun, T. *et al.* (2017) 'Ion beam radiation effects on natural halite crystals', *Nuclear Instruments and Methods in Physics Research Section B: Beam Interactions with Materials and Atoms*, 409, pp. 216–220. Available at: <https://doi.org/10.1016/j.nimb.2017.03.062>.
- Baliga, N.S. *et al.* (2004) 'Systems Level Insights Into the Stress Response to UV Radiation in the Halophilic Archaeon Halobacterium NRC-1', *Genome Research*, 14(6), pp. 1025–1035. Available at: <https://doi.org/10.1101/gr.1993504>.
- Banerdt, W. *et al.* (2020) 'Initial results from the InSight mission on Mars', *Nature Geoscience*, 13, pp. 1–7. Available at: <https://doi.org/10.1038/s41561-020-0544-y>.
- Beblo-Vranesevic, K. *et al.* (2017) 'The responses of an anaerobic microorganism, *Yersinia intermedia* MASE-LG-1 to individual and combined simulated Martian stresses', *PLOS ONE*, 12(10), p. e0185178. Available at: <https://doi.org/10.1371/journal.pone.0185178>.
- Benison, K.C. and LaClair, D.A. (2003) 'Modern and Ancient Extremely Acid Saline Deposits: Terrestrial Analogs for Martian Environments?', *Astrobiology*, 3(3), pp. 609–618. Available at: <https://doi.org/10.1089/153110703322610690>.
- Bibring, J.-P. *et al.* (2004) 'Perennial water ice identified in the south polar cap of Mars', *Nature*, 428(6983), pp. 627–630. Available at: <https://doi.org/10.1038/nature02461>.
- Bickel-Sandkötter, S., Gärtner, W. and Dane, M. (1996) 'Conversion of energy in halobacteria: ATP synthesis and phototaxis', *Archives of Microbiology*, 166(1), pp. 1–11. Available at: <https://doi.org/10.1007/s002030050349>.
- Carr, M.H. and Wänke, H. (1992) 'Earth and Mars: Water inventories as clues to accretional histories', *Icarus*, 98(1), pp. 61–71. Available at: [https://doi.org/10.1016/0019-1035\(92\)90207-N](https://doi.org/10.1016/0019-1035(92)90207-N).
- Chevrier, V., Hanley, J. and Altheide, T. (2009) 'Correction to "Stability of perchlorate hydrates and their liquid solutions at the Phoenix landing site, Mars"', *Geophysical Research Letters*, 36(18). Available at: <https://doi.org/10.1029/2009GL040523>.
- Clark, B.C. and Van Hart, D.C. (1981) 'The salts of Mars', *Icarus*, 45(2), pp. 370–378. Available at: [https://doi.org/10.1016/0019-1035\(81\)90041-5](https://doi.org/10.1016/0019-1035(81)90041-5).
- Daly, M.J. *et al.* (2004) 'Accumulation of Mn(II) in *Deinococcus radiodurans* Facilitates Gamma-Radiation Resistance', *Science*, 306(5698), pp. 1025–1028. Available at: <https://doi.org/10.1126/science.1103185>.
- Daly, M.J. *et al.* (2007) 'Protein Oxidation Implicated as the Primary Determinant of Bacterial Radioresistance', *PLoS Biology*. Edited by G.A. Petsko, 5(4), p. e92. Available at: <https://doi.org/10.1371/journal.pbio.0050092>.
- Dartnell, L.R. *et al.* (2007) 'Modelling the surface and subsurface Martian radiation environment: Implications for astrobiology', *Geophysical Research Letters*, 34(2). Available at: <https://doi.org/10.1029/2006GL027494>.
- D'Souza, S.E., Altekar, W. and D'Souza, S.F. (1997) 'Adaptive response of *Haloferax mediterranei* to low concentrations of NaCl (< 20%) in the growth medium', *Archives of Microbiology*, 168(1), pp. 68–71. Available at: <https://doi.org/10.1007/s002030050471>.

- Falkowski, P.G., Fenchel, T. and Delong, E.F. (2008) 'The Microbial Engines That Drive Earth's Biogeochemical Cycles', *Science*, 320(5879), pp. 1034–1039. Available at: <https://doi.org/10.1126/science.1153213>.
- Fang, X. *et al.* (2010) 'Escape probability of Martian atmospheric ions: Controlling effects of the electromagnetic fields', *Journal of Geophysical Research: Space Physics*, 115(A4). Available at: <https://doi.org/10.1029/2009JA014929>.
- Fendrihan, S. *et al.* (2009) 'Investigating the Effects of Simulated Martian Ultraviolet Radiation on *Halococcus dombrowskii* and Other Extremely Halophilic Archaeobacteria', *Astrobiology*, 9, pp. 104–12. Available at: <https://doi.org/10.1089/ast.2007.0234>.
- Formisano, V. *et al.* (2004) 'Detection of Methane in the Atmosphere of Mars', *Science*, 306(5702), pp. 1758–1761. Available at: <https://doi.org/10.1126/science.1101732>.
- Franz, H.B. *et al.* (2017) 'Large sulfur isotope fractionations in Martian sediments at Gale crater', *Nature Geoscience*, 10(9), pp. 658–662. Available at: <https://doi.org/10.1038/ngeo3002>.
- Gooding, J.L. (1992) 'Soil mineralogy and chemistry on Mars: Possible clues from salts and clays in SNC meteorites', *Icarus*, 99(1), pp. 28–41. Available at: [https://doi.org/10.1016/0019-1035\(92\)90168-7](https://doi.org/10.1016/0019-1035(92)90168-7).
- Hassler, D.M. *et al.* (2014) 'Mars' Surface Radiation Environment Measured with the Mars Science Laboratory's Curiosity Rover', *Science*, 343(6169), p. 1244797. Available at: <https://doi.org/10.1126/science.1244797>.
- Head, J.W. *et al.* (2003) 'Recent ice ages on Mars', *Nature*, 426(6968), pp. 797–802. Available at: <https://doi.org/10.1038/nature02114>.
- Hecht, M.H. *et al.* (2009) 'Detection of perchlorate and the soluble chemistry of martian soil at the Phoenix lander site', *Science (New York, N.Y.)*, 325(5936), pp. 64–67. Available at: <https://doi.org/10.1126/science.1172466>.
- Hong, S. *et al.* (2014) 'Radiation Resistance and Injury in Starved *Escherichia coli* O157:H7 Treated with Electron-Beam Irradiation in 0.85% Saline and in Apple Juice', *Foodborne Pathogens and Disease*, 11(11), pp. 900–906. Available at: <https://doi.org/10.1089/fpd.2014.1782>.
- Jones, D.L. and Baxter, B.K. (2016) 'Bipyrimidine Signatures as a Photoprotective Genome Strategy in G + C-rich Halophilic Archaea', *Life (Basel, Switzerland)*, 6(3). Available at: <https://doi.org/10.3390/life6030037>.
- Jones, D.L. and Baxter, B.K. (2017) 'DNA Repair and Photoprotection: Mechanisms of Overcoming Environmental Ultraviolet Radiation Exposure in Halophilic Archaea', *Frontiers in Microbiology*, 8. Available at: <https://doi.org/10.3389/fmicb.2017.01882>.
- Karan, R. *et al.* (2014) 'Bioengineering radioresistance by overproduction of RPA, a mammalian-type single-stranded DNA-binding protein, in a halophilic archaeon', *Applied Microbiology and Biotechnology*, 98(4), pp. 1737–1747. Available at: <https://doi.org/10.1007/s00253-013-5368-x>.
- Kellermann, M.Y. *et al.* (2016) 'Important roles for membrane lipids in haloarchaeal bioenergetics', *Biochimica et Biophysica Acta (BBA) - Biomembranes*, 1858(11), pp. 2940–2956. Available at: <https://doi.org/10.1016/j.bbamem.2016.08.010>.
- Kish, A. *et al.* (2009) 'Salt shield: intracellular salts provide cellular protection against ionizing radiation in the halophilic archaeon, *Halobacterium salinarum* NRC-1', *Environmental Microbiology*, 11(5), pp. 1066–1078. Available at: <https://doi.org/10.1111/j.1462-2920.2008.01828.x>.

- Kounaves, S.P. *et al.* (2014) ‘Evidence of martian perchlorate, chlorate, and nitrate in Mars meteorite EETA79001: Implications for oxidants and organics’, *Icarus*, 229, pp. 206–213. Available at: <https://doi.org/10.1016/j.icarus.2013.11.012>.
- Laskar, J., Levrard, B. and Mustard, J.F. (2002) ‘Orbital forcing of the martian polar layered deposits’, *Nature*, 419(6905), pp. 375–377. Available at: <https://doi.org/10.1038/nature01066>.
- Leuko, S. *et al.* (2015) ‘The Survival and Resistance of Halobacterium salinarum NRC-1, Halococcus hamelinensis, and Halococcus morrhuae to Simulated Outer Space Solar Radiation’, *Astrobiology*, 15. Available at: <https://doi.org/10.1089/ast.2015.1310>.
- LeukoStefan and RettbergPetra (2017) ‘The Effects of HZE Particles, γ and X-ray Radiation on the Survival and Genetic Integrity of Halobacterium salinarum NRC-1, Halococcus hamelinensis, and Halococcus morrhuae’, *Astrobiology* [Preprint]. Available at: <https://doi.org/10.1089/ast.2015.1458>.
- Lisse, C.M. *et al.* (2020) ‘A Geologically Robust Procedure for Observing Rocky Exoplanets to Ensure that Detection of Atmospheric Oxygen Is a Modern Earth-like Biosignature’, *The Astrophysical Journal Letters*, 898(1), p. L17. Available at: <https://doi.org/10.3847/2041-8213/ab9b91>.
- Mangold, N. *et al.* (2021) ‘Perseverance rover reveals an ancient delta-lake system and flood deposits at Jezero crater, Mars’, *Science*, 374(6568), pp. 711–717. Available at: <https://doi.org/10.1126/science.abl4051>.
- McCready, S. *et al.* (2005) ‘UV irradiation induces homologous recombination genes in the model archaeon, Halobacterium sp. NRC-1’, *Saline Systems*, 1(1), p. 3. Available at: <https://doi.org/10.1186/1746-1448-1-3>.
- Mendonca, A.F. *et al.* (2004) ‘Radiation resistance and virulence of Listeria monocytogenes Scott A following starvation in physiological saline’, *Journal of Food Protection*, 67(3), pp. 470–474. Available at: <https://doi.org/10.4315/0362-028x-67.3.470>.
- Mettler, F.A. (2012) ‘Medical effects and risks of exposure to ionizing radiation’, *Journal of Radiological Protection*, 32(1), pp. N9–N13. Available at: <https://doi.org/10.1088/0952-4746/32/1/N9>.
- Michalski, J.R. *et al.* (2022) ‘Geological diversity and microbiological potential of lakes on Mars’, *Nature Astronomy*, pp. 1–9. Available at: <https://doi.org/10.1038/s41550-022-01743-7>.
- Ojha, L. *et al.* (2015) ‘Spectral evidence for hydrated salts in recurring slope lineae on Mars’, *Nature Geoscience*, 8(11), pp. 829–832. Available at: <https://doi.org/10.1038/ngeo2546>.
- Oren, A., Elevi Bardavid, R. and Mana, L. (2014) ‘Perchlorate and halophilic prokaryotes: implications for possible halophilic life on Mars’, *Extremophiles*, 18(1), pp. 75–80. Available at: <https://doi.org/10.1007/s00792-013-0594-9>.
- Pollack, J.B. *et al.* (1987) ‘The case for a wet, warm climate on early Mars’, *Icarus*, 71(2), pp. 203–224. Available at: [https://doi.org/10.1016/0019-1035\(87\)90147-3](https://doi.org/10.1016/0019-1035(87)90147-3).
- Ramirez, R.M. and Craddock, R.A. (2018) ‘The geological and climatological case for a warmer and wetter early Mars’. Available at: <https://doi.org/10.1038/s41561-018-0093-9>.
- Robinson, C.K. *et al.* (2011) ‘A Major Role for Nonenzymatic Antioxidant Processes in the Radioresistance of Halobacterium salinarum’, *Journal of Bacteriology*, 193(7), pp. 1653–1662. Available at: <https://doi.org/10.1128/JB.01310-10>.
- Soppa, J. (2014) ‘Polyploidy in Archaea and Bacteria: About Desiccation Resistance, Giant Cell Size, Long-Term Survival, Enforcement by a Eukaryotic Host and Additional Aspects’, *Microbial Physiology*, 24(5–6), pp. 409–419. Available at: <https://doi.org/10.1159/000368855>.

- Stan-Lotter, H. and Fendrihan, S. (2015) 'Halophilic Archaea: Life with Desiccation, Radiation and Oligotrophy over Geological Times', *Life*, 5(3), pp. 1487–1496. Available at: <https://doi.org/10.3390/life5031487>.
- Stern, J.C. *et al.* (2015) 'Evidence for indigenous nitrogen in sedimentary and aeolian deposits from the Curiosity rover investigations at Gale crater, Mars', *Proceedings of the National Academy of Sciences*, 112(14), pp. 4245–4250. Available at: <https://doi.org/10.1073/pnas.1420932112>.
- Thomas, N.H. *et al.* (2019) 'Mars Science Laboratory Observations of Chloride Salts in Gale Crater, Mars', *Geophysical Research Letters*, 46(19), pp. 10754–10763. Available at: <https://doi.org/10.1029/2019GL082764>.
- Touma, J. and Wisdom, J. (1993) 'The Chaotic Obliquity of Mars', *Science*, 259(5099), pp. 1294–1297. Available at: <https://doi.org/10.1126/science.259.5099.1294>.
- Webb, K.M. *et al.* (2013) 'Effects of intracellular Mn on the radiation resistance of the halophilic archaeon *Halobacterium salinarum*', *Extremophiles*, 17(3), pp. 485–497. Available at: <https://doi.org/10.1007/s00792-013-0533-9>.
- Zerulla, K. and Soppa, J. (2014) 'Polyploidy in haloarchaea: advantages for growth and survival', *Frontiers in Microbiology*, 5. Available at: <https://doi.org/10.3389/fmicb.2014.00274>.
- Zorzano, M.-P. *et al.* (2009) 'Stability of liquid saline water on present day Mars', *Geophysical Research Letters*, 36(20). Available at: <https://doi.org/10.1029/2009GL040315>.
- David, N. L. and Cox, M. M. 2017. *Lehninger Principles of Biochemistry*. 7th ed. New York, NY: W.H. Freeman.

3.7 Supplementary info

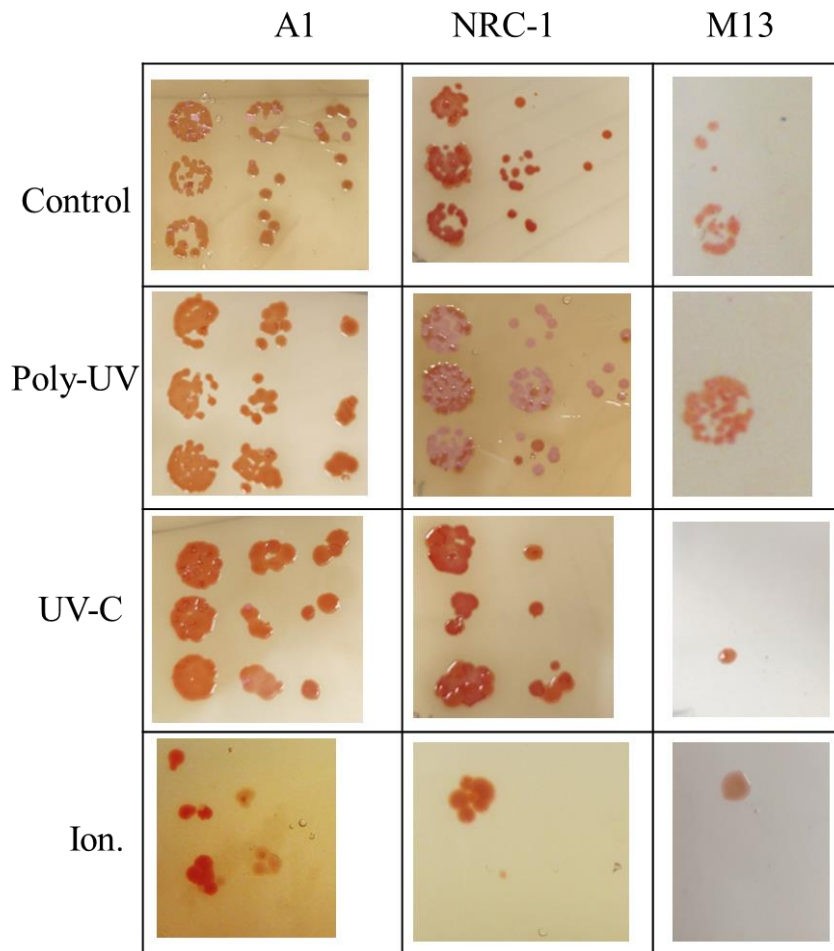


Figure S3.1. One picture from one replicate for each sample of the experiment C where the growth of both the single species tested and the contaminant were observed. The strain of each species is reported on the top, while on the side the type of radiation at which they were subjected.

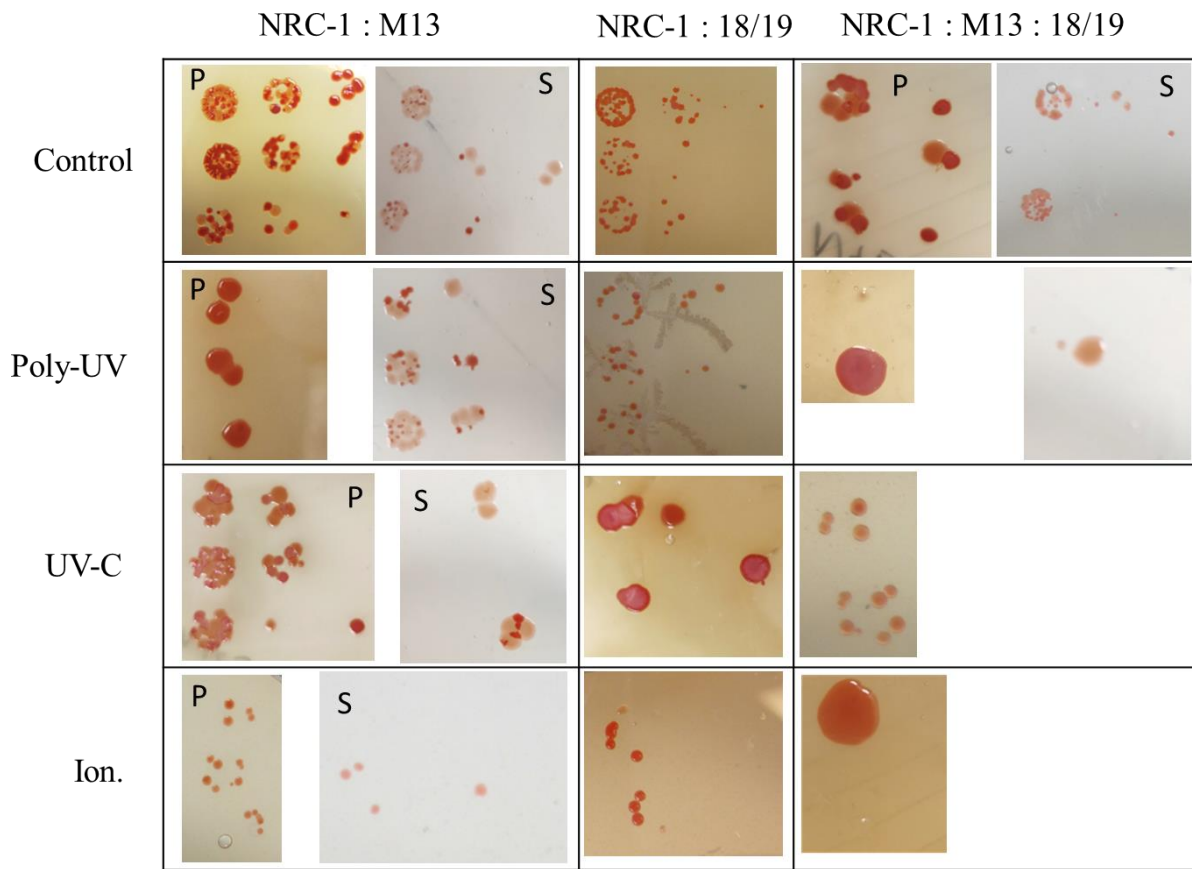


Figure S3.2. One picture from one replicate for each sample of the experiment C where the growth of both the single species tested in co-entombment and the contaminant were observed. The strain of each species is reported on the top, while on the side the type of radiation at which they were subjected.

Chapter 4: Differential protein expression in *Halobacterium salinarum* NRC-1 during entombment in lab-made halite

Abstract

4.1 Introduction

4.2 Phenotypical and genotypical signature of halophiles

4.3 Aims and objectives

4.2 Methodology

4.2.1 Microbial culture

*4.2.2 Entombment of *Halobacterium salinarum**

4.2.3 Protein extraction

4.2.4 Protein analysis

4.2.5 Statistical analysis

4.3 Results

4.3.1 Visualisation of proteins on SDS-PAGE precast gel

4.3.2 LC-MS/MS Shotgun Proteomic Analysis

4.3.3 Comparison of the proteome between T-0 and T-1

4.3.4 Comparison of the proteome between T-1 and T-2

4.3.5 Comparison of the proteome between T-0 and T-2

4.3.5.1 Differentially expressed ribosomal proteins

4.3.5.2 Differentially expressed proteins involved in the biosynthesis of new proteins

4.3.5.3 Up-regulation of enzymes involved in the Fermentative arginine degradation

4.3.5.4 Use of alternative electron acceptors

4.3.5.5 Other proteins significantly differentially expressed during the entombment

4.3.6 Contamination by Natrinema sp.

4.4 Discussion

4.4.1 Differentially expressed proteins involved in the biosynthesis of new proteins

4.4.2 Up-regulation of enzymes involved in the Fermentative arginine degradation

4.4.3 Use of alternative electron acceptors

4.4.4 Other proteins significantly differentially expressed during the entombment

4.5 Conclusions

4.6 References

4.7 Supplementary material

Chapter 4: Differential protein expression in *Halobacterium salinarum* NRC-1 during entombment in lab-made halite

Abstract

Halobacterium salinarum NRC-1 is a specialist in long-term survival, with optimum growth at saturated concentration of NaCl. To gain insight into its longevity and its ability to survive entombed in salt crystals (halite) over geological time, I investigated the proteome changes at 42 days of entombment compared with growth prior to entombment and the point at which halite formed. Proteins involved in transcription and translation were significantly less abundant after 42 days in fluid inclusions, suggesting that its energy is primarily devoted to maintenance, rather than growth and reproduction. In contrast to all other ribosomal proteins detected, ribosomal protein L13 had an elevated abundance at day 42, suggesting that it may have a role in haloarchaea connected with long-term survival. We also found a higher abundance of several proteins, including enzymes involved in the arginine fermentation, highlighting the existence of on-going anaerobic metabolic activities to respond to the changing environmental conditions in the fluid inclusions.

4.1 Introduction

Hypersaline environments are dynamic ecosystem with fluctuations between dissolution and precipitation of salt crystals, including halite. Microbial communities living in these environments may become entombed in halite when it precipitates (Norton and Grant 1988). Inside the fluid inclusions of halite, halophilic microbes such as *Dunaliella salina* are able to survive the entombment, however, for a limited time (two weeks survival) (see Chapter 2). Species of *Halobacterium* instead, have shown the ability to survive over months (see Chapter 1 and 2), and it has been reported in the literature that Haloarchaea are able to survive inside fluid inclusions of halite over geological time, specifically *Hbt. salinarum* (Mormile *et al.* 2003) (see Chapter 1). The question on how they survive is still open and the experiment reported here is an attempt to study what the intrinsic abilities of

Haloarchaea are to survive over geological time scale in a nutrient-limited, oxygen-limited, closed micro ecosystem (Figure 4.1).

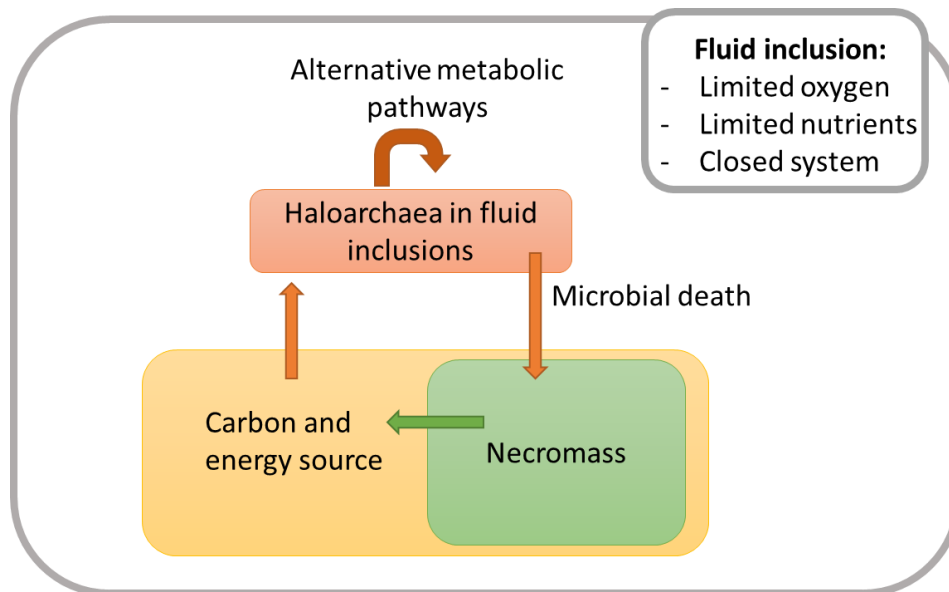


Figure 4.1. Schematic view of Haloarchaea entombed in a fluid inclusion inside the crystals of halite. As reported in the literature (see Introduction), Haloarchaea can feed on carbon and energy sources coming from organic matter that gets trapped in the fluid inclusions together with the Haloarchaea; dead cells of Haloarchaea can become part of this pool of carbon and energy source.

4.2 Phenotypical and genotypical signature of halophiles

The strategy adopted by extreme halophiles (discussed in Chapter 1) results in them having a proteome with an excess ratio of acidic to basic amino acids. To avoid problems such as unfolding and instability, proteins of *Halobacterium salinarum*, and Haloarchaea in general, are predominantly negatively charged with most of the negative charge occurring on surface amino acid residues (Oren 2013; Soppa 2006; Madern, Ebel, and Zaccari 2000). Different studies have investigated the stability of proteins with low hydrophobicity in halophiles, and proposed this as an additional molecular signature of life in hypersaline environments (Hutcheon *et al.*, 2005; Lanyi 1974). Also, Paul *et al.* (2008) investigated the physical and chemical principles sustaining the stability of proteins in high salt milieu mostly based on genomic analysis, and found that in the secondary structure of proteins from halophiles with salt-in strategy, coils are preferred to alpha helices. In the same study, they also

investigated the physical and chemical structure of the DNA of halophiles, to identify signatures of adaptation to high salt. They found evidence of specific selection on dinucleotide and synonymous codon usage that are preferred in halophiles, and how this is a salt-specific signature: in fact, the higher frequency of GA, AC and GT, reflects the preference of amino acids Asp, Glu, Thr and Val, typically more abundant in the proteome of halophiles (Paul *et al.* 2008). While this is inferred from the DNA sequence, there are also reports that have focussed on the protein structure (Graziano and Merlino 2014, and references therein). A famous example is the case of the malate dehydrogenase (hMDH) in *Haloarcula marimortui*: Dym *et al.* (1995) determined by X-ray crystallography the structure of the hMDH enzyme and clearly showed surface negative charges on the enzyme, preventing denaturation.

Halophiles tend to have a high mol% G&C content, possibly as an adaptation to intense UV radiation, and *Haloquadratum walsbyi* compensate for its lower GC-content (XX%) with more photolyases genes devoted repair UV damage (Jones and Baxter 2016). Paul *et al.* (2008) suggest an additional explanation to the high G&C-content of halophiles, and that is related to the DNA structure in high salt environments.

Halobacterium salinarum has been used as a model organism over the last decades to study many different biological processes. Several highly similar species of *Halobacterim* should be regarded as strains of *Halobacterium salinarum* (Oren and Ventosa 2017). The strain studied in this work is *Halobacterium salinarum* NRC-1, which is very similar to the strain R1, due to an important number of insertion sequences (ISH elements) (Brügger *et al.* 2002). To study the main difference that makes these two different strains, Pfeiffer *et al.* (2008) investigated the similarities between the genomes of NRC-1 and R1. Their results show that their chromosome is completely colinear and virtually identical, but their plasmids have differences, with regards to 210 kb of sequence occurring only in R1 and the remaining 350 kb are virtually identical. At the protein level, Pfeiffer *et al.* (2008) also found that 20% of protein sequences differ despite the similarity at the DNA level; they concluded that NRC-1 and R1 originate from the same natural isolate and are two different strains of *Halobacterium salinarum*.

4.3 Aims and objectives

When considering the existence of a pool of carbon and energy sources to sustain the metabolism of Haloarchaea in fluid inclusions of halite, there are important points to consider: 1) What are the

physiological adaptations of *Halobacterium salinarum* NRC-1 to survive in fluid inclusions of halite? 2) Is their survival fully dependent on the recycling of available organic matter? 3) How long can the recycling of carbon and energy sources sustain the metabolism of Haloarchaea? In order to answer these questions and to shed light onto the innate ability of Haloarchaea to survive over geological timescale, we investigated the changes in the proteome of *Halobacterium salinarum* NRC-1 over a period of 42 days entombed in lab-made halite to gain insights into possible mechanisms of long-term survival.

4.2 Methodology

4.2.1 Microbial culture

For the preparation of a starter culture, *Halobacterium salinarum* NRC-1 was grown aerobically in the dark at 30°C on a shaker at 100 rpm, in 15 ml of 20% NaCl Payne liquid medium (Chapter 2, Table S2.1), in a 50 ml falcon tube, until late-exponential phase. When the OD₆₀₀ reached the value of 0.900, 1 ml was inoculated into 100 ml of 20% NaCl Payne liquid medium, in 300 ml flasks, and cultured at 30°C in the dark on a shaker at 100 rpm until the late exponential phase (Figure S2.1).

4.2.2 Entombment of *Halobacterium salinarum*

When late-exponential phase was reached, 30 ml of culture was centrifuged (8500 g, 4°C, 20 min) and the cell pellet was washed in 25 ml of 25% NaCl; 2.5% MgSO₄·7H₂O twice and centrifuged again. Cells were resuspended in 100 ml of salt solution (25% NaCl; 2.5% MgSO₄·7H₂O) and cell concentrations were determined with a counting chamber (Helber chamber, Fisher) and adjusted to 5×10⁸ cells/ml. In order to get to the desired final cell concentration, where needed, an additional volume of culture was centrifuged, washed in salt solution, and added to the previous suspension. A volume of 100 ml of each suspension was then poured into sterile 145 mm diameter Petri dish and was left, with lids off, on a disinfected, unused laboratory bench. When the crystallization was completed, the petri dishes were stored with lids on.

4.2.3 Protein extraction

Proteins were prepared following a previously described method that is a personal communication of Igor Chernukhin and adapted by Gramain (Gramain, 2009). Three time points were selected in this experiment, representing respectively, the cells in the liquid culture at the late exponential phase (day -11: T-0), the moment of crystallisation (day 0: T-1) and 42 days after the crystallisation was completed (day 42: T-2) (Figure 4.2).

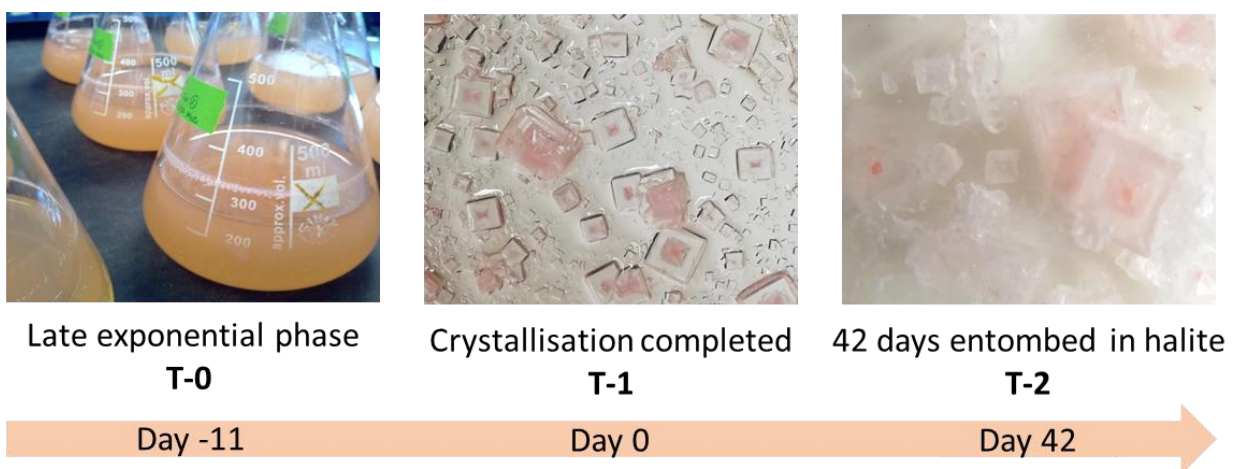


Figure 4.2. Pictures of the three time points chosen from which the proteins were extracted and analysed. T-0: *Halobacterium salinarum* NRC-1 grown aerobically in 20% NaCl modified Payne medium on a shaker (100 rpm) at 30°C until the late exponential phase. T-1: After eleven days the precipitation was completed, and the halite crystals were formed. T-2: The crystals were kept at ambient temperature closed in a petri dish, covered, for 42 days.

For the first time point, harvested cells were collected by centrifugation (8500 g, 4°C, 20 min) and the pellet washed in a solution composed of 15% w/v NaCl; 1.5% MgSO₄·7H₂O. The resulting pellet was then stored at -80°C until protein extraction. For the following two time points, 30 g of salt crystals with entombed cells of *Halobacterium salinarum* NRC-1 were dissolved in sterile MilliQ water to give a final concentration of 20% w/v salt. In order to facilitate the dissolution, the falcon tubes were placed on a shaker at 100 rpm at room temperature. Once the crystals were dissolved, the samples were centrifuged (8500 g, 4°C, 20 min), and the resulting pellet stored at -80°C until protein extraction. The frozen cell pellets were slowly thawed on ice and then resuspended in 2 ml of urea/mercaptoethanol solution (8 M, 20 mM, respectively). Separately, one tablet of Protease-inhibitor (cOmplete™, Mini, EDTA-free Protease Inhibitor Cocktail, Roche) was dissolved in 100 µl

of sterile MilliQ water, following manufacturer's protocol. Benzonase nuclease (Benzonase® Nuclease1 ≥ 250 units/ μL , $\geq 90\%$, Sigma) was diluted 1:10 in MilliQ water to obtain a final concentration of 25 units/ μL . Subsequently, 20 μL of Protease-inhibitor solution and 2 μL of diluted Benzonase nuclease were added to the sample. The suspension was then vortexed for one minute at maximum speed and incubated on ice for 20 minutes. The suspension was then centrifuged (8500 g, 4°C, 20 min) and the supernatant was transferred to a fresh 15 ml Falcon tube and treated with 1 volume of ice-cold acetone (100% v/v) for 15 minutes at -20°C. Subsequently, 10 μL of urea (8 M) was added, and the tube centrifuged (10,000 g, 4°C, 10 minutes). The resulting protein pellet was air-dried and resolubilized with 100 μL of resuspension buffer (42.04 g urea, 15.22 g thiourea, 4 g CHAPS, 2 ml mercaptoethanol made up to 100 ml with MilliQ water), as described by Tebbe *et al.* (2005), then stored at -80°C until use.

4.2.4 Protein analysis

Extracted proteins were stored at -80°C and were subsequently slowly defrosted in ice. In order to visualise the proteins by SDS-PAGE, 5 μL of sample was added to 5 μL of loading buffer and then incubated for 5 minutes in a water bath at 90°C. The loading-buffer stock solution was composed of 1.25 mL of TRIS-HCl (0.5 M, pH 6.8), 2.5 mL of glycerol, 2 mL of SDS (10% w/v), 0.2 mL of bromophenol blue (0.5% w/v) and 3.55 mL of Milli-Q water. A volume of 950 μL of loading-buffer stock solution was supplemented with 50 μL of 2-mercaptoethanol (Bio-Rad) before use.

The denatured samples were then loaded onto a Mini-PROTEAN TGX precast, 10% polyacrylamide gel (Bio-Rad), and run for one hour at 100 V, using a 1 \times running buffer (15 g of TRIS, 72 g glycine (Sigma-Aldrich) and 5 g of SDS pH 8.3 in 1 L of Milli-Q water). The gel was loaded with 5 μL of PageRuler™ prestained protein ladder (Thermo Fisher Scientific). The gel was then stained with Coomassie Brilliant Blue (0.1% Bio-Rad Coomassie Brilliant Blue R-250, 50% v/v methanol, 10% v/v glacial acetic acid) overnight, and then treated with destaining solution (40% v/v methanol, 10% v/v glacial acetic acid) for 3 h. The gel was then transferred into a transparent container with MilliQ water for observation.

Total protein in the final solution was determined using the modified Bradford protein assay, and a BSA standard. The dye reagent was prepared by diluting one part Dye Reagent (Bio-Rad Quick Start™ Bradford 1 \times Dye Reagent) concentrate with 4 parts MilliQ water. Five known dilutions of the protein standard Bovine Serum Albumin (Bio-Rad Protein Assay Standard II) were prepared. On the microtitre plate (Nunc™ Surface, Nunc™), 10 μL of each standard was added to triplicate wells of

the microtiter plate, and 10 μl of each sample dilution was added to triplicate wells. Subsequently, 200 μl of the diluted dye reagent was added to each well. The solution in each well was well mixed and incubated at room temperature for 5 minutes. The absorbance was then measured at 595 nm with a spectrophotometer and the data plotted against the standard concentration.

The in-gel trypsin digestion was performed by Dr. Gergana Metodieva and used to prepare the samples for the mass spectrometric identification of proteins. Briefly, the gel was sliced into small pieces of 1-2 mm and subsequently destained three times in a solution of 100 μl of 50% Acetonitrile (ACN)/50 mM NH_4HCO_3 . Gel slices were dehydrated with ACN 50%, rehydrated with 30 μl of Dithiothreitol (DTT) solvent and incubated for 30 minutes at 37°C. After the removal of DTT, 30 μl of iodacetamide were added and incubated in the dark at room temperature for 30 minutes. After the removal of the solvent, the samples were dehydrated with ACN 50% and subsequently rehydrated with 25 μl of trypsin solution (Sequencing Grade Trypsin, Promega). Up to a volume of 20 μl of 50 mM NH_4HCO_3 was added to the gel pieces to cover them and they were incubated overnight at 37°C. A volume of 5 μl of 5% formic acid was added and the peptide collected in a clean tube for extraction. The extraction was carried out with 50 μl of 50% ACN with 0.1 % v/v formic acid. The liquid was then collected, and peptides extracted with 50 μl of ACN 50%. Finally, the samples were dried in a vacuum concentrator. Through this method, the extracted proteins were cleaved into peptide fragments, that were then dried and reconstituted in 20 μl of LC/MS-grade water containing 0.1% (v/v) formic acid.

The LC-MS/MS analysis was performed by Dr. Metodi Metodiev using the protocol published in Greenwood *et al.* (2012). The samples were analysed on a hybrid linear LTQ/Orbitrap Velos instrument (Thermo Fisher) interfaced to a split-less nanoscale HPLC (Ultimate 3000, Dionex) following the method described by Greenwood *et al.* (2012). The fragmented peptide samples resulting from the in-gel digestion (2 μl) were injected automatically by the autosampler and desalted and concentrated online at a flow of 1 $\mu\text{l}\cdot\text{min}^{-1}$ on a 2 cm long, 0.1 mm inner diameter (i.d.) trap column packed with 5 μm C18 particles (Dionex). After concentration/desalting, the fragmented peptides were eluted from the trap column and separated in a 90-min gradient of 2-30% (v/v) acetonitrile in 0.1% (v/v) formic acid (flow rate 0.3 $\mu\text{l}\cdot\text{min}^{-1}$), and subsequently separated on a 15 cm-long, 0.1 mm i.d. pulled tip packed with 5 μm C18 particles (Nikkoy Technos Co., Tokyo, Japan). The elution of peptides was then electrosprayed directly into the mass spectrometer at a voltage of 1.75 kV using a liquid junction interface.

Data analysis was initially performed by Dr Metodi Metodiev in MaxQuant (Cox and Mann 2008) following a previously described method (Gregson *et al.*, 2019). Firstly, the raw data files from the LQT/Orbitrap Velos instrument, were converted to MSM files, through the MaxQuant “Quant”

module. As an integration of MaxQuant, Andromeda, an open-source search engine, was used to identify peptides in sequence databases by their fragmentation spectra (Cox *et al.*, 2011). To obtain the final data set, peptides and proteins were filtered at 0.3% false discovery rate (FDR). The number of MS/MS spectra matched to the corresponding proteins were counted to quantify the proteins. UniProt protein sequences from *Halobacterium salinarum* NRC-1 (Pfeiffer *et al.* 2008) were used to perform protein identification. The default settings in MaxQuant and Andromeda were used to validate proteins with a minimum of one peptide. Where proteins were validated with only one peptide, the peptides unique to the protein in question had to be distinctly identified. Proteins identified as contaminants from the LC-MS/MS sample preparation (*i.e.* trypsin and keratin), were removed from the data set. Furthermore, the final data set was filtered against *Natrinema pallidum* JCM 8980/*Natrinema altunense* JCM 12890 (100% similarity), as it was found as a contaminant in the experiment. Differences between runs were accounted for by normalization of spectral counts to total spectral counts (where total spectral counts varied from 817 to 1363 per run). As a result of the criteria used, the final data set included a total of 424 proteins.

4.2.5 Statistical analysis

To account for differences between runs, spectral counts were normalised against total spectral counts. The OMICS package of XLSTAT-Premium Version 2020.1.3 (Addinsoft), differential expression analysis was performed on the normalised spectral count data by analysis of variance (ANOVA). The Benjamini-Hochberg false discovery rate was used to correct post-hoc *p*-values (Benjamini and Hochberg 1995). Differentially expressed proteins were identified by Students t-test with Tukey's Honestly Significant Difference (HSD) post-hoc test for pairwise comparisons (e.g., time points over the process of entombment). Fold-changes in protein spectral counts between treatments were calculated by dividing the following time point spectral counts by the previous time point spectral counts (e.g., T-2 spectral counts divided by T-1 spectral counts). For the purpose of generating volcano plots, in order to include proteins with spectral counts of zero in one of the treatments, a value of 1 was added to the mean spectral count of each protein within the three time points analysed. This approach minimally altered the spectral count ratio while allowing the visualisation of all the proteins detected to be displayed on the volcano plots.

4.3 Results

4.3.1 Visualisation of proteins on SDS-PAGE precast gels

Prior to the LC-MS/MS analysis, extracted proteins were separated by SDS-PAGE. This gel gave a visual representation that proteins had been successfully extracted. Three out of four replicates were visualized of gel, and it clearly showed the proteome had changed with time (Figure 4.3).

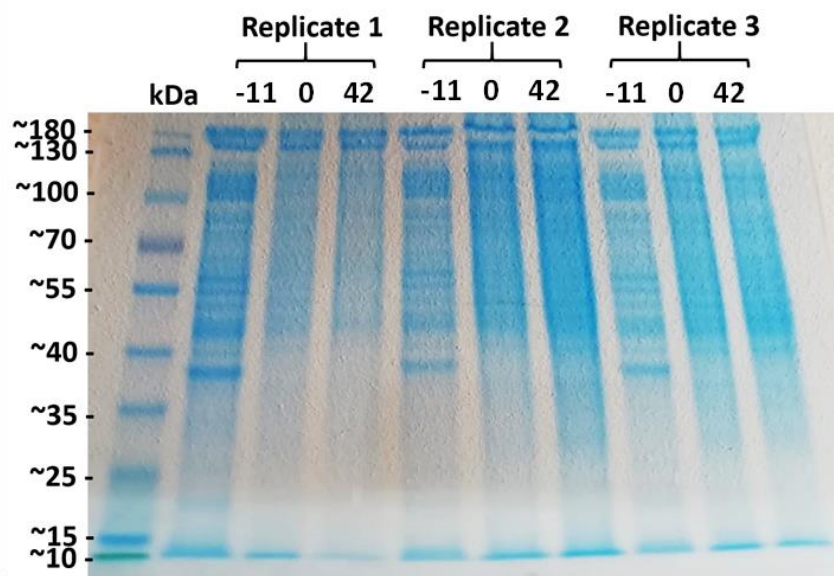


Figure 4.3. Precast gel showing three replicates of the three time points used and the separated proteins. -11, 0 and 42 indicate respectively T-0 (day: -11), T-1 (day: 0), and T-2 (day: 42). 10% Mini-PROTEAN® TGX™ Precast Gels (BioRad). A volume of 20 μ L of extracted proteins was loaded into the gel pockets and 5 μ L of the PageRuler™ Prestained Protein Ladder (ThermoFisher Scientific) was used as marker.

4.3.2 LC-MS/MS Shotgun Proteomic Analysis

Twelve LC-MS/MS runs were performed consisting of four independent biological replicates of three time points across the process of entombment in laboratory-made halite. The three time points represented respectively: the late exponential phase in optimum growth conditions, complete precipitation of salt, and 42 days inside the salt crystals (Figure 4.2). A total of 11891 MS/MS spectra

were assigned to 424 proteins (average of 998.4 spectral counts per replicate and ranging from 1 to 91 spectral counts per protein after filtering the data according to specified criteria (Section 4.2.5).

4.3.3 Comparison of the proteome of *Hbt. salinarum* NRC-1 between T-0 and T-1

Of the 424 proteins detected in the proteome of *Halobacterium salinarum* NRC-1 following entombment in salt crystals, 30 were significantly differentially expressed across the 11 days between T-0 and T-1. In this comparison, the relative abundance of 20 proteins was found to be significantly decreased and 10 were significantly increased (Figure 4.4).

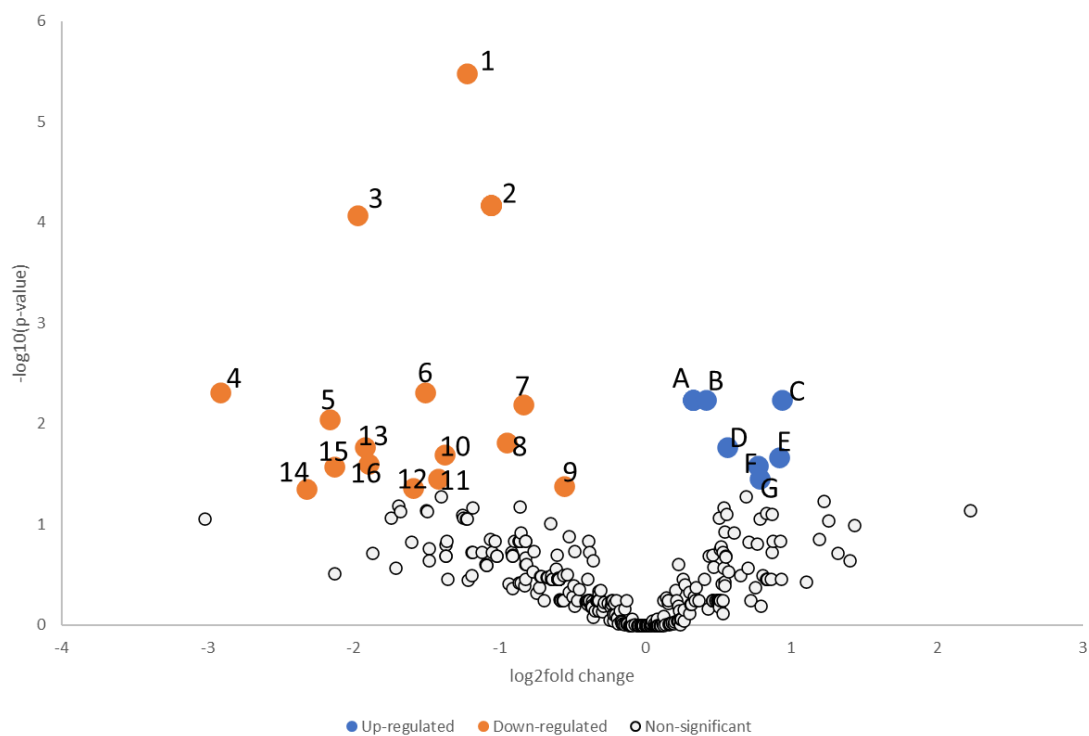


Figure 4.4. Volcano plot of normalised LC-MS/MS spectral counts comparing *Halobacterium salinarum* NRC-1 protein expression across 11 days of becoming entombed inside fluid inclusions (comparison between T-0 and T-1). Large circles (orange and blue) represent differentially expressed proteins with p-values (t-test) below 0.05 ($-\log_{10}(0.05) = 1.301$) and a fold change value ranging between 0.09 and 0.63 for proteins found in lower abundance, and a value ranging between 1.48 and 2.17 for proteins found in higher abundance (real values). Fold-changes in protein spectral counts between treatments were calculated by dividing the following time point spectral counts by the previous time point spectral counts (i.e., T-1/T-0). For the purpose of generating volcano plots, in order to include proteins with spectral counts of zero in one of the treatments, a value of 1 was added to the mean spectral count of each protein within the three time points analysed; this minimally altered the spectral count ratio while allowing the visualisation of all the proteins detected to be displayed on the volcano plots. Where there are multiple proteins in one point, the proteins are overlapped. Large, orange

circles containing numbers represent proteins with lower abundance at T-1 versus T-0 (Uniprot codes in brackets): **1:** D-3-phosphoglycerate dehydrogenase (Q9HMR0); **2:** Transducer protein Htr7 (P0DMI5), 50S ribosomal protein L24 (Q9HPC3), HGPRTase-like protein (Q9HRT1), AAA-type ATPase (Q9HPU1), PhoU domain protein (Q9HS09); **3:** Vng6208c (Q9HHV6); **4:** Thermosome subunit alpha (Q9HN70); **5:** 50S ribosomal protein L4 (Q9HPD3); **6:** Taxis protein CheF1 (Q9HQX2); **7:** Pyruvate kinase (Q9HSA5); **8:** 30S ribosomal protein S3Ae (Q9HRA5); **9:** Branched-chain-amino-acid aminotransferase (Q9HNF8); **10:** ABC-type transport system ATP-binding protein (Q9HMX3); **11:** Translation initiation factor 2 subunit gamma (Q9HNK9); **12:** Peptide chain release factor subunit 1 (Q9HNF0); **13:** 30S ribosomal protein S19e (Q9HNP2); **14:** ABC transporter, ATP-binding protein (Q9HRV7); **15:** DNA protection during starvation protein (Q9HMP7); **16:** Arginine-tRNA ligase (Q9HHN2). Large, blue circles containing letters represent protein with higher abundance at T-1 versus T-0: **A:** Putative dimethyl sulfoxide reductase iron-sulfur subunit B (Q9HR73), ParA domain protein (Q9HHU2), HD_domain domain-containing protein (Q9HR93), ABC transporter (Lipoprotein) (Q9HRA0); **B:** Glutamate-1-semialdehyde 2,1-aminomutase (Q9HMY8); **C:** Flagellin B1 (P61116); **D:** Pyruvate dehydrogenase alpha subunit (Q9HN77); **E:** TATA-box-binding protein B (Q48325); **F:** Putative dimethyl sulfoxide reductase catalytic subunit A (Q9HR74); **G:** Ornithine carbamoyltransferase, catabolic activity (Q48296).

4.3.4 Comparison of the proteome between T-1 and T-2

Of the 424 proteins detected in the proteome of *Halobacterium salinarum* NRC-1 following entombment in salt crystals, six proteins were significantly differentially expressed across the 42 days between T-1 (day: 0) and T-2 (day: 42). One protein had significantly lower abundance and five (some overlap) were significantly higher abundance (Figure 4.5).

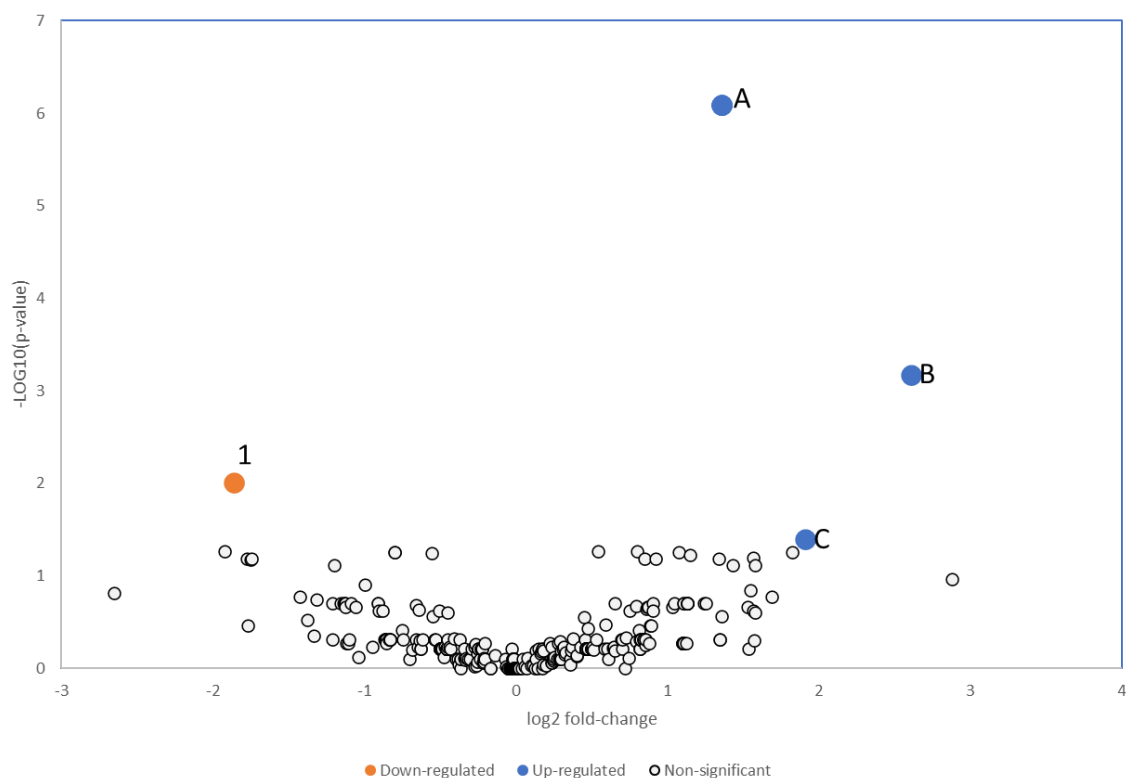


Figure 4.5. Volcano plot of normalised LC-MS/MS spectral counts comparing *Halobacterium salinarum* NRC-1 protein expression across 42 days of being entombed inside fluid inclusions (comparison between T-1 and T-2). Large circles (orange and blue) represent differentially expressed proteins with p-values (t-test) below 0.05 ($-\log_{10}(0.05) = 1.301$) and a fold change value of 0.169 for proteins found in lower abundance, and for proteins found in higher abundance, their spectral counts increased from 0 (T-1) to a value between 1.56 and 5.08 (real values). Fold-changes in protein spectral counts between treatments were calculated as indicated in Figure 4.4. Where there are multiple proteins in one point, the proteins are overlapped. Large, orange circles containing numbers represent lower abundant proteins over a period of 11 days of entombment (Uniprot codes in brackets): **1**: 30S ribosomal protein S12 (P0CX00). Large, blue circles containing letters represent the higher abundant proteins: **A**: Phosphoglycerate dehydrogenase (Q9HPW9), HAD superfamily hydrolase (Q9HQE2), DUF88 family protein (Q9HS40); **B**: 50S ribosomal protein L13 (Q9HQJ3), **C**: Histidine--tRNA ligase (Q9HNP5).

4.3.5 Comparison of the proteome between T-0 and T-2

Of the 424 proteins detected in the proteome of *Halobacterium salinarum* NRC-1 following entombment in salt crystals, 79 proteins were significantly differentially expressed across the 11 days until complete precipitation and 42 days inside fluid inclusions of laboratory-made halite, for a total of 53 days (comparison between T-0 and T-2). In this comparison it was found that 46 proteins had

significant lower abundance, whilst 33 had significant higher abundance (p -value > 0.05 ; T-test) (Figure 4.6).

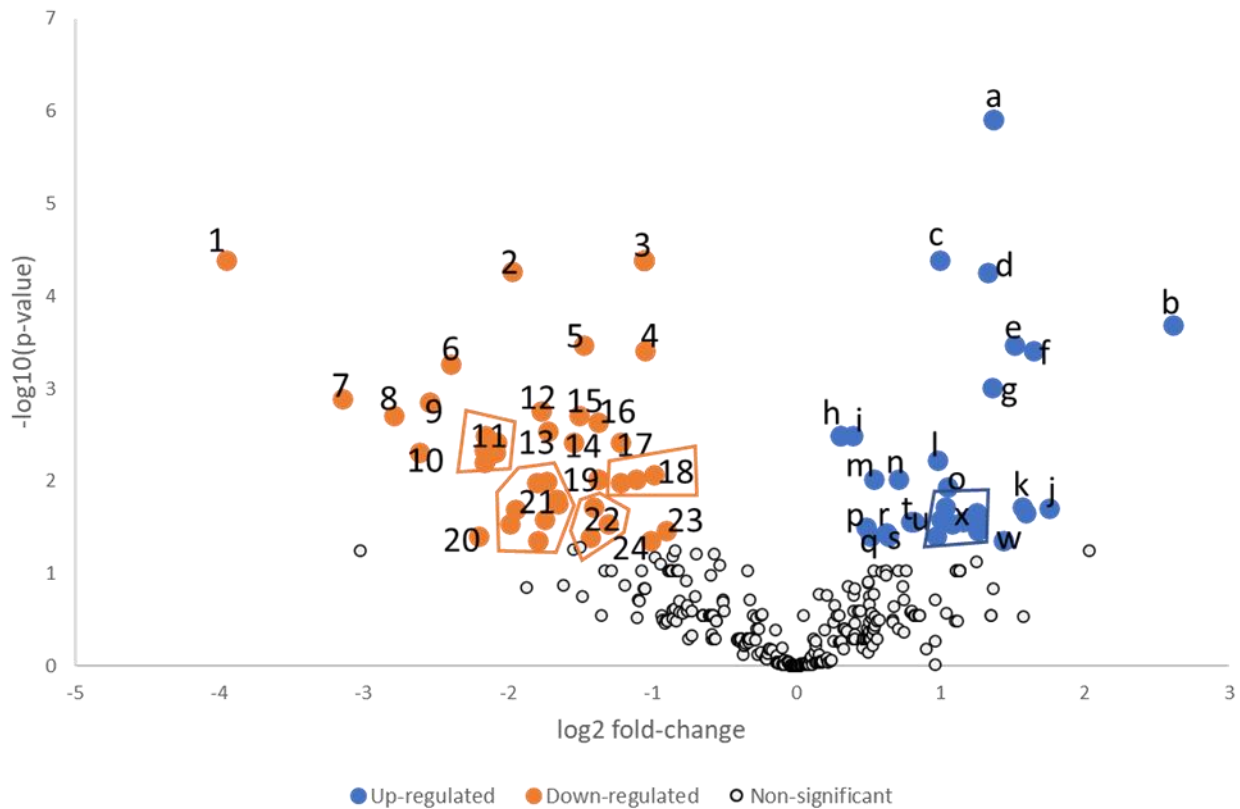


Figure 4.6. Volcano plot of normalised LC-MS/MS spectral counts comparing *Halobacterium salinarum* NRC-1 protein expression across 42 days of being entombed inside fluid inclusions (comparison between T-0 and T-2). Large circles (orange and blue) represent differentially expressed proteins with p -values (t-test) below 0.05 ($-\log_{10}(0.05) = 1.301$) and a fold change value ranging from 0.019 and 0.45 for proteins found in lower abundance, and a value ranging between 1.45 and 4.26 for proteins found in higher abundance. For some proteins, the spectral count in T-0 or T-2 was zero; these cases are further discussed in the Result section individually. Fold-changes in protein spectral counts between treatments were calculated as indicated in Figure 4. Where there are multiple proteins in one point, the proteins are overlapped. Large, orange circles containing numbers represent lower abundant proteins over a period of 11 days of entombment (Uniprot codes in brackets): **1**: Thermosome subunit alpha (Q9HN70); **2**: Vng6208c (Q9HHV6); **3**: Transducer protein Htr7 (P0DMI5), Signal recognition particle 54 kDa protein (Q9HMN5), 50S ribosomal protein L24 (Q9HPC3), Glycerol-3-phosphate dehydrogenase chain C (Q9HNS2), AAA-type ATPase (CDC48 subfamily) (Q9HPU1), FAD-dependent oxidoreductase (Homolog togeranylgeranyl reductase) (Q9HQE5); **4**: 50S ribosomal protein L10e (Q9HSS4); **5**: Pyruvate kinase (Q9HSA5); **6**: Transcription initiation factor IIB (Q9HSF7); **7**: 30S ribosomal protein S8e (Q9HPE9); **8**: 30S ribosomal protein S19e (Q9HNP2); **9**: Uncharacterized protein (Q9HS58); **10**: 30S ribosomal protein S3 (P15009); **11**: 30S ribosomal protein S13 (Q9V2W4), 50S ribosomal protein L4 (Q9HPD3), 30S ribosomal protein S3Ae (Q9HRA5), 50S ribosomal protein L32e (Q9HPB7), Serine--tRNA ligase (Q9HNJ8), Peptide chain release factor subunit 1 (Q9HNF0), 50S ribosomal protein L10 (P13553); **12**: 50S ribosomal protein L39e (Q9HMM9); **13**: 50S ribosomal protein

L18e (Q9V2W0); **14:** 50S ribosomal protein L3 (Q9HPD4); **15:** Taxis protein CheF1 (Q9HQX2); **16:** 30S ribosomal protein S7 (P0CX01); **17:** DNA-directed RNA polymerase (P0CX07); **18:** Aminopeptidase (Homolog to leucyl aminopeptidase/ aminopeptidase T) (Q9HSK5), 30S ribosomal protein S9 (Q9HQJ2), 50S ribosomal protein L2 (Q9HPD1); **19:** ABC-type transport system ATP-binding protein(Probable substrate dipeptide/oligopeptide) (Q9HMX3), 2-(3-amino-3-carboxypropyl)histidine synthase (Q9HR56); **20:** 50S ribosomal protein L22 (P15008); **21:** 50S ribosomal protein L10 (P13553), 50S ribosomal protein L15 (P05971), 30S ribosomal protein S12 (P0CX00), Succinate--CoA ligase [ADP-forming] subunit beta (Q9HPP1), 30S ribosomal protein S4 (Q9HQJ6), 50S ribosomal protein L19e (Q9HPB6), Repair helicase (Q9HMB4), Alpha/beta hydrolase fold protein (Q9HRJ0); **22:** DNA protection during starvation protein (Q9HMP7), Translation initiation factor 2 subunit gamma (Q9HMK9), Tubulin-like protein CetZ (Q9HNV2); **23:** Cell division protein FtsZ1 (Q9HS71); **24:** Arginine-tRNA ligase (Q9HHN2). Large, blue circles containing letters represent proteins up-regulated over a period of 42 days of entombment:**a:** Methenyltetrahydromethanopterin cyclohydrolase (Q9HPD7), Lipoate protein ligase (Q9HSK8); **b:** 50S ribosomal protein L13 (Q9HQJ3); **c:** NADH dehydrogenase-like complex subunit 1 (Q9HRL7); **d:** Ornithine carbamoyltransferase, catabolic (Q48296); **e:** V-type ATP synthase beta chain (Q9HNE4); **f:** Adenylosuccinate synthetase (Q9HQM6); **g:** Aminopeptidase (Homolog to leucyl aminopeptidase/ aminopeptidase T) (Q9HMP2); **h:** HD_domain domain-containing protein (Q9HR93), Acyl-CoA dehydrogenase (Q9HRI6); **i:** Glutamate-1-semialdehyde 2,1-aminomutase (Q9HMY8); **j:** PyrE-like protein (Q9HS16); **k:** Protein translation factor SUI1 homolog (Q9HME3); **l:** Elongation factor 1-alpha (Q9HM89); **m:** Pyruvate dehydrogenase alpha subunit (Q9HN77); **n:** Phosphoribosyl transferase (Q9HNW7); **o:** Carbamate kinase (Q48295); **p:** Aconitase (Q9HMF1); **q:** Formyltetrahydrofolate deformylase (Q9HNU0); **r:** V-type ATP synthase alpha chain (Q9HNE3); **s:** Putative dimethyl sulfoxide reductase catalytic subunit A (Q9HR74); **t:** Malate dehydrogenase (Q9HPI2); **u:** Proteasome-activating nucleotidase 1 (Q9HRW6); **v:** Succinate--CoA ligase [ADP-forming] subunit alpha (Q9HPP0); **w:** GNAT family acetyltransferase (Q9HRK6); **x:** HAD superfamily hydrolase (Q9HQE2), GMP synthase [glutamine-hydrolyzing] subunit B (Q9HP33), Probable glycine dehydrogenase (decarboxylating) subunit 2 (Q9HPK0), Bifunctional short chain isoprenyl diphosphate synthase (Q9HSA8), Probable thiosulfate sulfurtransferase (Q9HMT7), Archaeosine synthase (Q9HNT2), DRTGG domain protein (Q9HQY9), Cysteine synthase (Q9HRP3), Succinate--CoA ligase [ADP-forming] subunit alpha (Q9HPP0).

4.3.5.1 Differentially abundant ribosomal proteins

Among the 46 proteins that had significantly lower abundance at T-2 versus T-0, 21 were identified as ribosomal proteins (p-value < 0.05; t-test). This suggests that the ribosomal machinery responsible for the biosynthesis of new proteins is significantly down-regulated, which indicates that the cell is not devoting as much energy for growth and reproduction from T-0 to T-2 (Figure 4.7).

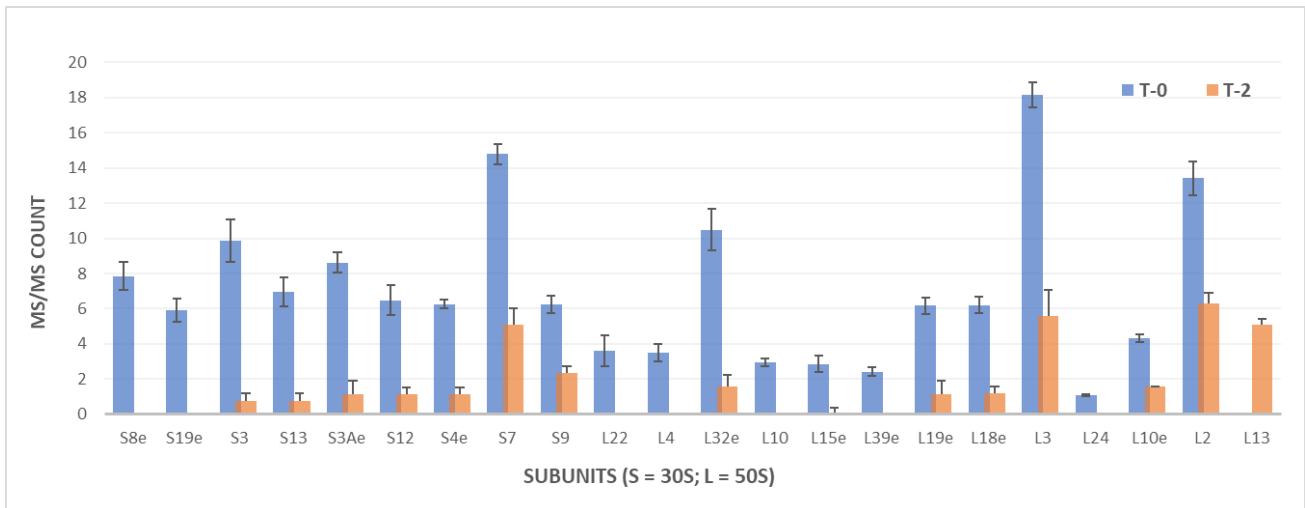


Figure 4.7. Normalised spectral counts of differentially expressed ribosomal proteins compared between T-0 (blue) and T-2 (orange). The mean of four replicates is plotted for the protein spectral counts. The spectral counts plotted all have a p-value < 0.05 and a fold change value ranging between 0.46 and 0.07, except for ribosomal proteins S8, S19e, L22, L4, L10, L15, L39e and L24 where the spectral count in T-2 is zero, and the ribosomal protein L13 that at T-0 has a spectral count of zero, and increases in abundance at T-2.

As the correct RNA folding cannot occur efficiently without these ribosomal proteins, as reported by Ramakrishnan and Moore (2001), these results indirectly suggest that the cells possibly were not growing or might have had slowed down growth. Although the relative abundance of the proteins detected in this experiment was low, collectively for ribosomal proteins 148 spectral counts in T-0, and 34 in T-2, there are proteins that have significantly higher abundance, highlighting that many metabolic activities continue during entombment. In Figure 4.7, it is clear that one ribosomal protein bucks this general trend. The 50S ribosomal protein L13 had significantly higher abundance (T-0 = 0, T-2 = 5.09 spectral counts).

4.3.5.2 Differentially abundant proteins involved in the biosynthesis of new proteins

Among the other proteins that had significantly lower abundance at T-2 (day: 42) versus T-0 (day: -11), and involved in the process of translation, there is the protein Translation Initiation Factor-2 subunit gamma (p-value < 0.05 (t-test) and fold change 0.142) (Figure 4.8).

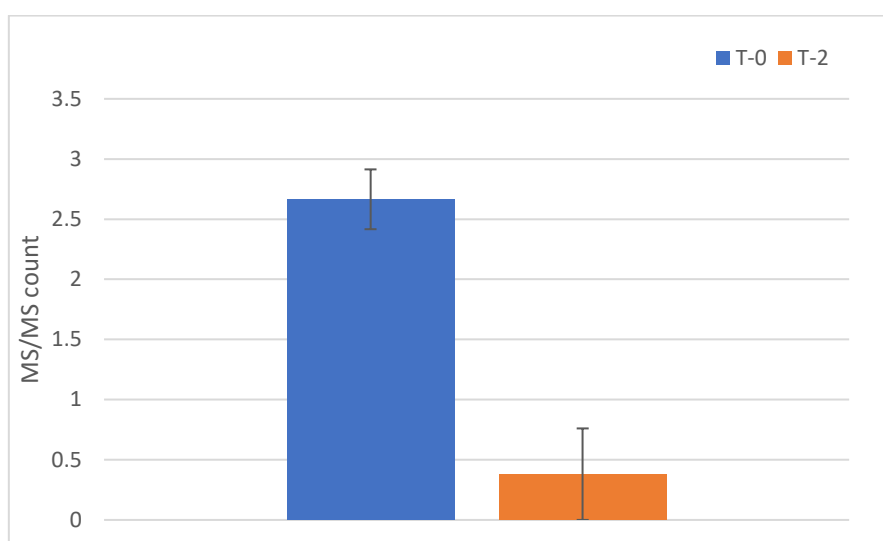


Figure 4.8. Normalised spectral counts of differentially abundant protein Translation initiation factor 2 subunit gamma over a period comprised between optimum growth (T-0) and 42 days entombed in laboratory-made halite. The mean of four replicates is plotted for the protein spectral counts (\pm S.E.). Significance: p -value < 0.05 (t-test) and a fold-change of 0.142).

The protein Translation initiation factor 2 (e/aIF2 – where “e” stands for Eukarya and “a” for Archaea) is composed of three subunits called alpha, beta and gamma. The genes are respectively coded by *SUI2*, *SUI3* and *GCD11*. The protein aIF2, together with GTP and methionylated initiator tRNA, binds to the small ribosomal subunit. It is in fact this initiation factor that delivers the Met-tRNA_i^{Met} and therefore responsible for the beginning of translation (Benelli et al., 2017; Schmitt et al., 2010). The subunit gamma is at the core of the entire structure of aIF2, and it is also responsible for binding GTP. If gamma is not present, the interaction between the subunits alpha and beta does not occur. In this dataset, The alpha and beta subunits have decreased from T-0 to T-2 but not significantly.

In the same comparison (T-0 and T-2), another protein involved in the translation process that was found to have significant lower abundance over time is the protein Peptide Chain Release Factor subunit 1 (p -value < 0.05 (t-test), spectral counts = 0 in T-2) (Figure 4.9). This protein acts as a codon-specific release factor (RF) and is part of the release factor class I, therefore its role is to recognize the stop codon in the aminoacyl site (A site) of the ribosome and catalyses the hydrolysis of the peptidyl-tRNA.

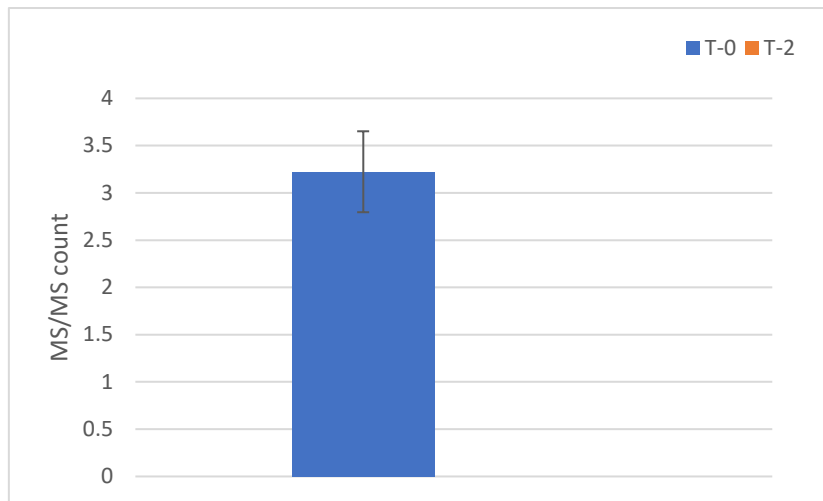


Figure 4.9. Normalised spectral counts of differentially expressed protein Peptide chain release factor 1 over a period comprised between optimum growth conditions and 42 days entombed in laboratory made Halite. The time points compared are T-0 (aerobic growth conditions) and T-2 (Entombment >42 days). The mean of four replicates is plotted for the protein spectral counts (\pm S.E.), p -value <0.05 (t-test), T-2 value is zero).

4.3.5.3 Up-regulation of enzymes involved in the fermentative arginine degradation

Enzymes involved in the fermentative arginine degradation were more abundant in T-2 compared to T-0 (Figure 4.10). Ornithine carbamoyltransferase and the carbamate kinase were significantly more abundant in T-2 compared to T-0, and the arginine deiminase was higher too, but not significantly. Overall, these results indicate that the organism might activate this pathway to produce ATP molecules, as for each arginine there is the production of a molecule of ATP (Ruepp and Soppa 1996). It should be noted that even at T-0, there is a relatively high abundance of these proteins, suggesting that even under apparently aerobic conditions, *Hbt. salinarum* may be carrying out arginine fermentation. In addition to the three enzymes involved in this pathway, I also found significantly higher abundance in T-2 of the Arginine t-RNA ligase, the enzyme responsible for the charging of the tRNA with its respective amino acid. Although not directly involved in the fermentative arginine degradation, the higher abundance in T-2 of this enzyme, might indicate that the organism is devoting the amino acid for the production of energy rather than the biosynthesis of proteins.

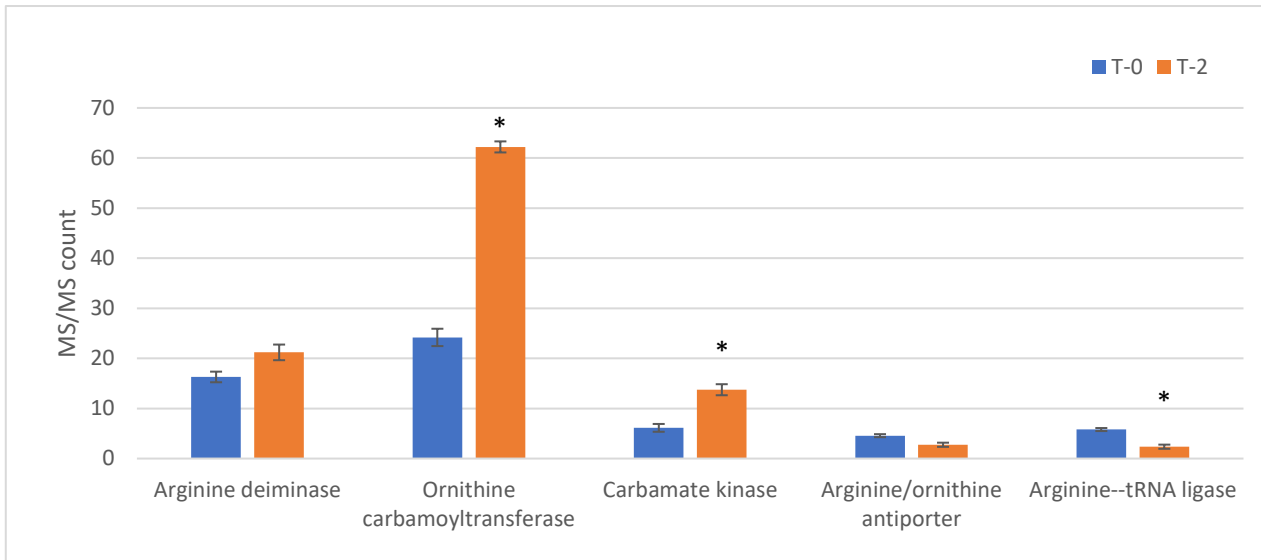


Figure 4.10. Normalised spectral counts of differentially abundant proteins involved in the fermentative arginine degradation and two additional proteins that are involved in arginine utilization, Arginine/Ornithine Antiporter (A/O antiporter) and the Arginine-tRNA ligase (A-tRNA, fold change = 0.40). The latter are less abundant in T-2, whereas the three enzymes arginine deiminase (ADI), carbamate kinase (CK, fold change = 2.24) and catabolic ornithine transcarbamylase (OTC, fold change = 2.57) are more abundant. The mean of four replicates is plotted for the protein spectral counts (\pm S.E.). * Indicates p -value < 0.05 (t-test).

4.3.5.4 Use of alternative electron acceptors

The enzyme DMSO reductase had significantly higher abundance in T-2 compared with T-0, with a fold change value of 1.81 (Figure 4.11). This enzyme catalyses the reduction of dimethyl sulfoxide (DMSO) to dimethyl sulphide (DMS) during anaerobic respiration, but can use as substrate also trimethylamine N-oxide (TMAO) (Müller and DasSarma 2005). The beta subunit of this enzyme is proposed to be involved in electron transfer, confirming its role as an alternative terminal electron acceptor (Müller and DasSarma 2005; Oren 2013). Müller and DasSarma (2005) demonstrated that is the absence of the oxygen, and not the presence of either DMSO or TMAO, that induces the *dms* gene cluster and that *dmsR*, one of the gene in the cluster, may respond directly to changing oxygen concentrations. The higher abundance of this protein might indicate that the oxygen levels in the fluid inclusions are triggering the transcription of the *dms* gene cluster. This is a different scenario compared to the fermentation (e.g., arginine fermentation), where, primarily, the process is induced by decreasing oxygen concentrations, but can still occur in the presence of oxygen.

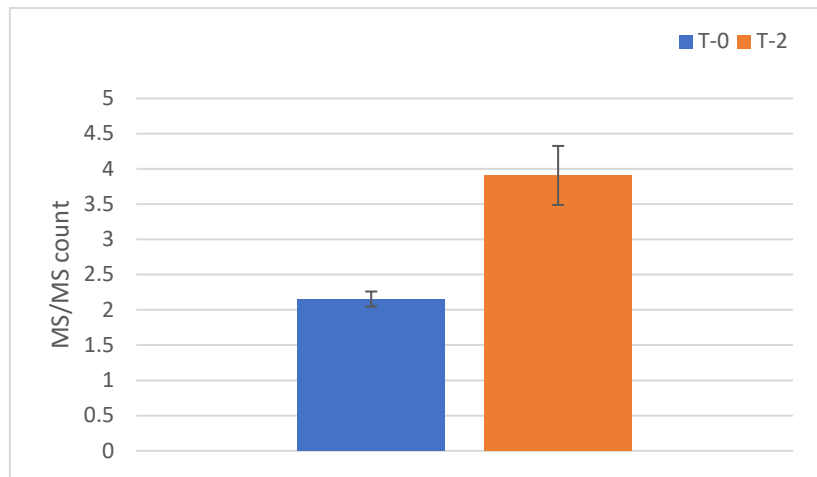


Figure 4.11. Normalised spectral counts of differentially expressed protein Putative dimethyl sulfoxide reductase iron-sulfur subunit B. This protein is significantly higher abundant in T-2, p-value < 0.05 (t-test) and fold change = 1.81. The mean of four replicates is plotted for the protein spectral counts (\pm S.E.).

4.3.5.5 Other proteins significantly differentially abundant after 42 days of entombment

Cell division protein FtsZ1 was significantly lower abundant in *Halobacterium salinarum* NRC-1 when entombed in fluid inclusions for 42 days (Figure 4.12). The protein Cell division protein FtsZ1 is an essential cell division protein that forms the so-called Z ring, a contractile structure at the division site of the dividing cell (Liao *et al.* 2021; Wang and Lutkenhaus 1996; Bernander and Ettema 2010). This result might indicate that the cell is actively reducing the rate of cellular division, by decreasing the relative abundance of the protein FtsZ1, one of the first molecule to assemble at the division site. Importantly, this protein specifically binds GTP, therefore, by reducing the relative abundance of FtsZ1, the organism might modulate the rate of cellular division and avoid unnecessary utilisation of high-energy molecules like GTP. We detected also the protein Cell division protein FtsZ2, and in the comparison between T-0 and T-2 it was found to be higher, however, not significantly. Liao *et al.*, (2021) found that in *Haloferax volcanii* the cell division cannot be performed properly without the interaction of the two proteins FtsZ1 and FtsZ2, therefore a down-regulation of FtsZ1 impacts the interaction with FtsZ2, affects the rate of cellular division, and avoids unnecessary GTP expenses.

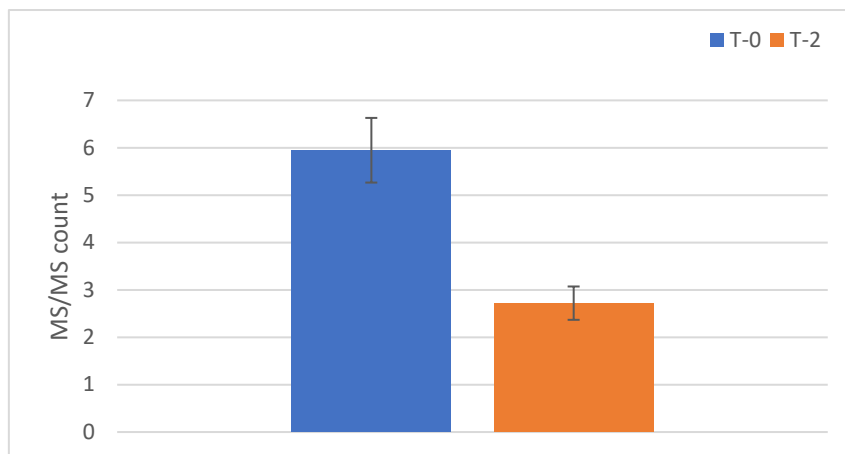


Figure 4.12. Normalised spectral counts of differentially expressed cell division protein FtsZ1. This protein is significantly lower abundant in T-2 compared to T-0. The mean of four replicates is plotted for the protein spectral counts (\pm S.E.). Significance: p -value < 0.05 ; fold-change: 0.45.

Interestingly, the protein DNA-directed RNA polymerase subunit A also had lower abundance in T-2 compared to T-0 (Figure 4.13). Transcription in Archaea has been defined as a hybrid of Eukarya and Bacteria (Bell and Jackson 1998), and RNA polymerases (RNAPs) are composed by multiple subunits, among which, the subunit A found in this experiment. Since its relative abundance was significantly lower in T-2, it is possible to speculate that there is a down-regulation also of the transcription process. Additionally, another protein involved in the transcription, namely the protein Translation initiation factor IIB 7 was also found lower abundant in T-2 compared to T-0, in line with the hypothesis that the transcription process is down-regulated (Figure 4.14).

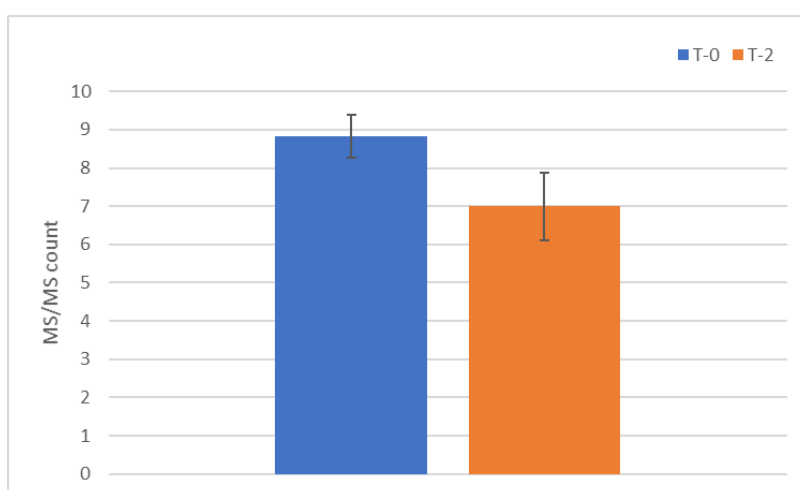


Figure 4.13. Normalised spectral counts of differentially expressed protein DNA-directed RNA polymerase subunit A. This protein is significantly lower abundant in T-2 compared to T-0. The mean of four replicates is plotted for the protein spectral counts (\pm S.E.). p -value < 0.05 ; fold-change: 0.35.

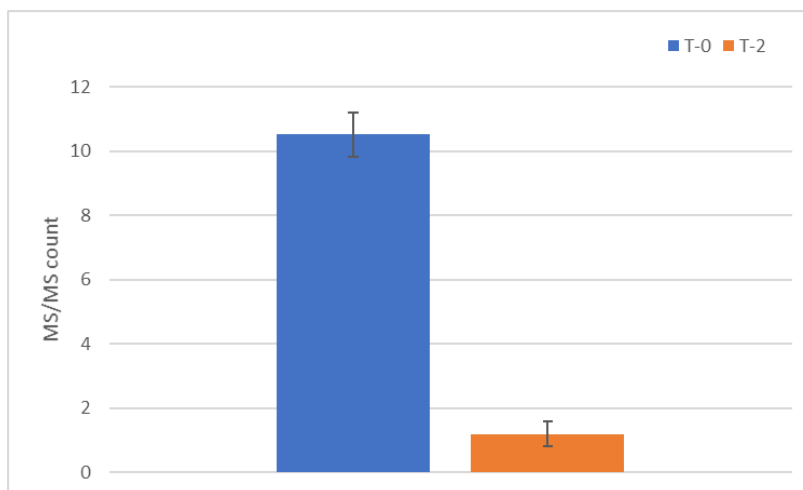


Figure 4.14. Normalised spectral counts of differentially expressed protein Transcription initiation factor IIB 7. This protein is significantly lower abundant in T-2 compared to T-0. The mean of four replicates is plotted for the protein spectral counts (\pm S.E.), p -value < 0.05 ; fold-change: 0.11.

4.3.6 Contamination by *Natrinema* sp.

During the proteomics analysis, contamination by another Haloarchaea was found in the samples. Following the methods described in Chapter 2, the two growing isolates were indicated as “dark red colonies” and “light orange colonies” (Figure 4.15). The 16S rRNA gene sequence analysed was then analysed: the dark red colonies had 100% 16S rRNA identity to *Halobacterium salinarum* NRC-1 studied in this experiment, and *Halobacterium salinarum* 91-R6, and the light orange colonies were 100% similar to *Natrinema pallidum* and *Natrinema altunense* (Figure 4.16).



Figure 4.15. Colonies on solid media (20% NaCl modified Payne) of two different colours, “dark red colony” on the left that is *Halobacterium salinarum* NRC-1 and “orange light colony” on the right that is *Natrinema* sp.

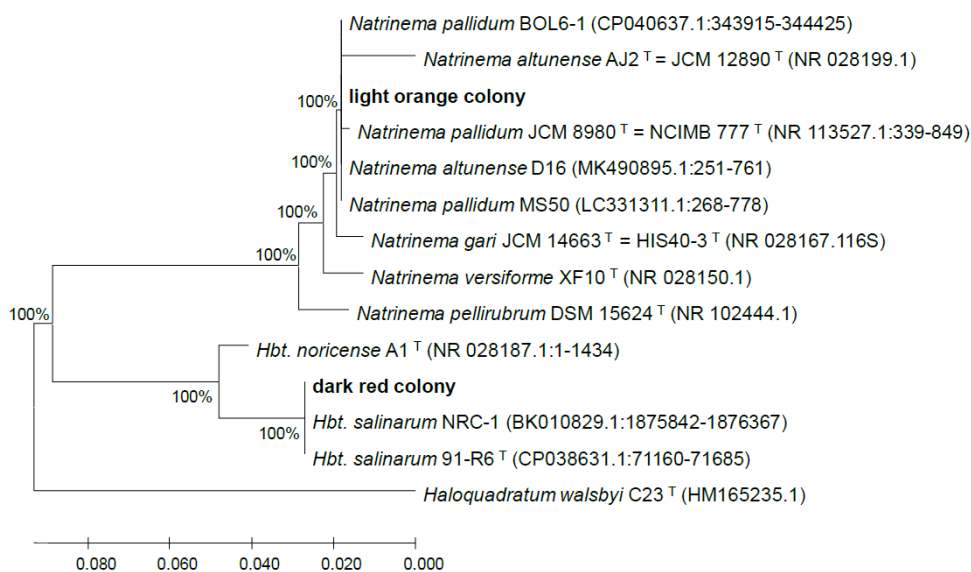


Figure 4.16. Neighbour-Joining phylogenetic tree based on the 16S rRNA sequence (primers used: 515F (Parada et al., 2016) and 806R (Aprill *et al.* 2015), obtained from the “light orange colony” and “dark red colony”. The phylogenetic tree was generated from a MUSCLE alignment of the sequences. The neighbour-joining method was used and the evolutionary distances were computed using the Kimura 2-parameter method in MEGA7 software (Kumar et al., 2016). The phylogenetic analysis was performed by Nora Georgiev (Georgiev, 2020).

4.4 Discussion

4.4.1 Differentially abundant proteins involved in the biosynthesis of new proteins

Ribosomal proteins, together with rRNA and translation factors, orchestrate the mRNA-directed protein biosynthesis. Each of these factors has different functions and they are regulated throughout the entire process. The ribosomes, constituted by ribosomal proteins and rRNA, undergo important conformational rearrangements both between the two subunits and within each subunit (Ramakrishnan and Moore 2001). As reported in Table 4.1, each ribosomal protein has a specific role, some of which are still unclear. In this experiment, the majority of the ribosomal proteins that are responsible for stabilizing the tertiary structure of the RNA in the ribosomal architecture (Ramakrishnan and Moore 2001) had significantly lower abundance, along with other ribosomal proteins with a diverse array of functions, summarized in Table 4.1. The expression of ribosomal

proteins is tightly co-regulated and responds collectively to a variety of nutritional and environmental stimuli (de la Cruz *et al.* 2018): in this study, the authors highlight the fact that the assembly of the ribosomal subunits, and the transcription of the respective genes, are highly interdependent and do not happen simultaneously. Therefore, the lower abundance of ribosomal proteins, crucial for the correct folding of the rRNA, is enough to compromise the entire ribosomal functional structure, resulting in deceleration of translation efficiency, which in turn, results in a low-rate cell division.

Table 4.1 Summary of ribosomal proteins and their role in translation. In bold, ribosomal proteins significantly differentially expressed in this experiment (comparison T-0 – T-2). Other ribosomal proteins known to be important for the RNA folding, but not statistically significant in this experiment, are: S10, S11, S17, L21e, L37e and L44e.

Detected in this experiment (p-value > 0.05) in the comparison T0 versus T2	Function	Reference
S9; S13	Tendrils contact P-site-bound tRNA	
S10; S11; S17	Not specified	Ramakrishnan and Moore, 2001
S12	Binds mRNA and IF factors	
S19		
S3; S3Ae	Binds mRNA and IF factors	
S4; S7	Repressors in the regulation of ribosomal protein synthesis (in E. coli)	Maguire and Zimmermann, 2001
S4	Binds mRNA and IF factors	
S8e		
L2; L3; L4	Presumably required to maintain the conformation of the rRNA at the active site	
L2; L3; L4; L15	Transfers peptide to aminoacyl-tRNA	
L2	Binds fMet-tRNA and peptidyl-tRNA	Ramakrishnan and Moore, 2001
L3	Helps form a constriction in the tunnel from the peptidyl-transferase site	
L19; L39e	Not specified	
L21e; L37e; L44e	Not specified	
L18e; L24	Binds fMet-tRNA and peptidyl-tRNA	
L22	Helps form a constriction in the tunnel from the peptidyl-transferase site	Maguire and Zimmermann, 2001
L10; L10e; L32e	Not specified	
L13	Might be involved in regulation of transcription	Mazumder et al., 2003

Against this trend of lower abundance, the ribosomal protein L13 was significantly more abundant at T-2 compared to T-0. In the model proposed by Mazumder *et al.* (2003) for Eukarya, when L13a is integrated in the 60S ribosomal subunit, the efficiency of the translation is enhanced. The phosphorylation of L13a leads to its release from the ribosome, and it binds, possibly in a complex with auxiliary proteins, and silences translation. In this model, the ribosome functions not only as a protein synthesis machine, but also as a depot for regulatory proteins that modulate translation. Based on the similarities that Archaea share with Eukarya (Dennis 1997; Benelli *et al.*, 2017; Schmitt *et al.* 2020, and references therein), especially at the initiation step of the translation process (Schmitt *et al.*, 2010), L13a studied by Mazumder and colleagues (2003) and L13 found in *Halobacterium salinarum*, might have similar functions. According to the model proposed by Mazumder *et al.* (2003) there are four possible mechanisms for translational silencing: 1) inhibiting function of one or more components of the cap-binding complex (a structure found at the 5' end of eukaryotic mRNA), eIF4F; 2) blocking recruitment of the 43S pre-initiation complex; 3) preventing scanning of the 43S complex to the initiation codon; 4) blocking 60S ribosomal subunit joining. This modification activates the 50S ribosomal protein L13 to bind a mRNA structure (possibly together with other co-factors) and lead to different scenarios summarized in Figure 4.17, that eventually, individually or concurrently, affects negatively the translation efficiency (see Conclusions for future perspectives).

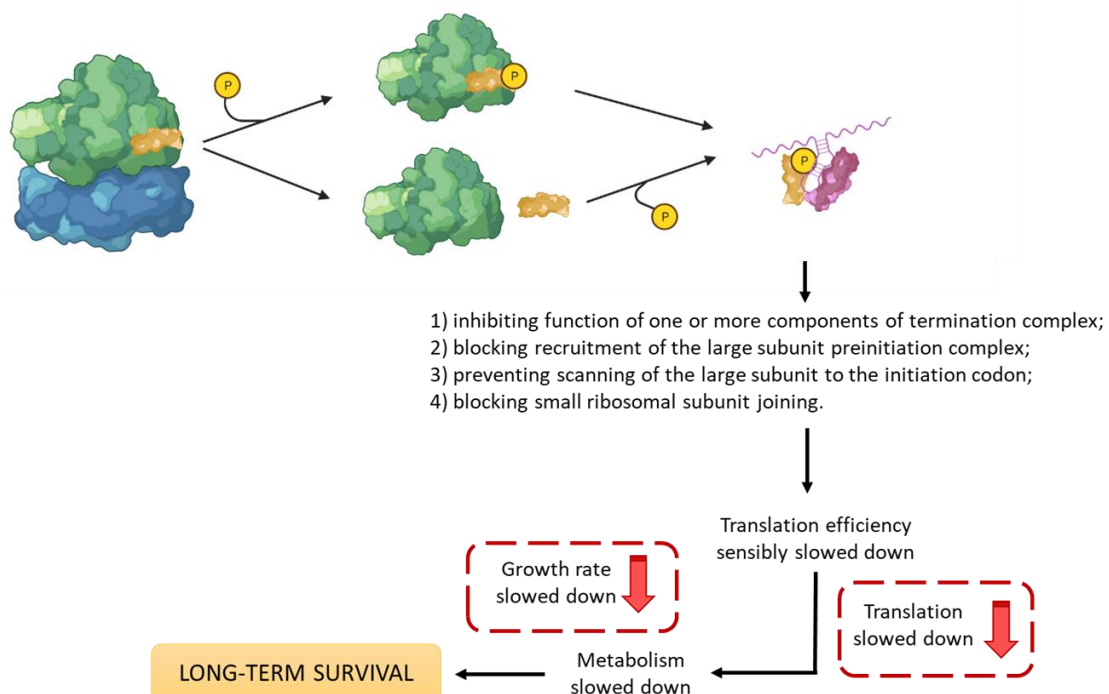


Figure 4.17. Proposed model for the regulation of translation by the ribosomal protein L13. In the model proposed by Mazumder *et al.* (2003), the ribosome functions also as a depot for regulatory proteins that modulate translation. This figure was created in BioRender.

The initiation step, similar in Archaea and Eukarya, is characterized by many different factors, finely regulated, among which the protein Translation initiation factor 2 (a/eIF2), composed by alpha, beta and gamma subunits. The gamma subunit, which significantly decreased in abundance from T-0 to T-2, is responsible for binding the methionylated tRNA and GTP. The alpha and beta subunits, which showed no significant difference from T-0 to T-2, provide the protein aIF2 its full tRNA binding affinity, and contributes in small part to the overall stability of the heterotrimeric protein, respectively (reviewed in Schmitt *et al.*, 2010). The decrease in gamma subunit might indicate an efficient mechanism that regulates the biosynthesis of new proteins: the translation process is slowed down at the upstream level. By regulating the relative abundance of the gamma subunit, that is responsible for the correct pairing between the initiation codon and the initiator tRNA anticodon and the hydrolysis of GTP, *Halobacterium salinarum* may modulate the initiation step of the translation. In addition, the regulation of the sole subunit that has GTPase activity avoids unnecessary coupling of GTP (high energy content molecule) with the gamma subunit, therefore, limiting the consumption of energy. Although the number of spectral counts was low, these results indicate that there may be an active modulation of the physiology, with downstream consequences that eventually may lead to the long-term survival (Figure 4.18). Previous studies reported that the genes coding for the three subunits of eIF2 were vital for yeast cell viability (Donahue *et al.* 1988; Hannig *et al.* 1993). However, further studies have shown that deletion mutation in *GCD11* (GCD: general control depressed) altered the translation efficiency at the transcription activator *GCN4* (GCN: general control non-inducible) AUG codon (Benelli *et al.*, 2017; Schmitt *et al.*, 2010), meaning that the gamma subunit has an independent role from alpha and beta in *Saccharomyces cerevisiae* (Hannig *et al.* 1993). Another study reported a slow-growth phenotype in *S. cerevisiae* related to a mutation in the gene coding for the gamma subunit (Erickson *et al.* 2001). Experiments by Schmitt *et al.* (2010) confirmed the role of the protein Translation initiation factor aIF2 in delivering Met-tRNA_i^{Met} to the ribosome, and also for selecting the correct translation start site (Schmitt *et al.*, 2010). Once the assemblage between aIF2, the initiation codon and the initiation tRNA anticodon is correct, GTP-bound to e/aIF2 is hydrolysed irreversibly. The protein e/aIF2-GDP subsequently dissociates from the initiator tRNA and from the ribosome. The 60S ribosomal subunit joins (the reaction is catalysed by eIF5B, and the elongation

step begins) (Schmitt *et al.* 2020; Schmitt *et al.*, 2010). It is the irreversible GTP hydrolysis on e/aIF2 that controls the accuracy of the translation initiation process, preventing initiation at non-AUG codons. In Eukarya, eIF2B is responsible for the regeneration of GTP on eIF2-GDP, thereby recycling the activity of the protein and so promoting the rate of the translation initiation and cell growth (Schmitt *et al.*, 2010). So far, equivalent of the catalytic subunit of eIF2B has not been found in Archaea; it is thought that the GTP recycling on aIF2 is likely to occur spontaneously (Schmitt *et al.* 2020).

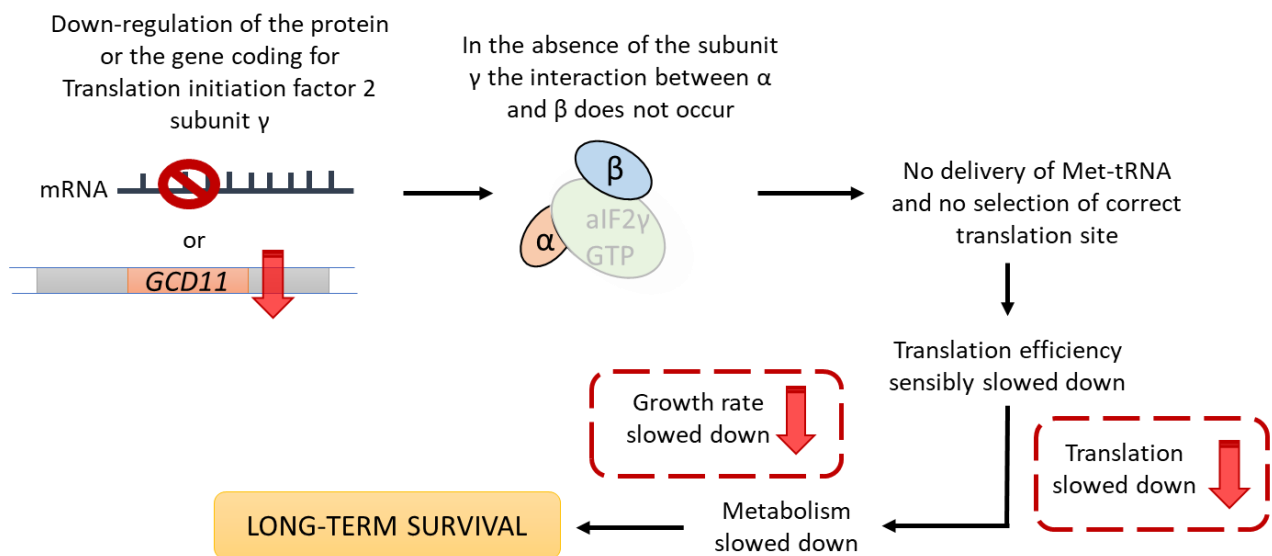
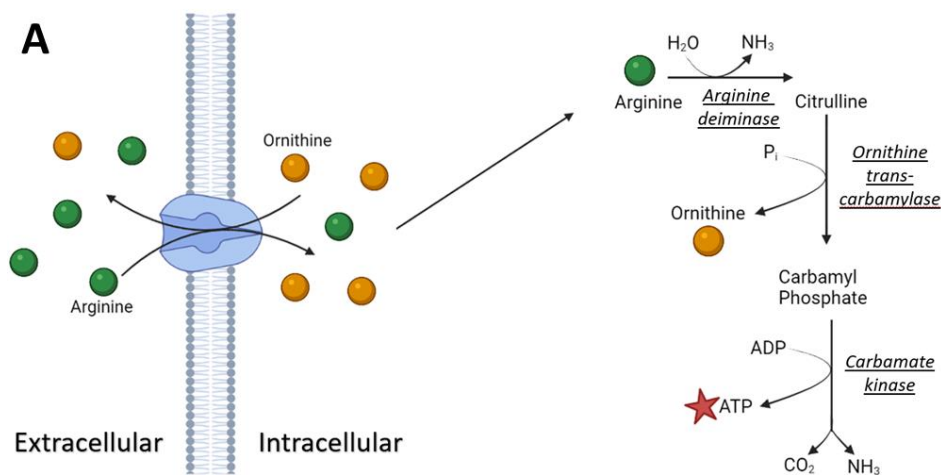


Figure 4.18. Proposed reactions explaining the lower abundance found in T-2 of the product of the *GCD11* gene coding for the gamma subunit of the protein aIF2 (Translation initiation factor 2), The heterotrimeric protein cannot be assembled in the absence of the gamma subunit, causing a decrease in translation efficiency that results in a slow-growth phenotype. The selective down-regulation of the gene *GCD11* or the down-regulation of the protein expression may lead to the long-term survival. This figure was created in BioRender.

4.4.2 Up-regulation of enzymes involved in the fermentative arginine degradation

In this experiment, enzymes involved in the fermentative arginine degradation were found to be significantly more abundant at T-2 compared to T-0 (Figure 4.10), namely the ornithine carbamoyltransferase and the carbamate kinase. The arginine deiminase was higher too, but not

significantly. Generally, in organisms able to perform the arginine deiminase pathway, the different concentration of arginine/ornithine at the two sides of the membrane is the driver to the activation of this pathway, and it has been proposed that the presence of the arginine/ornithine antiporter helps to control the levels of these two amino acids at the two sides of the membrane (Poolman et al., 1987). Since the nutrients from the medium were removed (see Methodology section of this chapter), it is possible to speculate that the arginine that *Hbt. salinarum* NRC-1 might be using to produce energy via the fermentation, comes from the intracellular milieu (Figure 4.19). To support this hypothesis, the lower abundance of the Arginine tRNA ligase in T-2 might be an indication that the organism is using the amino acid to produce ATP (via the fermentation of arginine) rather than making new proteins. This is a matter of speculation as it is not known what the mechanisms for intracellular regulation of ornithine and arginine are in this case, and whether or not the arginine deiminase pathway activates independently from the intracellular levels of these two amino acids. The arginine not used for the biosynthesis of new proteins (down-regulation of the Arginine-tRNA ligase), can enter in the arginine fermentation pathway, that eventually will allow the organism to have one molecule of ATP for each molecule of arginine used. The lower abundance, although not significant, of the arginine/ornithine antiporter might indicate that there might be alternative ways to accumulate arginine intracellularly. Furthermore, the lower abundance of the Arginine-tRNA ligase in T-2 is also consistent with the findings that the translation process is slowed down (See section 4.3.5).



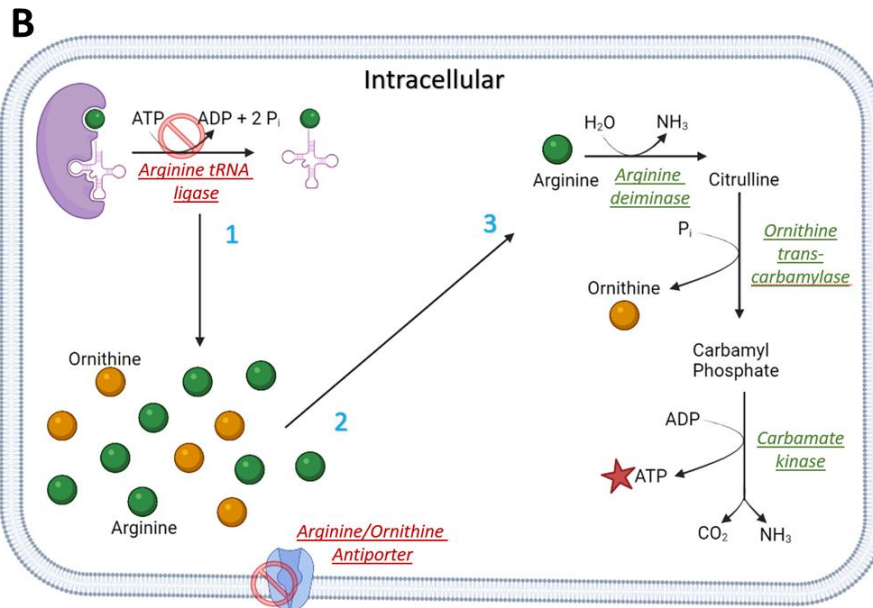


Figure 4.19. Schematic view of the arginine deiminase pathway (A) and a proposed model for the arginine deiminase pathway occurring at the intracellular level in *Halobacterium salinarum* NRC-1 entombed for 42 days in fluid inclusions with no nutrients (B). (A) On the two sides of the membrane there is a different concentration gradient of arginine (extracellular) and ornithine (intracellular). This different gradient is the driver to the extracellular release of ornithine and the concomitant intracellular uptake of arginine. The arginine deiminase pathway results in the formation of a molecule of ATP and the high intracellular ornithine pool is maintained through the reaction guided by the Ornithine transcarbamylase, that, together with a phosphate group, catalyses the formation of ornithine and carbamyl-phosphate starting from citrulline. (B) In *Halobacterium salinarum* entombed for 42 days in fluid inclusions with no additional nutrients, the arginine is accumulating intracellularly through a different mechanism: (B1) the enzyme Arginine-tRNA ligase is significantly down-regulated, therefore the arginine is not used to synthesize new proteins, instead, it accumulates intracellularly; (B2) the enzyme involved in the formation of the arginine/ornithine antiporter is significantly down-regulated, therefore, the intracellular pool of these two amino acids must be controlled intracellularly, however, it is not known which are the mechanisms maintaining the balance, if present. The arginine not used for the biosynthesis of new proteins, can enter in the arginine deiminase pathway, that eventually will allow the organism to have one molecule of ATP for each molecule of arginine. This figure was created in BioRender.

4.4.3 Use of alternative electron acceptors

In this experiment, the alpha and beta subunit were both more abundant at T-2 compared to T-0, however, only for the alpha subunit was the increase statistically significant (Section 4.3.5.4). Several Haloarchaea can use dimethyl sulfoxide (DMSO) and trimethylamine-*N*-oxide (TMAO), nitrate and

to some extent fumarate, as alternative terminal electron acceptor (Oren and Trüper 1990; Müller and DasSarma 2005; Gruber *et al.* 2004). There are many enzymes belonging to the DMSO reductase family, including DMSO reductase, TMAO reductase, Nitrate reductase and Perchlorate reductase. The atom that coordinates the cofactor determines the type of protein (Miralles-Robledillo *et al.* 2019). In the DMSO reductase, the genes transcribing for the alpha (catalytic) and beta (electron transfer) subunits are co-transcribed in the same operon (Müller and DasSarma 2005). A typical feature of DMSO and TMAO reductase from halophilic microorganisms is that the aspartate coordinates the cofactor: interestingly, when looking at the sequence of the protein DMSO reductase detected in this experiment, DmsA has its own branch (Miralles-Robledillo *et al.* (2019). This, on one hand confirms that the protein detected is DMSO reductase, on the other, that *Halobacterium salinarum* NRC-1 can use both DMSO and TMAO as substrate, which might be the reason why this protein shows some evolutionary distinctiveness. As reported by Müller and DasSarma (2005), the *dms* operon is induced during anaerobic respiration, and the absence of a terminal electron acceptor (e.g., oxygen) is essential to activate the operon. The significant increase of the DMSO reductase alpha subunit over time might indicate that the levels of oxygen are decreasing, resulting in the activation of the operon, which is consistent with the increase in proteins involved in arginine fermentation (Section 4.4.2).

4.4.4 Other proteins significantly differentially expressed during the entombment

The results show that the cell-division protein FtsZ1 is significantly less abundant in T-2 compared to T-0. This protein is essential in forming the so-called Z ring, a contractile structure at the division site of the dividing cell (Liao *et al.* 2021; Wang and Lutkenhaus 1996; Bernander and Ettema 2010). FtsZ1 is among the first molecules to assemble at the division site, and among the most conserved cell division protein in bacteria (de Boer *et al.*, 1992). This tubulin-like protein, is localized on the site where the division constriction starts, and has been found in *Haloferax volcanii*, indicating is conserved also in Archaea (Wang and Lutkenhaus 1996). de Boer *et al.* (1992) found that the protein FtsZ specifically binds and hydrolyses GTP, therefore the bond between FtsZ and GTP is necessary to enable the cell division. The results of the same study showed that it is the cellular concentration of FtsZ that regulated the frequency of division, and not the GTP concentration. In fact, FtsZ is also a target for several division inhibitors (de Boer *et al.*, 1992, and references therein). This can explain its down-regulation during the 42 days entombed in halite; in order to reduce the rate of cellular

division, the down-regulation of the FtsZ1, one of the first molecule to assemble at the division site, and most importantly, specifically binds GTP, is a very effective and efficient way to modulate the rate of cellular division and avoid unnecessary utilisation of high-energy molecules like GTP. Additionally, Liao *et al.* (2021) found that in *Haloferax volcanii* cell division cannot be performed properly without the interaction of the two proteins FtsZ1 and FtsZ2, therefore a down-regulation of FtsZ1 impacts the interaction with FtsZ2, affects the rate of cellular division, and avoids unnecessary GTP expenses. The protein FtsZ2 was also detected, however its difference in relative abundance was not significant. One explanation for this might be that, since it is FtsZ1 the protein binding GTP, *Hbt. salinarum* NRC-1 might actively modulate its relative abundance, and indirectly, avoid GTP usage. The significantly lower abundance of the protein DNA-directed RNA polymerase subunit A and on the Translation initiation factor IIB 7, add to the hypothesis that the cell division rate might be slowed down, as these proteins are among the essential proteins involved in transcription.

4.5 Conclusions

The set-up of this experiment allowed us to use proteomics analysis as a window of the metabolic activities of *Halobacterium salinarum* NRC-1 when entombed inside fluid inclusions of halite (Figure 4.20 right).

There were limitations in this experiment, these relate to the low biomass retrieved from the lab-made halite crystals and the contamination by *Natrinema* sp.; for these reasons, the results in this experiment should be considered as indications of the modifications happening in the proteome of the analysed species, and they should be confirmed in the future. Some findings are very clear, *e.g.* reduced activity whereas others need further proteomic analysis and further testing by other means. Based on the results and limitations of this experiment, I carried out another experiment, where also additional questions were asked (Chapter 5). Nevertheless, these results provide new insights into the ability of this species to modulate its physiology, and can be used to understand what lies at the base of their longevity.

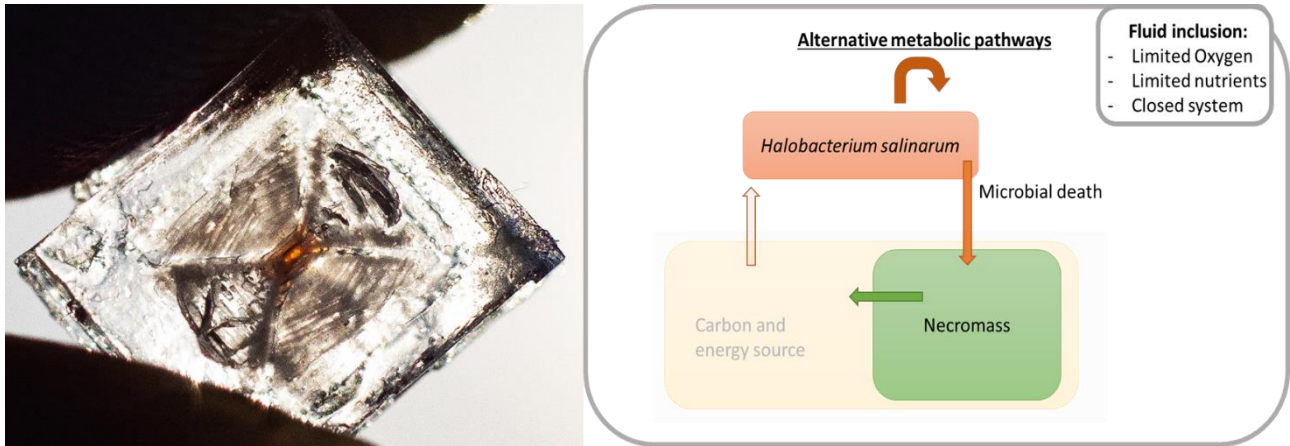


Figure 4.20. (Left) Halite crystal with red colouration in the middle due to high abundance of cells of *Halobacterium salinarum* NRC-1. It is also possible to clearly distinguish the primary fluid inclusions banding in chevron halite, as previously described by Benison and Goldstein (1999). (Right) Scheme representing a fluid inclusion with the set-up of this experiment, where cells of *Halobacterium salinarum* were entombed in fluid inclusions of lab-made halite, after all the nutrients and leftovers from the growing media were washed away.

Table 4.2. List of the findings of this experiment discussed in this chapter. The listed proteins are all statistically differentially expressed (p-value: < 0.05). The comparison is between the first time point (T-0) and the last time point (T-2). This comparison was chosen in order to understand the changes happening between optimum growth conditions and 42 days inside fluid inclusions of lab-made halite crystals.

Protein (s)	Relative abundance in T-2 compared to T-0	Function
Ribosomal proteins (20)	Lower	Stability and functionality of the ribosome
Ribosomal protein L13	Higher	Probable regulatory protein for translation
Translation initiation factor 2 subunit gamma	Lower	Binds GTP, together with other two subunits, it is responsible for the initiation of the translation
Peptide chain release factor subunit 1	Lower	Codon-specific release factor, involved in the termination of the translation using ATP
Ornithine transcarbamoylase; Carbamate kinase	Higher	Involved in the fermentation of the arginine, a pathway that produces energy
Arginine tRNA ligase	Lower	Involved in the biosynthesis of new proteins

Putative DMSO sulfoxide reductase	Higher	Alternative terminal electron acceptor
Cell division protein FtsZ1	Lower	Essential cell division protein, also involved in the shape of the cell, binds GTP
DNA-directed RNA polymerase subunit A	Lower	Essential protein for the correct assemblage of the RNA polymerase
Transcription initiation factor IIB 7	Lower	Essential transcription factor involved in the initiation step

Translation and protein biosynthesis are essential for cell growth and division, however, the synthesis of proteins true to the information present on the mRNA requires energy. Many reactions require high-energy phosphate groups; at the initiation step, the subunit gamma of the translation initiation factor 2 (aIF2) consume one GTP for every new protein (Schmitt *et al.* 2020), for each aminoacyl-tRNA there is the consumption of two high-energy phosphate groups, during the elongation step, there is GTP consumption for the formation of each peptide bond of a newly-synthetising protein, and ATP is consumed every time an amino acid is incorrect (David and Cox, 2017), at the termination step there is also consumption of ATP, to release the protein and dissociate the ribosome. If we consider the error rate of the ribosome, the estimates in prokaryotes are 10^4 , compared to the 10^8 of the DNA polymerase (Ninio 1991). The results in this experiment highlight the possibility that translation happens with the regulation of specific proteins and enzymes, ensuring a cascade effect, that eventually results in efficient energy utilization, maintenance of cellular functions, and possibly, long-term survival (summarized in Figure 4.21).

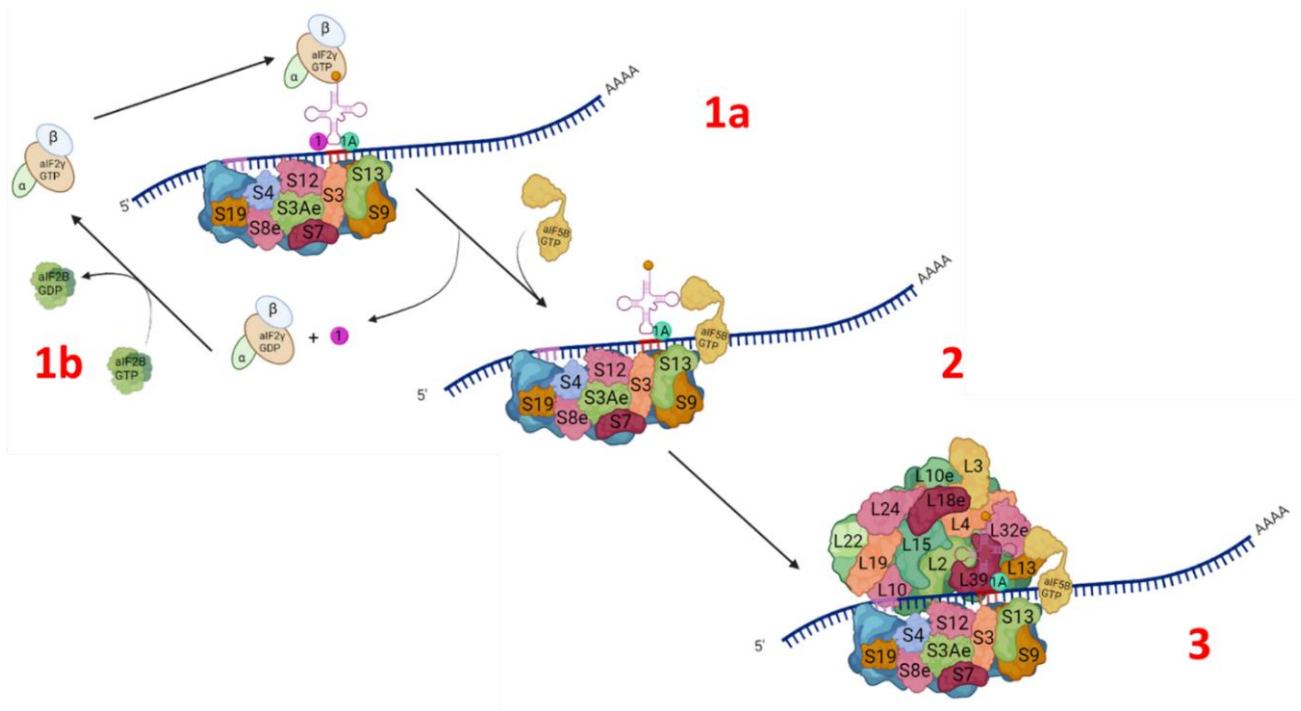


Figure 4.21. Model summarizing the initiation step of the translation. The 30S subunit of the ribosome, together with the first tRNA attached to aIF2, scans the mRNA until the start codon is found, subsequently, the ribosome sits such that the P site is located on the start codon, thanks to the base-pairing with the tRNA anticodon (1A) aIF1 and aIF1A participate in accuracy of start codon selection. When the codon and anticodon are paired, GTP-bound to aIF2 is hydrolysed irreversibly. The protein aIF2-GDP subsequently dissociates from the initiator tRNA and from the ribosome. The protein aIF2B, although not clear, might be a guanine nucleotide exchange factor, that will recycle aIF2 and aIF1 (1B). The initiation factor aIF5B is recruited to facilitate joining of the large ribosomal subunit (2). After the 60S ribosomal subunit joins, a reaction is catalysed by eIF5B, aIF1A and aIF5B are released and the elongation step begins (3). Modified from (Schmitt *et al.*, 2020). The ribosomal proteins highlighted in the ribosome were detected in this experiment, and with the exception of L13, they were all found to be significantly down-regulated. This figure was created in BioRender.

The hypothesis that NRC-1 is actively modulating its metabolic activities, is also supported by the modulation of the relative abundance of proteins binding high energy compounds, namely ATP and GTP. This might indicate that an adaptation to avoid unnecessary use of energy exists.

Liao and colleagues (2021) found that low abundance of the protein FtsZ1 correlates with a slow growth rate in *Haloferax volcanii*. The same study also reported that FtsZ1 influences the cell shape, which might be involved in the phenomenon observed by Winters and colleagues of size reductions and shape transitions from rods to cocci when cells of *Halobacterium salinarum* were starved

(Winters *et al.*, 2015). This, from an ecological perspective, is an advantage, as the conversion from rods to cocci and a decreased cell size allow a greater surface to volume ratio that optimize the functionality of intracellular communication, and also, the intake of nutrients when these are very low in concentration. The regulation of this protein can be among the physiological modification, finely regulated, that are at the base of the longevity of Haloarchaea.

From a metabolic perspective, the modulation of enzymes involved in the arginine deiminase pathway (ADI), and the higher abundance of the DMSO reductase in T-2, indicate a possible need for an alternative metabolic pathway to produce energy (in the case of ADI), and the need of an alternative electron acceptor (DMSO reductase).

The lag observed by Müller and DasSarma (2005) in the growth rate in cells of *Halobacterium salinarum* moved from aerobic to anaerobic conditions, can also explain why not all the cells are able to rapidly adapt to the limiting availability of oxygen. This lag phase is therefore a crucial step that might be at the basis of which cells among the entire population is able to survive in the fluid inclusions of halite. The DMSO reductase might be preferred to the nitrate reductase (same family of reductases (Miralles-Robledillo *et al.* 2019), as its synthesis requires less energy, which might be preferred in nutrient-depleted conditions.

In the case of the Arginine tRNA ligase, the available data is not sufficient to understand if the activity (or affinity) of this enzyme is influenced by the enzymes involved in the fermentation of arginine, but it is not possible to exclude a connection, direct or indirect.

In a possible scenario, the lack of energy affects the tRNA charging, as for each amino acid charged on the tRNA there is the consumption of ATP. The unsuccessful charging of the Arginine on the tRNA might bring to an intracellular accumulation of arginine, which in turn can be sequestered by the Arginine deiminase, activating the arginine fermentation pathway.

As the aim of this experiment was to mimic the conditions of deposited layers of ancient halite, alternative ways possessed by Haloarchaea to produce energy using the sunlight were not investigated.

In conclusions, the results in this experiment represent, to the best of my knowledge, the first indication of the existence of intrinsic abilities of *Halobacterium salinarum* to actively respond to the fluid inclusion microenvironment; abilities that might explain how they are able to survive over geological time scale, in a nutrient-depleted, oxygen-depleted, high ionic strength, closed system. Lastly, this study can be part of the effort to understand the limit of life on Earth, as the Haloarchaea are living not only at the extreme of salt, but also of time.

4.6 References

- Aivaliotis, Michalis, Boris Macek, Florian Gnad, Peter Reichelt, Matthias Mann, and Dieter Oesterhelt. 2009. 'Ser/Thr/Tyr Protein Phosphorylation in the Archaeon *Halobacterium Salinarum*—A Representative of the Third Domain of Life'. Edited by Ulrich Dobrindt. *PLoS ONE* 4 (3): e4777. <https://doi.org/10.1371/journal.pone.0004777>.
- Apprill, Amy, Sean McNally, Rachel Parsons, and Laura Weber. 2015. 'Minor Revision to V4 Region SSU RRNA 806R Gene Primer Greatly Increases Detection of SAR11 Bacterioplankton'. *Aquatic Microbial Ecology* 75 (June). <https://doi.org/10.3354/ame01753>.
- Bell, Stephen D, and Stephen P Jackson. 1998. 'Transcription and Translation in Archaea: A Mosaic of Eukaryal and Bacterial Features'. *Trends in Microbiology* 6 (6): 222–28. [https://doi.org/10.1016/S0966-842X\(98\)01281-5](https://doi.org/10.1016/S0966-842X(98)01281-5).
- Benelli, Dario, Anna La Teana, and Paola Londei. 2017. 'Translation Regulation: The Archaea-Eukaryal Connection'. In *RNA Metabolism and Gene Expression in Archaea*, edited by Béatrice Clouet-d'Orval, 71–88. Nucleic Acids and Molecular Biology. Cham: Springer International Publishing. https://doi.org/10.1007/978-3-319-65795-0_3.
- Benjamini, Yoav, and Yosef Hochberg. 1995. 'Controlling the False Discovery Rate: A Practical and Powerful Approach to Multiple Testing'. *Journal of the Royal Statistical Society. Series B (Methodological)* 57 (1): 289–300.
- Bernander, Rolf, and Thijs JG Ettema. 2010. 'FtsZ-Less Cell Division in Archaea and Bacteria'. *Current Opinion in Microbiology, Growth and development: eukaryotes/prokaryotes*, 13 (6): 747–52. <https://doi.org/10.1016/j.mib.2010.10.005>.
- Boer, Piet de, Robin Crossley, and Lawrence Rothfield. 1992. 'The Essential Bacterial Cell-Division Protein FtsZ Is a GTPase'. *Nature* 359 (6392): 254–56. <https://doi.org/10.1038/359254a0>.
- Brügger, Kim, Peter Redder, Qunxin She, Fabrice Confalonieri, Yvan Zivanovic, and Roger A Garrett. 2002. 'Mobile Elements in Archaeal Genomes'. *FEMS Microbiology Letters* 206 (2): 131–41. <https://doi.org/10.1111/j.1574-6968.2002.tb10999.x>.
- Cox, Jürgen, and Matthias Mann. 2008. 'MaxQuant Enables High Peptide Identification Rates, Individualized p.p.b.-Range Mass Accuracies and Proteome-Wide Protein Quantification'. *Nature Biotechnology* 26 (12): 1367–72. <https://doi.org/10.1038/nbt.1511>.

Cox, Jürgen, Nadin Neuhauser, Annette Michalski, Richard A. Scheltema, Jesper V. Olsen, and Matthias Mann. 2011. 'Andromeda: A Peptide Search Engine Integrated into the MaxQuant Environment'. *Journal of Proteome Research* 10 (4): 1794–1805. <https://doi.org/10.1021/pr101065j>.

Cruz, Jesús de la, Fernando Gómez-Herreros, Olga Rodríguez-Galán, Victoria Begley, María de la Cruz Muñoz-Centeno, and Sebastián Chávez. 2018. 'Feedback Regulation of Ribosome Assembly'. *Current Genetics* 64 (2): 393–404. <https://doi.org/10.1007/s00294-017-0764-x>.

Dennis, Patrick P. 1997. 'Ancient Ciphers: Translation in Archaea'. *Cell* 89 (7): 1007–10. [https://doi.org/10.1016/S0092-8674\(00\)80288-3](https://doi.org/10.1016/S0092-8674(00)80288-3).

Donahue, Thomas F., A. Mark Cigan, Edward K. Pabich, and Beatriz Castilho Valavicius. 1988. 'Mutations at a Zn(II) Finger Motif in the Yeast EIF-2 β Gene Alter Ribosomal Start-Site Selection during the Scanning Process'. *Cell* 54 (5): 621–32. [https://doi.org/10.1016/S0092-8674\(88\)80006-0](https://doi.org/10.1016/S0092-8674(88)80006-0).

Dym, O., M. Mevarech, and J. L. Sussman. 1995. 'Structural Features That Stabilize Halophilic Malate Dehydrogenase from an Archaeobacterium'. *Science* 267 (5202): 1344–46. <https://doi.org/10.1126/science.267.5202.1344>.

Erickson, F Les, Joseph Nika, Scott Rippel, and Ernest M Hannig. 2001. 'Minimum Requirements for the Function of Eukaryotic Translation Initiation Factor 2'. *Genetics* 158 (1): 123–32. <https://doi.org/10.1093/genetics/158.1.123>.

Graziano, Giuseppe, and Antonello Merlino. 2014. 'Molecular Bases of Protein Halotolerance'. *Biochimica et Biophysica Acta (BBA) - Proteins and Proteomics* 1844 (4): 850–58. <https://doi.org/10.1016/j.bbapap.2014.02.018>.

Greenwood, Christina, Gergana Metodieva, Khalid Al-Janabi, Berthold Lausen, Louise Alldridge, Lin Leng, Richard Bucala, Nelson Fernandez, and Metodi V. Metodiev. 2012. 'Stat1 and CD74 Overexpression Is Co-Dependent and Linked to Increased Invasion and Lymph Node Metastasis in Triple-Negative Breast Cancer'. *Journal of Proteomics*, *Proteomics: The clinical link*, 75 (10): 3031–40. <https://doi.org/10.1016/j.jprot.2011.11.033>.

Gregson, Benjamin H., Gergana Metodieva, Metodi V. Metodiev, and Boyd A. McKew. 2019. 'Differential Protein Expression during Growth on Linear versus Branched Alkanes in the Obligate Marine Hydrocarbon-Degrading Bacterium *Alcanivorax Borkumensis* SK2T'. *Environmental Microbiology* 21 (7): 2347–59. <https://doi.org/10.1111/1462-2920.14620>.

Gruber, Claudia, Andrea Legat, Marion Pfaffenhüemer, Christian Radax, Gerhard Weidler, Hans-Jürgen Busse, and Helga Stan-Lotter. 2004. 'Halobacterium Noricense Sp. Nov., an Archaeal Isolate from a Bore Core of an Alpine Permian Salt Deposit, Classification of Halobacterium Sp. NRC-1 as a Strain of *H. Salinarum* and Emended Description of *H. Salinarum*'. *Extremophiles* 8 (6): 431–39. <https://doi.org/10.1007/s00792-004-0403-6>.

Hannig, E M, A M Cigan, B A Freeman, and T G Kinzy. 1993. 'GCD11, a Negative Regulator of GCN4 Expression, Encodes the Gamma Subunit of EIF-2 in *Saccharomyces Cerevisiae*'. *Molecular and Cellular Biology* 13 (1): 506–20. <https://doi.org/10.1128/mcb.13.1.506-520.1993>.

Hutcheon, George W., Nishi Vasisht, and Albert Bolhuis. 2005. 'Characterisation of a Highly Stable Alpha-Amylase from the Halophilic Archaeon *Haloarcula Hispanica*'. *Extremophiles: Life Under Extreme Conditions* 9 (6): 487–95. <https://doi.org/10.1007/s00792-005-0471-2>.

Jones, Daniel L., and Bonnie K. Baxter. 2016. 'Bipyrimidine Signatures as a Photoprotective Genome Strategy in G + C-Rich Halophilic Archaea'. *Life (Basel, Switzerland)* 6 (3). <https://doi.org/10.3390/life6030037>.

Koning, Bart de, Fabian Blombach, Stan J. J. Brouns, and John van der Oost. 2010. 'Fidelity in Archaeal Information Processing'. *Archaea* 2010 (September): e960298. <https://doi.org/10.1155/2010/960298>.

Kumar, Sudhir, Glen Stecher, and Koichiro Tamura. 2016. 'MEGA7: Molecular Evolutionary Genetics Analysis Version 7.0 for Bigger Datasets'. *Molecular Biology and Evolution* 33 (7): 1870–74. <https://doi.org/10.1093/molbev/msw054>.

Lanyi, J K. 1974. 'Salt-Dependent Properties of Proteins from Extremely Halophilic Bacteria.' *Bacteriological Reviews* 38 (3): 272–90.

Liao, Yan, Solenne Ithurbide, Christian Evenhuis, Jan Löwe, and Iain G. Duggin. 2021. 'Cell Division in the Archaeon *Haloferax Volcanii* Relies on Two FtsZ Proteins with Distinct Functions in Division Ring Assembly and Constriction'. *Nature Microbiology* 6 (5): 594–605. <https://doi.org/10.1038/s41564-021-00894-z>.

Madern, D., C. Ebel, and G. Zaccai. 2000. 'Halophilic Adaptation of Enzymes'. *Extremophiles* 4 (2): 91–98. <https://doi.org/10.1007/s007920050142>.

Mazumder, Barsanjit, Prabha Sampath, Vasudevan Seshadri, Ratan K. Maitra, Paul E. DiCorleto, and Paul L. Fox. 2003. 'Regulated Release of L13a from the 60S Ribosomal Subunit as A Mechanism of Transcript-Specific Translational Control'. *Cell* 115 (2): 187–98. [https://doi.org/10.1016/S0092-8674\(03\)00773-6](https://doi.org/10.1016/S0092-8674(03)00773-6).

Miralles-Robledillo, Jose María, Javier Torregrosa-Crespo, Rosa María Martínez-Espinosa, and Carmen Pire. 2019. 'DMSO Reductase Family: Phylogenetics and Applications of Extremophiles'. *International Journal of Molecular Sciences* 20 (13): 3349. <https://doi.org/10.3390/ijms20133349>.

Mormile, Melanie R., Michelle A. Biesen, M. Carmen Gutierrez, Antonio Ventosa, Justin B. Pavlovich, Tullis C. Onstott, and James K. Fredrickson. 2003. 'Isolation of Halobacterium Salinarum Retrieved Directly from Halite Brine Inclusions'. *Environmental Microbiology* 5 (11): 1094–1102. <https://doi.org/10.1046/j.1462-2920.2003.00509.x>.

Müller, Jochen A., and Shiladitya DasSarma. 2005. 'Genomic Analysis of Anaerobic Respiration in the Archaeon Halobacterium Sp. Strain NRC-1: Dimethyl Sulfoxide and Trimethylamine N-Oxide as Terminal Electron Acceptors'. *Journal of Bacteriology* 187 (5): 1659–67. <https://doi.org/10.1128/JB.187.5.1659-1667.2005>.

Ninio, J. 1991. 'Connections between Translation, Transcription and Replication Error-Rates'. *Biochimie* 73 (12): 1517–23. [https://doi.org/10.1016/0300-9084\(91\)90186-5](https://doi.org/10.1016/0300-9084(91)90186-5).

Norton, C. F., and W. D. Grant. 1988. 'Survival of Halobacteria Within Fluid Inclusions in Salt Crystals'. *Microbiology* 134 (5): 1365–73. <https://doi.org/10.1099/00221287-134-5-1365>.

Oren, Aharon. 2013. 'Life at High Salt Concentrations, Intracellular KCl Concentrations, and Acidic Proteomes'. *Frontiers in Microbiology* 4 (November): 315. <https://doi.org/10.3389/fmicb.2013.00315>.

Oren, Aharon, and Hans G. Trüper. 1990. 'Anaerobic Growth of Halophilic Archaeobacteria by Reduction of Dimethylsulfoxide and Trimethylamine N-Oxide'. *FEMS Microbiology Letters* 70 (1): 33–36. <https://doi.org/10.1111/j.1574-6968.1990.tb03772.x>.

Oren, Aharon, and Antonio Ventosa. 2017. 'Halobacterium'. In *Bergey's Manual of Systematics of Archaea and Bacteria*, 1–12. American Cancer Society. <https://doi.org/10.1002/9781118960608.gbm00482.pub2>.

Parada, Alma E., David M. Needham, and Jed A. Fuhrman. 2016. 'Every Base Matters: Assessing Small Subunit rRNA Primers for Marine Microbiomes with Mock Communities, Time Series and Global Field Samples'. *Environmental Microbiology* 18 (5): 1403–14. <https://doi.org/10.1111/1462-2920.13023>.

Paul, Sandip, Sumit K. Bag, Sabyasachi Das, Eric T. Harvill, and Chitra Dutta. 2008. 'Molecular Signature of Hypersaline Adaptation: Insights from Genome and Proteome Composition of Halophilic Prokaryotes'. *Genome Biology* 9 (4): R70. <https://doi.org/10.1186/gb-2008-9-4-r70>.

Pfeiffer, F., S. C. Schuster, A. Broicher, M. Falb, P. Palm, K. Rodewald, A. Ruepp, J. Soppa, J. Tittor, and D. Oesterhelt. 2008. 'Evolution in the Laboratory: The Genome of Halobacterium Salinarum Strain R1 Compared to That of Strain NRC-1'. *Genomics* 91 (4): 335–46. <https://doi.org/10.1016/j.ygeno.2008.01.001>.

Poolman, B, A J Driessen, and W N Konings. 1987. 'Regulation of Arginine-Ornithine Exchange and the Arginine Deiminase Pathway in *Streptococcus Lactis*'. *Journal of Bacteriology* 169 (12): 5597–5604. <https://doi.org/10.1128/jb.169.12.5597-5604.1987>.

Ramakrishnan, V., and P. B. Moore. 2001. 'Atomic Structures at Last: The Ribosome in 2000'. *Current Opinion in Structural Biology* 11 (2): 144–54. [https://doi.org/10.1016/s0959-440x\(00\)00184-6](https://doi.org/10.1016/s0959-440x(00)00184-6).

Ruepp, A., and J. Soppa. 1996. 'Fermentative Arginine Degradation in *Halobacterium Salinarium* (Formerly *Halobacterium Halobium*): Genes, Gene Products, and Transcripts of the ArcRACB Gene Cluster'. *Journal of Bacteriology* 178 (16): 4942–47. <https://doi.org/10.1128/jb.178.16.4942-4947.1996>.

Schmitt, Emmanuelle, Pierre-Damien Coureux, Ramy Kazan, Gabrielle Bourgeois, Christine Lazennec-Schurdevin, and Yves Mechulam. 2020. 'Recent Advances in Archaeal Translation Initiation'. *Frontiers in Microbiology* 11. <https://doi.org/10.3389/fmicb.2020.584152>.

Schmitt, Emmanuelle, Marie Naveau, and Yves Mechulam. 2010. 'Eukaryotic and Archaeal Translation Initiation Factor 2: A Heterotrimeric TRNA Carrier'. *FEBS Letters*, Transfer RNA, 584 (2): 405–12. <https://doi.org/10.1016/j.febslet.2009.11.002>.

Soppa, Jörg. 2006. 'From Genomes to Function: Haloarchaea as Model Organisms'. *Microbiology* 152 (3): 585–90. <https://doi.org/10.1099/mic.0.28504-0>.

Spudich, J. L., and W. Stoeckenius. 1980. 'Light-Regulated Retinal-Dependent Reversible Phosphorylation of *Halobacterium* Proteins'. *The Journal of Biological Chemistry* 255 (12): 5501–3.

Wang, Xunde, and Joe Lutkenhaus. 1996. 'FtsZ Ring: The Eubacterial Division Apparatus Conserved in Archaeobacteria'. *Molecular Microbiology* 21 (2): 313–20. <https://doi.org/10.1046/j.1365-2958.1996.6421360.x>.

Winters, Yaicha D., Tim K. Lowenstein, and Michael N. Timofeeff. 2015. 'Starvation-Survival in Haloarchaea'. *Life* 5 (4): 1587–1609. <https://doi.org/10.3390/life5041587>.

Nelson, David L., and Michael M. Cox. 2017. *Lehninger Principles of Biochemistry*. 7th ed. New York, NY: W.H. Freeman.

Georgiev, N. 2020. Understanding how halophiles survive in evaporites. Master thesis. University of Essex

Chapter 5: Investigation into the microbial communities associated with Dead-Sea halite

Abstract

5.1 Introduction

5.1.1 Stratigraphy of halite section in Ein Gedi, Dead Sea

5.1.2 Diversity of microorganisms inhabiting the Dead Sea waters

5.1.3 Aim of the study

5.2 Methodology

5.2.1 Samples and sampling sites

5.2.2 Halite sampling

5.2.3 Halite surface sterilization

5.2.4 Halite dissolution and filtration

5.2.5 DNA extraction from halite samples

5.2.6 Water sampling

5.2.7 DNA extraction from water samples

5.2.8 PCR amplification

5.2.9 Sequencing and bioinformatic analysis

5.3 Results

5.3.1 Amplification 16S rRNA genes for detection of archaeal and bacterial DNA

5.3.2 Preliminary analysis

5.3.3 Identification of Archaea in different sample types.

5.4 Discussion

5.5 Conclusion

5.6 References

5.7 Supplementary info

Chapter 5: Investigation into the microbial communities associated with Dead-

Sea halite

Abstract

The Dead Sea with its constant precipitation of halite, extreme salinity, bitter brines, and radiation fluxes, presents fascinating challenges to the life inhabiting its waters. Previous studies have showed that a variety of extremely halophilic microorganisms is adapted to survive here, especially from the domain of Archaea. Reduced inflow has led to a drop in water level by about 1 metre per year, resulting in halite precipitation and the formation of well-dated halite layers, deposited in the past four decades. We asked whether amplifiable DNA could be extracted from the Dead Sea halite and whether different forms and ages of halite housed different microbes. To this end, we collected samples of halite from different layers, samples of mud and water. Preliminary results show that archaeal and occasionally bacterial 16S rRNA genes were amplified from these halite crystals and water samples. The archaeal MSBL1 Candidate Division was found preferentially in bottom-growth halite, whereas species from the genus *Halorhabdus* were preferentially found in cumulate halite. These two different halite structures result from different environmental conditions at the time of precipitation. This preliminary analysis may open to the possibility that entombed microbes may reflect depositional settings of salt giants. The findings of this study may have implications about the survival of life on Earth and opens the possibility of life elsewhere.

5.1 Introduction

The Dead Sea was formed along the left-lateral transform boundary between the Arabian and Sinai plates. The transform motion together with the pull-apart started at about 15 million years ago. During the lengthening process the crust under the basin was stretched and thinned, which caused its subsidence due to normal faulting. The basin formation was also accompanied by uplifting of ≥ 1 km (Garfunkel and Ben-Avraham 1996). It is the only deep hypersaline lake on Earth; due to its geology, hydrology and chemistry. It represents an open-air laboratory to study the architecture of salt giants of Earth. The Dead Sea waters are characterized by brines highly concentrated in Mg^{2+} and Ca^{2+} cations (1.8 and 0.4 M, respectively), relatively low pH (5.95 – 6.56), saturated levels of NaCl, and the deposition of halite is constant throughout the year (Bodaker *et al.* 2009). The precipitation of halite presents differences in winter and in summer: Sirota *et al.* (2021) provided a description of the differences between halite precipitated in the two seasons. During summer, halite is dissolved at the shallow part of the basin, as bottom-growth halite, whereas during winter, halite precipitates both at the shallow part and at the bottom of the basin, as cumulate halite (Sirota *et al.*, 2017).

The hypersalinity of the lake interferes with measurements of trace metals and nutrients, resulting in inconsistent measurements; nevertheless, it has been reported that the phosphate concentrations are relatively low, sulphate and inorganic carbon concentrations are caused to precipitate by the high Ca^{2+} concentrations, and the O_2 is limited (Oren 1988, and references therein). From a geological perspective, the Dead Sea is a prime target to study salt giants, as its sediment record span thousands of years of climatic variations (Torfstein *et al.* 2009). In the last four decades, the Dead Sea water level has decreased constantly, with a rate of about 1 m per year, leading to halite precipitation and exposing layers of deposited halite, as well as creating regression terraces along the coast. In 2020 the lake level was at 434 m below sea level (Israel Hydrological Service, 2020), and its maximum depth was about 290 m. These dramatic changes are caused by anthropogenic pressures: the important decrease in runoff (in particular from the Jordan River) and the use of Dead Sea water brought, concomitantly with other factors, to a drop in sea level as high as 1m/year, a mean annual rainfall level of 50 mm and potential evaporation rate of 1.1-1.2 m/year (Lensky *et al.* 2005). From the 1980s, halite has been constantly precipitating at the bottom of the Dead Sea, as well as along the coast, which has influenced the water column conditions, creating a unique scenario that can be used to understand the formation of salt giants. The constant precipitation of halite is leaving behind harsh brines, making the Dead Sea a hypersaline chloride lake (Oren 1988), with salt concentration reaching extremely high levels (348 g/L (Oren and Gunde-Cimerman 2012)). These extreme conditions is the

reason why there is little growth of microorganisms and even the most adapted are found in low concentration ($<10^4$ cell·ml⁻¹ (Ionescu *et al.* 2012)). Systematic monitoring since 1980 has shown that microbial blooms do occur, however the right conditions are met only after major rain events. Since the monitoring started, two high-density microbial blooms have been documented, one in the 1980 and another one in 1992. In 1992, the upper part of the water column was highly diluted, supporting a microbial cell density of $3.5 \cdot 10^7$ cells/ml (Oren and Gurevich 1995). On that occasion, the Chlorophyte, *Dunaliella salina* bloomed for the last recorded time, until disappearing entirely from 1996 onwards. Since then, the number of microbes never exceeded $5 \cdot 10^5$ cells/ml (Bodaker *et al.* 2010).

5.1.1 Stratigraphy of halite section in Ein Gedi, Dead Sea

Before the 1980s, the Dead Sea waters were stratified, resulting in meromictic conditions (non-mixing layers) that defined a stable diluted epilimnion (upper part of the water column) (Neev and Emery 1967). However, due to the negative water balance from after the 1980s, it became a holomictic lake (mixed layers), with summer stratification and a warm and salty stable epilimnion (depth of thermocline *ca* 25 m), and mixing layers of the water column during winter (Arnon *et al.*, 2016). As a result, the deposition rates of halite, though constant, vary with season. During summer halite dissolves, and the highest halite precipitation rates happen during winter. Although this may sound counterintuitive, this behaviour can be explained by the phenomenon of Double Diffusion (DD) salt fingering, which creates a unique asymmetry in the deep hypersaline lake (Arnon *et al.*, 2016). Briefly, DD salt fingering is a buoyancy-driven flow with fluid density depending on two scalar components, temperature, and salinity. The density of the water depends linearly on both temperature and salinity; in the Dead Sea, the upper layer has higher temperature and salinity than the lower layer (Yang *et al.*, 2016). This results in a clear stratification between the epilimnion and hypolimnion (Figure 5.1). The warm temperature of the summer stabilizes the stratification, as the warmer water tends to float above colder water. However, due to the high evaporation, the warmer upper layer is also saltier than the lower layer, and therefore heavier. These conditions are needed in order for the DD salt fingering to occur. This creates the unique asymmetry of the DD salt fingering represented in Figure 5.1. It has been suggested by Arnon *et al.* (2016) that it is through the DD salt fingering that the salt is transferred to the bottom, and not the salt precipitation alone, although more observations are needed to confirm this hypothesis. Nevertheless, this phenomenon might be the

explanation why the higher rates of halite precipitation occur during winter and can also explain the formation of bottom growth halite and cumulate halite precipitation. Evaporation at the upper part of the water column sets in motion, intricately coupled mechanisms involving the diffusive and convective transport of heat and dissolved salt, driving halite deposition on the basin floor (Sirota *et al.* 2020).

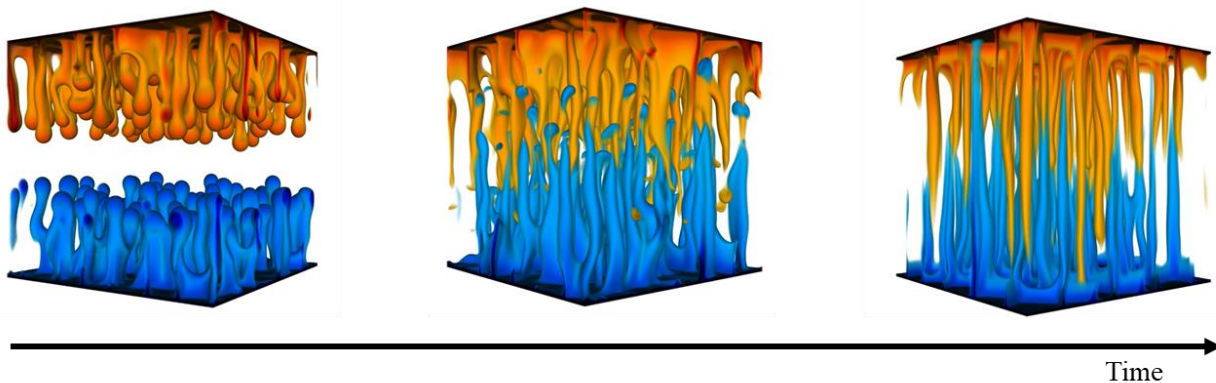


Figure 5.1. Dynamics of the Double Diffusion salt fingering (adapted from Yang *et al.* (2016)). The upper part in orange represents the warmer and saltier epilimnion, the lower part in blue represents the colder and less salty hypolimnion. The salt fingers keep the same horizontal locations for a very long time. The temperature and salinity distributions are the factors creating this asymmetry, that eventually influences the precipitation of halite (Sirota *et al.*, 2017).

Understanding how salts precipitate in deep salt lakes, like the Dead Sea, can aid the interpretation of ancient halite deposition better than shallow salterns, as the models used in the past were built on shallow hypersaline environments. The Dead Sea, being a deep hypersaline lake, makes a better analogue for halite sequence analysis. This premise is important to understand the stratigraphy of the modern halite section present in Ein Gedi, proposed as a model to study the formation of thick halite sequences, extensively studied by Sirota *et al.* (2016, 2017).

The analysed sequence is composed of alternating bottom growth-cumulate halite annual couplets, where the cumulate are formed during winter and the bottom growth during summer, conglomerates and mud layers deposited from suspensions caused by flash flood events (Figure 5.2) (Sirota *et al.* 2021). The terminology that refers to halite crystals morphology, follows the same used by Sirota *et al.* (2017).

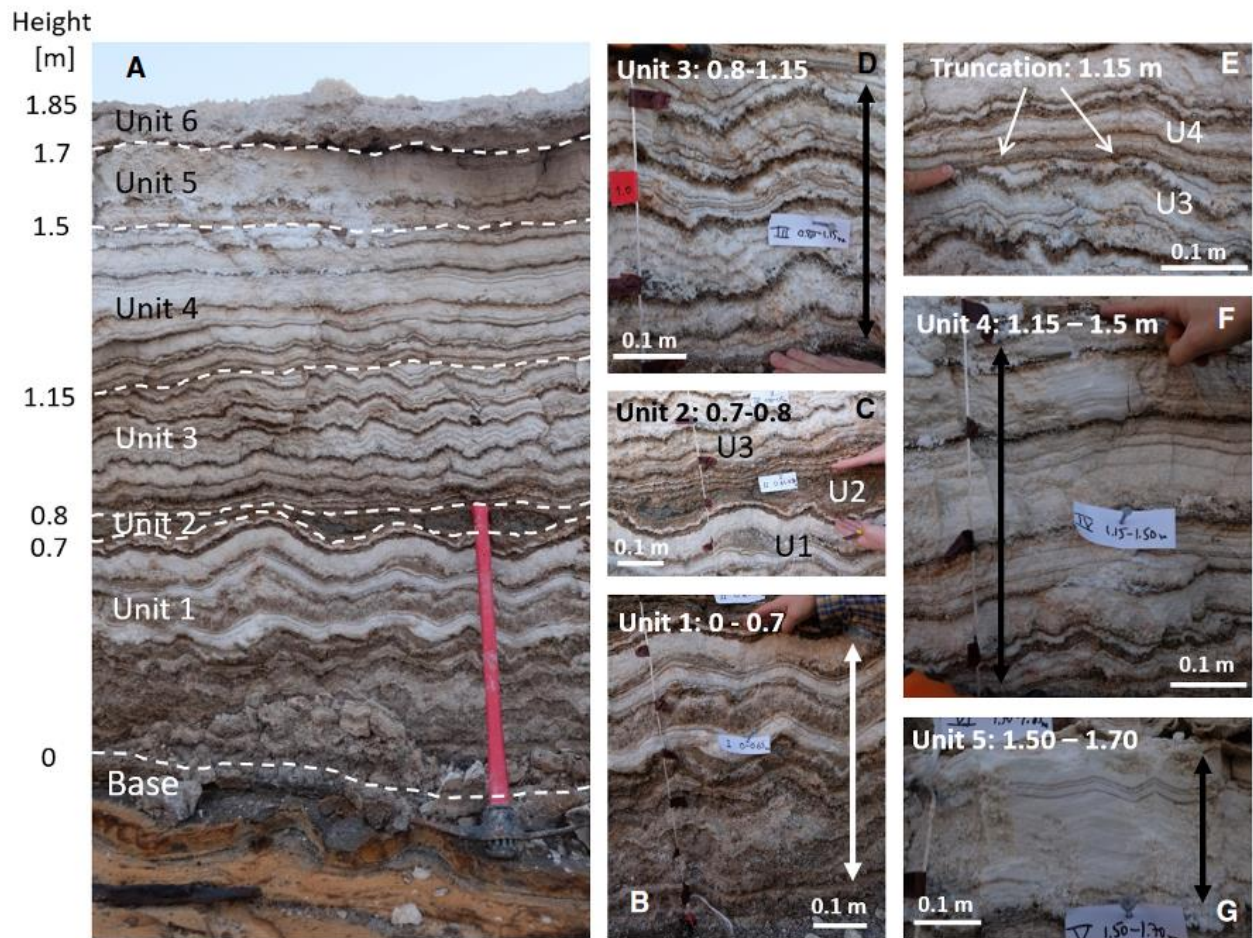


Figure 5.2. (A) Modern halite section situated in Ein Gedi formed from the negative water balance of the last four decades in the Dead Sea. (B to G) Details of the different units according to sedimentological characteristics that change along the section. The base was deposited until 1982, Unit 1 up to 3 were deposited until 1992. Units 4 and 5 correspond to halite precipitated from 2003 to 2016. Taken and modified from Sirota *et al.* (2021).

5.1.2 Diversity of microorganisms inhabiting the Dead Sea waters

The extreme chemical composition of the present-day Dead Sea water is the primary factor contributing to the low biomass found in its water; with brines characterized by 1.8 M of Mg^{2+} and 0.4 M of Ca^{2+} , the microbial cell number is $<10^4$ cell mL^{-1} (Ionescu *et al.* 2012). Additionally, the concentration of nutrients is also a limiting factor, and analysis to determine real concentrations is often difficult as the extreme salt concentrations interfere with the measurements, especially when these measurements are done during changing conditions (*e.g.* rainy events, high evaporation rates)

(Oren 1988). It is assumed that most organisms living in the Dead Sea waters are adapted to tolerate these conditions. From a geological perspective, the extreme conditions in the present-day Dead Sea have settled only in recent times. In fact, it has been reported the presence of diatoms and anaerobic bacteria involved in the carbon and sulphur cycle in its old sediment (Bartov *et al.* 2002; Thomas *et al.*, 2014; Torfstein *et al.*, 2005), suggesting that in the past, humid periods sustained more diversity, characterized by a different composition of the water column. There are very few records of measurements of microorganisms before 1979, when the lake was meromictic with an anaerobic hypolimnion. Some of them included microscopic counts of *Dunaliella* and prokaryotes measured in the period between 1963 and 1965 (Kaplan and Friedmann, 1970). Oren (2010) characterized the microbial community in the Dead Sea and compared the results with the metagenome of microbial bloom material recovered in 1992. The results of his study suggested that the microbial communities (detected by 16S rRNA gene surveys) are dynamic, and phylotypes related to the genera *Halorhabdus*, *Haloplanus*, *Natronomonas* and others, that compared with the very homogeneous cluster related to *Halobacterium salinarum* found in the material collected in 1992, suggested that the microbial composition of the Dead Sea water at the time of the study was dynamic, and exhibited important shifts in species composition. In the same study species of *Halorhabdus* were also recovered. Bodaker *et al.* (2010) performed a metagenomic study to characterize the perennial microbial community of the Dead Sea, comparing microbial DNA from Dead Sea brine (2007) and the last Dead-Sea bloom in 1992. Similar to what Oren (2010) concluded, Bodaker *et al.* (2010) found that the microbial community in the 1992 bloom was less diverse than that from the in the 2007 sample. In the 2007 sample, they found species related to the genera *Halorhabdus*, *Halorubrum*, *Halobacterium*, *Natronomonas* and others, while in the microbial material from the bloom, the majority was composed by *Halobacterium* species (Bodaker *et al.* 2010).

Thomas *et al.* (2015) analysed how the diversity present in the sediments with different depositional conditions changes through time. The core was 456 m long, and they subsampled intervals representing specific periods of lake sedimentation. They compared the diversity from the core samples with those of a microbial mat from the shore of the present Dead Sea, as a reference of an active sedimentary microbial community. They found that the subsurface microbial diversity was largely composed by the *Euryarchaeota* phylum, with the *Halobacteriaceae* that were ubiquitous. In line with previous mentioned studies, Bacteria were scarce. The diversity analysed in the subsurface aragonite sample showed a high abundance of the archaeal MSBL1 and bacterial KB1 candidate divisions. In gypsum samples the most retrieved species were from the family *Halobacteriaceae*. The study concluded that different biological conditions in the water column influenced the microbial diversity, as aragonite and gypsum have different depositional conditions, respectively, one

precipitates during humid periods and stratified lake while the other result from a holomictic lake (Thomas et al., 2015). In agreement with this conclusion, another study published by Thomas *et al.* (2014), where they showed that distinct communities of Archaea are associated with two different sedimentary facies of the Dead Sea, namely gypsum and aragonite. In aragonite samples, the abundance of MSBL1 lead to the hypothesis that methanogenesis could occur in the Dead Sea, whereas in gypsum, 95% of the taxonomically identifiable Archaea were members of the class *Halobacteria* (Thomas et al., 2014).

5.1.3 Aim of the study

In recent years Sirota, Lensky and colleagues have investigated the stratigraphy of a well-dated modern halite section, deposited in the past four decades (Sirota *et al.* 2021). The diversity of the layers is the direct result of different hydrological conditions resulting from the negative water balance and the geology of the basin, that being a deep hypersaline lake, presents unique phenomena. In this study we asked whether the microbial communities trapped in deposited layers of halite reflect: 1) the environmental conditions of the Dead Sea at the time of deposition and 2) a specific diversity associated with different layers of deposited halite.

To this end, we collected samples of halite, water and mud and the DNA was extracted for a 16S rRNA survey analysis. The water samples serve as a reference of microbial diversity living in the current chemistry of the basin.

5.2 Methodology

5.2.1 Samples and sampling sites

Halite was sampled at the end of November 2021 along the modern well-dated halite outcrop situated at the western Dead Sea coast, in Ein Gedi (Figure 5.3; 5.4), and its sedimentology and stratigraphy

is described in Sirota *et al.* (2021). Specific care was taken to avoid any external or cross-contamination as detailed later. Halite samples were preserved in sterile plastic bags and kept at room temperature until arrival in the laboratory. The mud samples were collected from the bottom part of the halite section. Samples were then handled in a clean laboratory using sterile tools. Based on the stratigraphic description published in Sirota *et al.* (2021), samples of halite were collected from the different ages and sample types (Figure 5.4). The oldest samples (A) correspond to the onset of modern halite deposition and the holomictic phase, commenced in 1982. The second oldest samples (E and F) were taken from the base of the sequence that is composed of alternating bottom growth/cumulate halite annual couplets, deposited during holomictic conditions. The white layer E represents cumulate halite and the brown layer F represents bottom growth halite and trapped clay etc. In 1992, in meromictic conditions, it was recorded the last bloom of *Dunaliella salina*; halite samples were collected from this layer too. Lastly, bottom growth/cumulate annual couplets deposited in holomictic conditions: in particular, bottom growth halite deposited in 2002 (D) represent the last layer of the Unit 3 (Figure 5.4), characterized by couplets of cumulate and bottom growth layers, whereas the cumulate halite deposited 2003 (C) were also collected and represented the base of Unit 4 (Figure 5.4), where in addition to cumulate layers including bottom growth laminae, thin mud layers are also present. Water samples were collected on the surface (top 4 cm) near the shore, except for the water sample collected in Einot Tzukim, where the brine surface sample was taken at buoy. During the days before the sampling, rain events caused the upper part of the basin to be diluted.

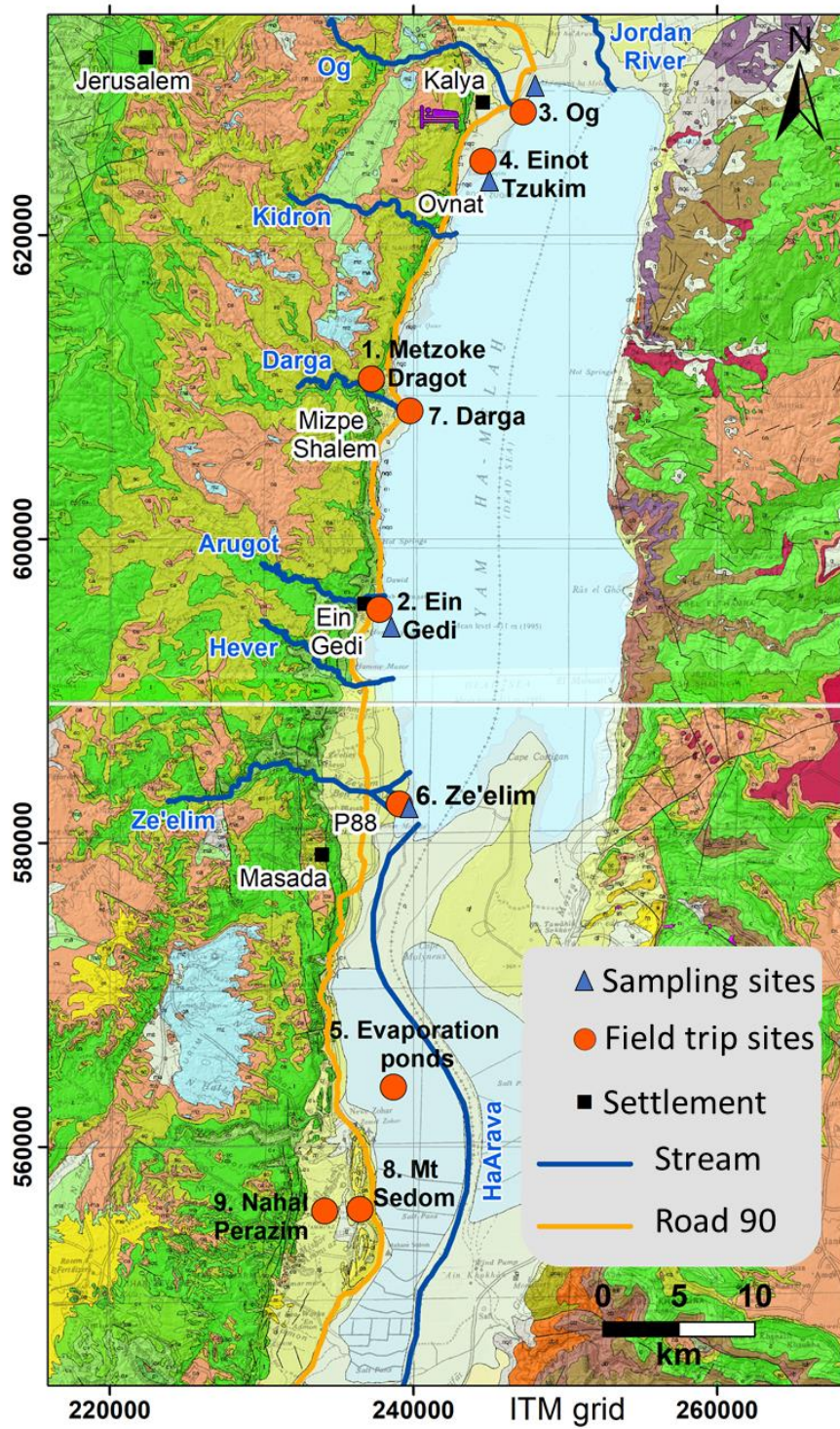


Figure 5.3. Geological map of the study area (Modified from: Sneh et al.,1998). The sampling sites (indicated by blue triangles) for halite and mud samples was Ein Gedi, whereas samples of water were collected in Ze'elim, Ein Gedi, Einot Tzukim and Og.

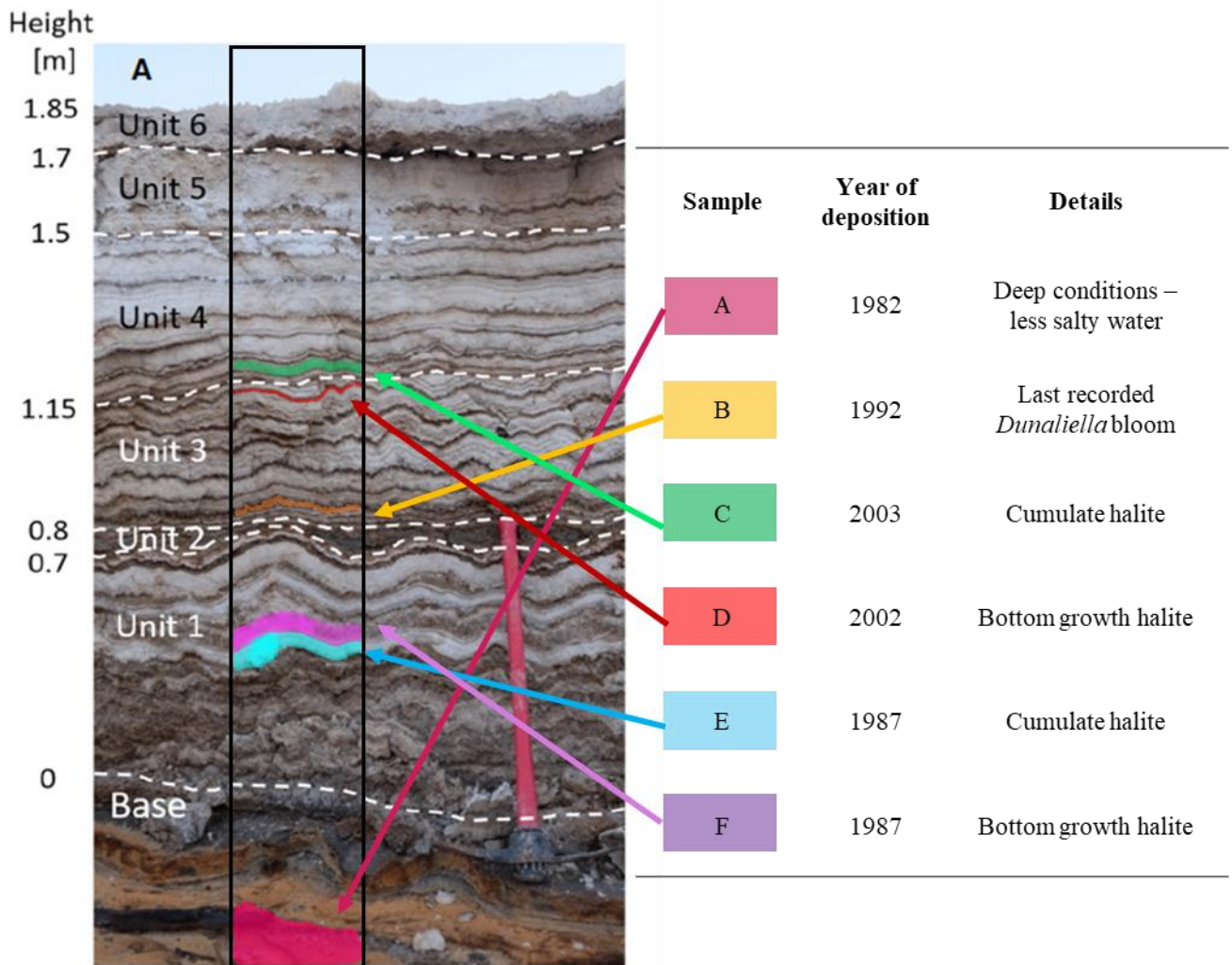


Figure 5.4. Halite section in Ein Gedi where the halite samples were taken. Halite section photograph and description of it was taken from Sirota et al (2021). As described in Sirota et al (2021), the entire modern halite sequence at the Ein Gedi area was deposited following the level decline of the past 40 years. The base represents the onset of halite deposition. Unit 1 is composed of alternations between bottom-growth and cumulate halite layers. Unit 3 is composed of alternations between cumulate and thinned bottom growth layers. Unit 4 is composed of cumulate layers; in this unit, thin non-continuous bottom growth halite and mud layers are randomly distributed along the unit.

5.2.2 Halite sampling

Halite samples from the Ein Gedi section (Figure 5.3) were collected on the 22nd of November 2021 at six different heights. In order to prevent contamination, halite samples were collected using sterile forceps, sterile spatulas and disinfected gloves. Specifically, the bottom growth halite crystals were collected utilizing sterile forceps, and at the bottom of the section, big halite crystals were picked by hand wearing disinfected gloves and stored in sterile plastic bags. For the cumulate halite crystals, these were scratched from the section with sterile spatulas and then collected in sterile plastic bags placed underneath the sampling point. The samples were kept at room temperature during the transportation to the laboratory at the University of Essex (UK). In the laboratory, the samples were stored at room temperature in boxes until use.

5.2.3 Halite surface sterilization

The protocol used for the surface-sterilisation of halite crystals was optimized by and published in Gramain *et al.* (2011). Halite crystals were weighed in falcon tubes on a sterile bench and scale, and their mass measured. The crystals were then submerged in 6% sodium hypochlorite for 20 min, soaked for 5 min saturated NaCl, and then. After the removal of the saturated NaCl, the samples were submerged in 10 M NaOH for 5 min, then washed twice with saturated NaCl for a total of 5 min. After the saturated NaCl was discarded, the crystals were submerged in 10.53 M of HCl for 20 min, followed by a wash with saturated Na₂CO₃/NaCl for 20 min. Finally, the crystals were washed twice in saturated NaCl for 5 min. From the last wash with saturated NaCl, 100 µl was poured onto agar plates, as well as liquid growth media (modified 20% NaCl Payne) in order to confirm the successful surface-sterilisation. This procedure was used to surface sterilise only intact and big halite crystals (e.g., bottom growth halite). Fragile and powdery crystals (e.g., cumulate halite) were not surface sterilised in order to prevent dissolution. Controls were included at this stage: lab-made halite crystals precipitated from sterile brine in the lab were also surface-sterilised.

5.2.4 Halite dissolution and filtration

The surface-sterilised crystals, as well as the non-surface-sterilised crystals, were placed into 25 ml of 10% NaCl to start the dissolution. The falcon tubes with the dissolving crystals were placed on a shaker at 50 rpm in order to mix the sample and speed up the dissolution. Every 15 minutes 1 ml of sterile MilliQ water was added until complete dissolution. The filtering units were assembled using

SWINNEX 47-mm filter holder (Millipore) onto which membrane filters of 0.1 µm pore size (Millipore) were placed. The dissolved halite was collected with a sterile syringe and filtered through the filtration units. In this step, negative controls were added, respectively, laboratory-made halite without microbial entombment, surface-sterilised laboratory-made halite without microbial entombment (produced as described in Chapter 2) and 10% NaCl solution used to dissolve the surface-sterilised crystals.

5.2.5 DNA extraction from halite samples

The DNA was extracted from filtered cells from the halite samples following the procedure published by Griffith and colleagues (2001). Briefly, the dissolved halite were poured into a 2ml bead-beating tube containing glass beads, where it was added 0.5 ml of 5% CTAB/Phosphate buffer (120 mM pH 8) and 0.5 ml of Phenol:Chloroform:Isoamyl alcohol (25:24:1) (pH 8). The bead-beating tubes were then placed in the bead beater (Precellys Evolution (Bertin), USA), and run for 30 seconds twice (with a break of 10 seconds) at 2000 rpm. The tubes were then cooled on ice and placed in a centrifuge for five minutes at maximum speed (10,000 x g). Subsequently, 450 µl of the upper layer was transferred into a sterile microfuge tube with 1 ml of 30% PEG 6000/1.6 M NaCl to the DNA-containing layer, inverted a few times and left, with lids closed, at room temperature overnight. The following day, the tubes were centrifuged for five minutes at maximum speed, and the DNA pellet was washed with 1ml of 70% v/v ice cold ethanol and centrifuged again. The resulting pellet was left in a sterile cabinet to dry for 20 minutes, subsequently rehydrated with 50 µl of sterile deionised water. The three negative controls described in the previous section (5.2.4) were also included in the DNA extraction procedure, and subsequently tested via PCR as controls.

5.2.6 Water sampling

Water samples from the Dead Sea were collected between the 22nd and the 24th of November 2021 at three different sites (Figure 5.4). All samples were collected on the shore, except the one collected in Einot Tzukim, that was collected from a buoy, at about 1 km from the shore. The samples were collected using sterile equipment (gloves, syringe, plastic bottles). The water was filtered in the field using Sterivex filters (SUPPLIER) with 0.22 µm pore size. Two ml of Longmire buffer was added to the Sterivex filters, which were then sealed (Longmire *et al.* 1997) (Table S5.1). Filters were stored

at 4°C and transported at room temperature (1 day) and then stored again at 4°C the laboratory at the University of Essex (UK).

5.2.7 DNA extraction from water samples

The volume of 2 ml of Longmire buffer present in the Sterivex was removed with a syringe and placed in 2ml Eppendorf and preserved. The DNA was extracted from Sterivex using the DNeasy® PowerWater® Sterivex™ Kit (Qiagen) following the manufacturer's protocol. The Longmire buffer was preserved in order to check whether DNA was also present. The rationale behind that was related to the possibility that halophilic cells might have lysed due to osmotic stress in the Longmire buffer. In this case, the DNA was extracted following the protocol described in Griffith *et al.* (2001), and the DNA amplified.

5.2.8 PCR amplification

The archaeal 16S rRNA gene and the bacterial 16S rRNA gene were targeted for amplification from each DNA extract, respectively, using the universal primers 344F and 915F, 27F and 1492R. For sequencing at Novogenes (Cambridge UK) prokaryotic primers 515F and 806R (Caporaso *et al.*, 2010) were used (Table 5.1). The polymerase chain reaction was performed using 2.5 µl of template DNA, 1 µl of each primer, 12.5 µl of app*Taq* RedMix (2×) DNA polymerase (Appleton Woods Ltd), 8 µl of PCR-grade water, for a final volume of 25 µl. Negative controls described in section 6.2.4 were included in this step, as well as a PCR-negative control of 2.5 µl PCR-grade water as a template. DNA extracts that had previously amplified using the same primers were included in the PCR reaction as positive controls. To amplify the archaeal 16S rRNA gene, thermocycling conditions were 94° C for 3 min followed by 36 cycles of 94 °C for 15 sec, 60 °C for 15 sec, 72 °C for 15 sec then 72 °C for 5 min and 4 °C on hold. To amplify the bacterial 16S rRNA gene, thermocycling conditions were 94° C for 3 min followed by 36 cycles of 94 °C for 15 sec, 56 °C for 15 sec, 72 °C for 22 sec then 72 °C for 5 min and 4 °C on hold. The amplified PCR products were visualised by agarose gel electrophoresis (1% w/v), stained with ethidium bromide for 20 minutes, de-stained in water for 5 minutes and viewed on a Gel Doc™ EZ gel documentation system (Bio-Rad). Samples with amplification, indicated by the presence of a band a band of the correct size, were selected for sequencing.

Table 5.1 Primers used for PCR amplification and Illumina MiSeq metagenetic sequencing.

Target gene/region	Primer	Sequence (5'-3')	Method
16S rRNA (Archaea)	344F	ACGGGGYGCAGCAGGCGCGA	PCR
	915R	GTGCTCCCCCGCCAATTCCT	
16S rRNA (Bacteria)	27F	AGAGTTTGATCCTGGCTCAG	PCR
	1492R	CGGTTACCTTGTTACGACTT	
16S rRNA (Archaea and Bacteria)	515F	GTGCCAGCMGCCGCGGTAA	Illumina
	806R	GGACTACHVGGGTWTCTAAT	

5.2.9 Sequencing and bioinformatic analysis

The 36 samples that amplified in the PCR were sent to Novogene (Cambridge) for sequencing of the 16S rRNA gene using prokaryotic primers 515F and 806R. In order to check for cross-contamination, three controls were sent, respectively, a negative control for surface-sterilised lab-made halite, a negative control for lab-made halite and a negative control for the 10% NaCl salt solution used to dissolve the surface-sterilised halite samples. At Novogene, the DNA samples that passed the quality control were used for amplicon sequencing (30k raw tags and p.e. 250). The raw data obtained by sequencing were cleaned by splicing and filtering by Novogenes. The cleaned data were filtered out using DADA2 to obtain the final ASVs (Amplicon Sequence Variants). By applying QIIME2's classify-sklearn algorithm (Bokulich *et al.* 2018; Bolyen *et al.* 2019), a pre-trained Naive Bayes classifier is used for species annotation of each ASV. The representative sequence of each ASV was annotated to obtain the corresponding species information and abundance distribution. The initial analysis was as follows: the raw ASV data were sorted so that ASVs with most reads were at the top. ASVs with any reads in the archaeal and bacterial PCR positive controls, as well as in the freshwater river sample, were removed. The remaining sequences were therefore less likely to be contaminants. At this step, ASV sequences with less than 200 base pairs (bp) were removed. In order to have a balance between sufficient coverage in each sample and enough samples to do statistical analysis, samples with less than 350 reads were also removed. Differences in read number between samples

was accounted for by normalization of reads to total reads (where total reads varied from 366 and 18767). As a result of the criteria used, the final data set included a total of 18 samples and 145 ASVs of the top 300 ASVs. Reads values were then converted in percentages. The taxonomic assignments were manually curated using Blast, under the scrutiny of Terry McGenity; where the genus was not possible to assign (low confidence score), the highest taxonomy level, with a higher confidence score, was assigned. Taxa were subsequently grouped, focussing on Archaea, by matching the taxonomic level.

5.3 Results

5.3.1 Amplification 16S rRNA genes for detection of archaeal and bacterial DNA

The presence of DNA extracted from the different samples was tested with PCR. Using archaeal primers, DNA was amplified from water samples and halite crystals decades old, including those that were surface sterilised (Figure 5.5 and 5.6). Crucially, there was no amplification in the process-negative controls that represent lab-made halite, including surface sterilised, and saturated solution of NaCl used to dissolve halite crystals (respectively, X1, X2 and X3 in Figure 5.6). With the bacterial primers, DNA was amplified from water samples and halite crystals decades old, including those that were surface sterilised (Figure 5.5 and 5.6).

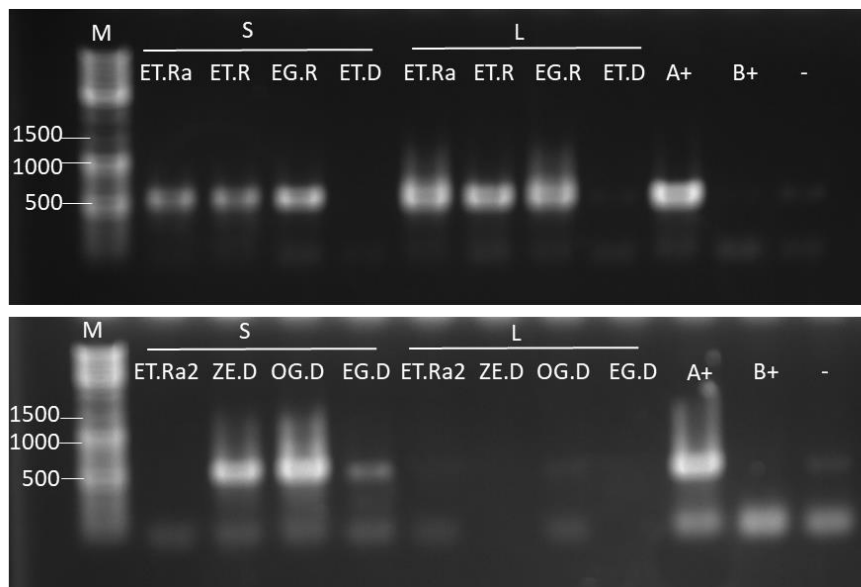


Figure 5.5. PCR amplification of the 16S rRNA gene from water samples using archaeal primers 344F and 915R. The molecular marker (M) is on the left side, showing the different bands. Numbers on the side indicate base pairs (bp). The

first four samples (S) in both gels are samples of extracted DNA using the DNeasy® PowerWater® Sterivex™ Kit (Qiagen). The next four samples (L) in both gels are samples of extracted DNA from Longmire buffer, using the protocol by Griffith *et al.* (2001). There are two positive controls, respectively for Archaea (A+) and Bacteria (B+). A negative control is present on the last lane (-). For samples details see Table 5.2.

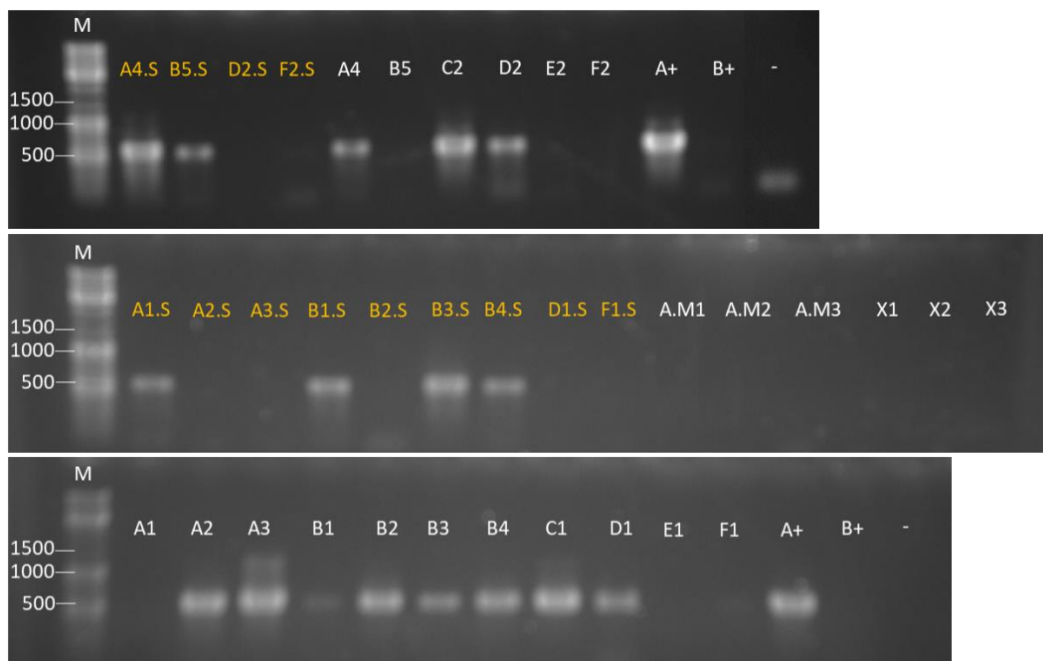


Figure 5.6. PCR amplification of the 16S rRNA gene using archaeal primers 344F and 915R. The molecular marker (M) is on the left side, showing the different bands. Numbers on the side indicate base pairs (bp). The name of samples in yellow indicates surface-sterilised halite crystals. Samples A.M1, A.M2 and A.M3 refer to DNA amplified from mud samples. Samples C1, C2 and C3 refer to DNA amplified from the negative controls for the halite surface-sterilisation described in section 6.2.4. There are positive controls for Archaea (A+) and Bacteria (B+). The DNA was extracted using the protocol by Griffith *et al.* (2001). A negative control is present on the last lane (-). For samples details see Table 5.2.

5.3.2 Preliminary analysis

The removal of ASVs with any reads in the controls, and the removal of short sequences (less than 250 bp), left 145 quality ASV sequences. After the removal of samples with less than 350 reads, 18 samples remained for further analysis. The samples were grouped based on similar characteristics, e.g., cumulate halite, bottom growth halite, bottom growth surface-sterilised halite, and one sample from the Dead Sea water also remained. Analysis of these most abundant and quality controlled ASVs showed that nearly all reads from the Dead Sea water were archaeal (Table 5.2). The samples that contained the highest abundance of bacterial ASVs were the surface sterilised halite crystals

precipitated in 1982, 1987 and 2002, whereas the non-surface sterilised crystals from 1982, 1987, 1992 and 2003 had higher abundance of archaeal ASVs (Table 5.2).

Table 5.2. Summary of the results. Suffixes of the sample code are: EG = Ein Gedi; (EG_)A, B, C, D, F, E = different layers of the halite section (see Figure 6.4); S = surface sterile; X = controls; EG, ET, ZE, OG = location of water samples; R = river plume; D = Dead Sea surface water.

Description (year of deposition)	Sample code	PCR amplification		QC	Criteria used in section 6.2.9	% Archaea	% Bacteria
		Arch	Bac				
Surface sterilised halite (1982)	EG_A1_S	yes	yes	passed	passed	6.71	93.29
	EG_A2_S	no	no	passed	passed	5.43	94.57
	EG_A4_S	yes	no	passed	passed	82.84	17.16
Surface sterilised halite (1992)	EG_B1_S	yes	no	failed	\	\	\
	EG_B3_S	yes	yes	passed	passed	89.27	10.73
	EG_B4_S	yes	no	failed	\	\	\
Surface sterilised bottom-growth halite (2002)	EG_B5_S	yes	no	passed	passed	6.12	93.88
	EG_D1_S	no	no	passed	passed	7.74	92.26
Surface sterilised bottom-growth halite (2002)	EG_D2_S	yes	no	passed	passed	7.05	92.95
	EG_F1_S	no	no	passed	passed	7.33	92.67
Halite (1982)	EG_A1	no	no	failed	\	\	\
	EG_A2	yes	yes	passed	passed	83.38	16.62
	EG_A3	yes	yes	passed	passed	81.26	18.74
	EG_A4	yes	no	passed	\	\	\
Halite (1992)	EG_B1	yes	no	passed	passed	79.87	20.13
	EG_B2	yes	no	passed	passed	69.25	30.75
	EG_B3	yes	no	passed	passed	39.84	60.16
	EG_B4	yes	no	failed	\	\	\
	EG_B5	yes	no	passed	passed	99	1
Cumulate halite (2003)	EG_C1	yes	yes	passed	passed	80.6	19.4
	EG_C2	yes	no	passed	passed	87.82	12.8
Bottom-growth halite (2002)	EG_D1	yes	no	passed	\	\	\
	EG_D2	yes	no	passed	\	\	\
Cumulate halite (1987)	EG_E2	yes	no	passed	\	\	\
Bottom-growth halite (1987)	EG_F1	no	no	passed	passed	96.18	3.82
Mud collected at the base of the halite section in EG	EG_A_M3	no	yes	passed	\	\	\
Lab-made halite surface sterilised	X1	yes	no	passed	*	\	\
Lab-made halite	X2	no	yes	passed	*	\	\
Saturated NaCl solution	X3	no	no	failed	\	\	\
River plume	ET_RA	yes	no	failed	\	\	\
	ET_R	yes	yes	failed	\	\	\
	EG_R	no	no	passed	\	\	\
Dead Sea surface water	ET_D	no	no	failed	\	\	\
	ZE_D	yes	no	passed	\	\	\
	OG_D	yes	no	passed	passed	98.22	1.78
	EG_D	yes	no	passed	\	\	\

5.3.3 Identification of Archaea in different sample types.

The Archaea in the Dead Sea water sample was dominated by the class of *Halobacteria* (> 98%) including the family of *Haloarculaceae*, *Halobacteriaceae* and *Haloferacaceae* (Table 5.2). Very few ASVs were identified at the genus level, thus indicating that there was a high abundance of unknown Haloarchaea in the Dead Sea. Crystal types were grouped in three different groups, respectively, cumulate, bottom-growth and surface sterilised bottom-growth. As reported in Table 5.2, in cumulate crystals precipitated in 2003, the majority of ASVs detected were archaeal, respectively 80.6% and 87.82%, where *Halobacteriales* constituting 32.59% of ASVs detected; these could not be classified below order level. Among the *Halobacteriales* detected in cumulate halite crystals, the most abundant genus were *Halorhabdus* (10.85%) and *Halorussus* (9.51%). The bacterial ASVs detected in cumulate halite were represented by the class *Bacilli* (7.65%), whereby the most abundant genus was *Bacillus* (4.37%), and the genus *Geodermatophilus* (3.55%) from the class *Actinobacteria*.

In surface-sterile bottom-growth crystals precipitated in 1982, 1987 and 2002, the majority of ASVs detected were bacterial, respectively 92.26%, 92.95% and 92.67%, represented by the order *Bacillales*. Archaeal ASVs in these samples constituted a minor part, represented by species of the order *Halobacteriales* (71.51%), of which the most abundant genus were *Halorhabdus* and *Halorientalis*, respectively 7.46% and 5.84%. On the contrary, bottom-growth crystals non surface sterilised, the majority of ASVs detected was archaeal were the most abundant were species of the class *Halobacteria* (17.71%); these could not be classified below order level.

Table 5.3. Archaea detected in water sample Dead Sea water and halite from samples: cumulate halite, bottom growth surface-sterile and bottom growth non surface sterile. Values represent mean percentages of all reads (both Bacteria and Archaea). Standard error is reported for each group on the last three columns, and values are expressed as \pm SE. The

number of samples per category is indicated. Where the genus level was not available, the level with the highest confidence score was chosen (g = genus, f = family, o = order, c = class, k = kingdom).

Taxonomy	Dead Sea n=1	cumulate n=2	bottom growth surface- sterile n=8	bottom growth n=7	c SE	bgSS SE	bgSE
k_Archaea	0.00	1.71	0.00	0.77	1.71	0.00	0.29
k_Archaea:p_Crenarchaeota;c_Nitrososphaeria;o_Nitrososphaerales:f_Nitrososphaeraceae	0.00	0.15	0.00	0.19	0.15	0.00	0.19
k_Archaea:p_Nanohaloarchaeota;c_Nanosalinia;o_Nanosalinales:f_Candidate_Nanosalina	0.00	0.15	0.00	1.00	0.15	0.00	0.97
k_Archaea:p_Thermoplasmata;c_Thermoplasmata	0.00	0.00	0.68	0.04	0.00	0.37	0.04
k_Archaea:p_Hadarchaeota;c_Hadarchaeia;o_Hadarchaeia:f_Hadarchaeales:g_MSBL1	0.00	0.11	17.71	3.36	0.11	9.35	1.20
k_Archaea:p_Halobacterota;c_Methanonatronarchaeia;o_Methanonatronarchaeales:f_Methanonatronarchaeaceae	0.00	0.46	0.28	1.52	0.08	0.17	0.35
k_Archaea:p_Halobacterota;c_Halobacteria	64.29	5.19	0.59	18.13	1.64	0.55	7.40
k_Archaea:p_Halobacterota;c_Halobacteria;o_Halobacterales	7.35	32.59	0.00	4.79	4.57	0.00	1.59
k_Archaea:p_Halobacterota;c_Halobacteria;o_Halobacterales:f_Haloarculaceae	2.49	8.52	0.01	3.43	0.32	0.01	1.08
k_Archaea:p_Halobacterota;c_Halobacteria;o_Halobacterales:f_Haloarculaceae:g_Haloglomus	0.00	0.69	0.00	0.43	0.13	0.00	0.37
k_Archaea:p_Halobacterota;c_Halobacteria;o_Halobacterales:f_Haloarculaceae:g_Halomicrobium	0.00	4.42	0.02	2.39	4.42	0.02	0.86
k_Archaea:p_Halobacterota;c_Halobacteria;o_Halobacterales:f_Haloarculaceae:g_Halorhabdus	3.32	10.85	0.16	7.46	2.38	0.15	0.94
k_Archaea:p_Halobacterota;c_Halobacteria;o_Halobacterales:f_Haloarculaceae:g_Halorientalis	0.00	0.84	0.25	4.84	0.84	0.22	0.90
k_Archaea:p_Halobacterota;c_Halobacteria;o_Halobacterales:f_Halobacteriaceae	0.00	1.25	1.30	5.05	1.25	1.04	0.95
k_Archaea:p_Halobacterota;c_Halobacteria;o_Halobacterales:f_Halobacteriaceae:g_Halanaeroarchaeum	0.00	0.00	0.02	0.74	0.00	0.02	0.48
k_Archaea:p_Halobacterota;c_Halobacteria;o_Halobacterales:f_Halobacteriaceae:g_Halobacterium	0.00	1.65	0.97	0.02	1.08	0.73	0.02
k_Archaea:p_Halobacterota;c_Halobacteria;o_Halobacterales:f_Halobacteriaceae:g_Halodesulfurarchaeum	0.00	0.06	0.04	1.14	0.06	0.03	0.40
k_Archaea:p_Halobacterota;c_Halobacteria;o_Halobacterales:f_Halobacteriaceae:g_Halomicrococcus	0.00	0.08	2.21	3.04	0.08	1.72	1.15
k_Archaea:p_Halobacterota;c_Halobacteria;o_Halobacteriales:f_Halobacteriaceae:g_Halorussus	1.54	9.51	1.37	5.37	2.24	1.14	1.37
k_Archaea:p_Halobacterota;c_Halobacteria;o_Halobacterales:f_Halobacteriaceae:g_Salararchaeum	0.00	0.00	0.04	0.39	0.00	0.04	0.22
k_Archaea:p_Halobacterota;c_Halobacteria;o_Halobacterales:f_Halobacteriaceae:g_Salinibaculum	4.98	1.17	0.00	0.97	1.17	0.00	0.53
k_Archaea:p_Halobacterota;c_Halobacteria;o_Haloferacales	0.00	0.26	0.62	2.61	0.26	0.50	1.78
k_Archaea:p_Halobacterota;c_Halobacteria;o_Haloferacales:f_Haloferacaceae	13.88	0.00	0.13	2.70	0.00	0.12	2.30
k_Archaea:p_Halobacterota;c_Halobacteria;o_Haloferacales:f_Haloferacaceae:g_Halobellus	0.36	0.20	0.01	2.41	0.20	0.01	0.98
k_Archaea:p_Halobacterota;c_Halobacteria;o_Haloferacales:f_Haloferacaceae:g_Haloplanus	0.00	1.01	0.00	1.80	1.01	0.00	0.89
k_Archaea:p_Halobacterota;c_Halobacteria;o_Haloferacales:f_Halorubraceae:g_Halohasta	0.00	0.03	0.14	0.79	0.03	0.11	0.49
k_Archaea:p_Halobacterota;c_Halobacteria;o_Haloferacales:f_Halorubraceae:g_Halorubrum	0.00	0.01	0.00	2.97	0.01	0.00	2.15
k_Archaea:p_Halobacterota;c_Halobacteria;o_Natrialbales:f_Natrialbaeae:g_Salinarchaeum	0.00	3.29	0.00	0.06	0.80	0.00	0.04

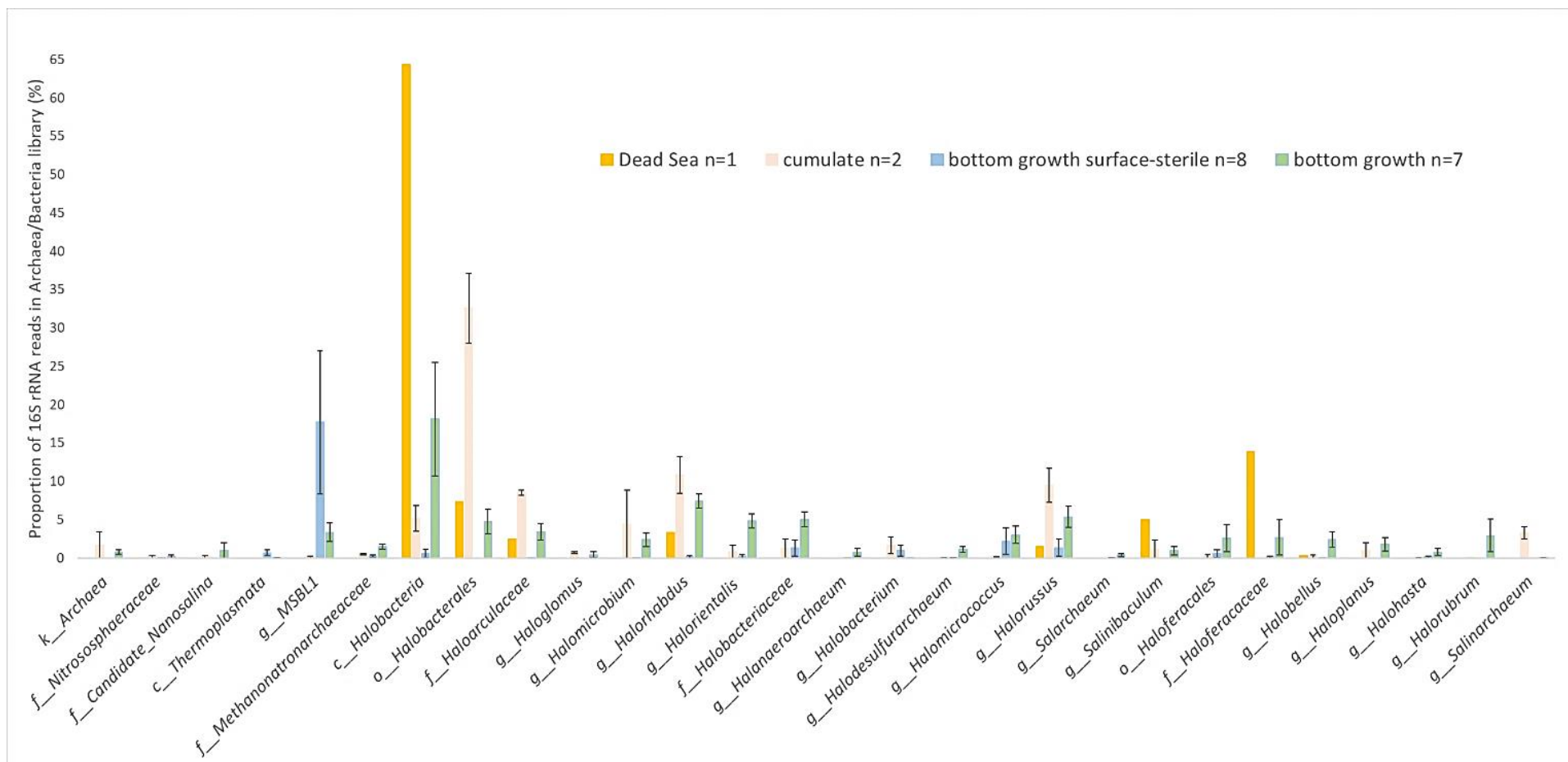


Figure 5.7. Distribution of 16S rRNA archaeal reads in Dead Sea water, cumulate halite (2 samples), bottom growth surface-sterile (8 samples) and bottom growth halite. The diversity is identified at the genus level. Where the genus level was not available, the level with the highest confidence score was chosen (g = genus, f = family, o = order, c = class, k = kingdom). The mean of replicates is plotted for each read (\pm S.E.).

5.4 Discussion

Based on the stratigraphic description published in Sirota *et al.* (2021), samples of halite were collected from the halite sequence (Figure 5.8). The preliminary analysis on this study showed that the microbial community detected in the water sample was largely dominated by the class of *Halobacteria* (> 98%). Members of the class of *Halobacteria* are the rare inhabitants of the modern Dead Sea, as a reflection of their successful “salt-in” osmotic adaptation. Bacterial community members were very scarce, highlighting that their physiological adaptation is less suitable in this environment.

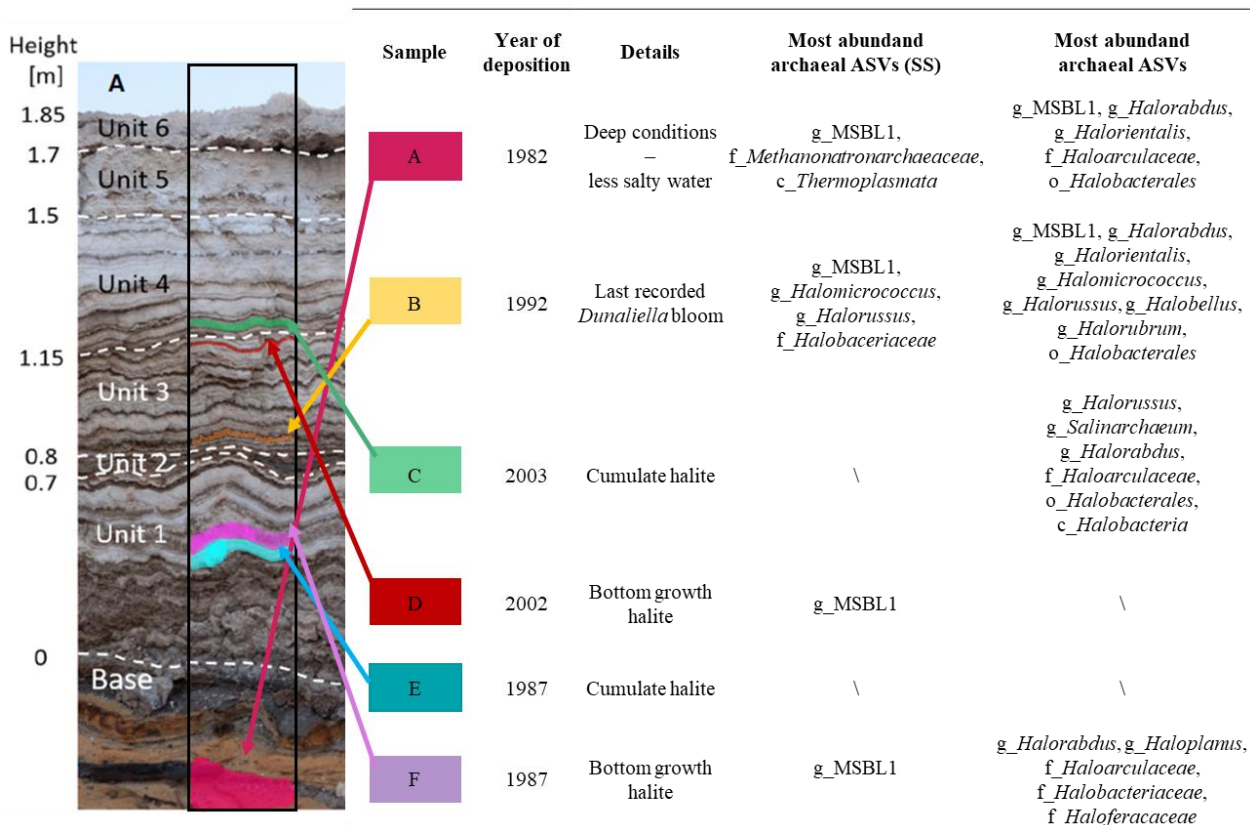


Figure 5.8. Scheme showing the most abundant ASVs found in the different samples collected from the halite section in the comparison between bottom-growth crystals and cumulate crystals. The halite section was taken from Sirota *et al.* (2021) and used to reference the samples collected. (SS) indicates surface sterilised halite.

The microbial community detected in the bottom growth halite, both surface-sterilised and non, had the highest abundance of the genus MSBL1 (17.71% in surface-sterilised halite, and 3.36% in the rest). This genus was not detected in the water sample and constituted only 0.11% of the microbial

community detected in the cumulate halite. The candidate Division MSBL1 (Mediterranean Sea Brine Lakes 1) is part of an abundant lineage found deep hypersaline anoxic basins (DHABs) in the Mediterranean Sea, the Red Sea and the Gulf of Mexico, and it has been suggested, based on their phylogenetic position, that the metabolism they possess is methanogenesis (Borin *et al.* 2009; Oren 2011; van der Wielen *et al.* 2005; Yakimov *et al.* 2013). Our understanding of this uncultured monophyletic group is still little; another study, based on metabolic reconstruction, suggested that they are not methanogen, but sugar-fermenting microbes able to grow autotrophically, concluding that such a mixotrophic strategy could offer survival advantage (Mwirichia *et al.* 2016). A common feature reported in these studies, however, is that MSBL1 is found in deep hypersaline environments, which is also in line with the findings of this study. The terminology proposed by Sirota *et al.* (2017), allows the distinction of bottom-growth and cumulate halite, and they differ based on the type of precipitation of the crystal, and the environmental conditions in which they precipitate. In fact, bottom-growth crystals are mainly characterized by coarse crystals vertically oriented, and they are deposited during the summer, whereas cumulate crystals are finer (*ca.* 0.1 mm) randomly oriented, and are deposited during the winter (Sirota *et al.* 2021). The other important difference is in the way the two precipitates: bottom-growth halite, as the name suggests, precipitates at the bottom of the Dead Sea basin, whereas cumulate halite precipitates from the upper part of the water column. Theoretically, these two different locations of precipitation might carry along a different microbial composition, as suggested by the results of this study. MSBL1 has been preferentially found in bottom-growth halite, and species of *Halorhabdus* resulted more abundant in cumulate halite samples. A study conducted on the Red Sea sediment from the Discovery Deep brine-pool, found high abundance of *Natronomas*, *Halococcus*, *Halobacterium* and *Halorhabdus* species, known to be capable of reducing oxidized nitrogen (Siam *et al.* 2012). In line with studies mentioned, also in this study, species of *Halorhabdus* and MSBL1 are located separately, as MSBL1 is significantly more abundant in bottom-growth halite, whereas *Halorhabdus* species are more abundant in cumulate samples. In particular, Thomas *et al.* (2015), found that MSBL1 was the most abundant species in intervals of alternating aragonite and mud in the longest core retrieved from the deepest point in the Dead Sea, and separately, in layers mainly composed of halite and gypsum, *Halorhabdus* species were the most abundant. There is a clear separation between MSBL1 and *Halorhabdus* species, suggesting that the distribution of microbial population depends on the chemical and biological conditions of the water column at the time of deposition. It is possible that MSBL1 is more abundant at the bottom of the basin and remain entrapped in halite forming at the bottom (bottom-growth halite), whereas *Halorhabdus* species become entrapped in the upper part of the water column, where cumulate halite starts to form. MSBL1 in this study has also been detected in bottom-growth crystal

non surface sterilised: this might be due to the fact that the microbial community detected in those samples are present on the surface of the samples, and therefore, they accumulated on the surface layer after the formation of bottom-growth halite. Additionally, the diversity detected in the bottom growth samples, compared to the surface-sterilised ones, showed a higher abundance, probably due to the removal of species by the surface-sterilisation procedure. However, the different species found in non-surface-sterilised halite, were not detected in the controls, therefore it is possible to speculate that these are species found in the layer where the samples were taken, and not the result of contamination.

Consistent with findings from previous studies (see section 5.1.2), Archaea were the dominant microbes in the Dead Sea, and in halite crystals. The DNA extracted from halite samples does not indicate whether organisms detected were alive or dead, however, there is evidence that some of the DNA sequences detected derives from live cells, as Utsav isolated species of *Salarchaeum* and *Halorhabdus* (Utsav et al., unpublished). In order to identify the main microbes, present in the halite, mud, Dead Sea and inflowing river samples, PCR and sequencing was performed at Novogenes using a set of primer that amplifies both Bacteria and Archaea. The sequence results had to be analysed and must be interpreted with caution because the two controls (lab-made halite and surface-sterilised lab-made halite), included in the samples sent at Novogene, showed amplification. While this was expected as the lab-made halite precipitation occurs on a sterile bench with lids opened, therefore not sterile conditions, it should be taken into account as cross-contamination might have occurred. However, as reported in the Methodology (section 5.2), all the ASVs found in these controls were removed from the discussed samples.

5.5 Conclusion

The unique opportunity the architecture of the Dead Sea offers to study the origin of salt giants on Earth is not limited to geology but opens to the possibility of understanding the co-evolution between the biology of its water and how this has changed with changing water dynamics throughout decades. The studies conducted by Sirota et al., (2021) offered the description of a sedimentological library, reporting exhaustive information about the stratigraphy of this well-dated, high-resolution modern Dead Sea halite sequence. The aim of the study was to provide a view of diversity found in the Dead Sea halite layers, and whether this diversity reflects the different environmental settings at the time of deposition. The results showed that MSBL1 and *Halorhabdus* had a different abundance in bottom-

growth halite and cumulate halite; the question arises on whether MSBL1, are preferentially found in deep sea brine lakes, and if this is the case, there is potential to use microbes to contribute to the study of depositional conditions. Species of *Halorhabdus* resulted more abundant in cumulate halite samples. In the near future, the analysis of this dataset will continue and will try to address the questions on whether different environmental conditions, resulting in different deposited layers of halite, clearly influences the microbial composition of the water column, and whether the most abundant species are found throughout the halite section and what this can tell us. Additionally, future studies can see how bio-energetic modelling could be used to ask questions regarding time and energy limits of survival of entombed microbes. To this end, a first step might be to calculate power availability from necromass utilization within halite crystals. These values could be bracketed by some assumptions about the amount of biomass of surviving populations, and the amount of necromass that is produced by those organisms that die out, an approach similar to previous studies (Bradley, et al., 2019; 2018).

These preliminary results show that the archaeal MSBL1 Candidate Division was found preferentially in bottom-growth halite, whereas species from the genus *Halorhabdus* were preferentially found in cumulate halite. This preliminary analysis may open to the possibility that entombed microbes may reflect depositional settings of salt giants. The findings of this study may have implications about the survival of life on Earth and opens the possibility of life elsewhere.

5.6 References

- Arnon, A., J. S. Selker, and N. G. Lensky. 2016. 'Thermohaline Stratification and Double Diffusion Diapycnal Fluxes in the Hypersaline Dead Sea'. *Limnology and Oceanography* 61 (4): 1214–31. <https://doi.org/10.1002/lno.10285>.
- Bartov, Yuval, Mordechai Stein, Yehouda Enzel, Amotz Agnon, and Ze'ev Reches. 2002. 'Lake Levels and Sequence Stratigraphy of Lake Lisan, the Late Pleistocene Precursor of the Dead Sea'. *Quaternary Research* 57 (January): 9–21. <https://doi.org/10.1006/qres.2001.2284>.
- Bodaker, Idan, Oded Beja, Itai Sharon, Roi Feingersch, Mira Rosenberg, Aharon Oren, Muna Y Hindiyeh, and Hanan I Malkawi. 2009. 'Archaeal Diversity in the Dead Sea: Microbial Survival under Increasingly Harsh Conditions', 9.
- Bodaker, Idan, Itai Sharon, Marcelino T. Suzuki, Roi Feingersch, Michael Shmoish, Ekaterina Andreishcheva, Mitchell L. Sogin, *et al.* 2010. 'Comparative Community Genomics in the Dead Sea: An Increasingly Extreme Environment'. *The ISME Journal* 4 (3): 399–407. <https://doi.org/10.1038/ismej.2009.141>.
- Bokulich, Nicholas A., Benjamin D. Kaehler, Jai Ram Rideout, Matthew Dillon, Evan Bolyen, Rob Knight, Gavin A. Huttlely, and J. Gregory Caporaso. 2018. 'Optimizing Taxonomic Classification of Marker-Gene Amplicon Sequences with QIIME 2's Q2-Feature-Classifer Plugin'. *Microbiome* 6 (1): 90. <https://doi.org/10.1186/s40168-018-0470-z>.
- Bolyen, Evan, Jai Ram Rideout, Matthew R. Dillon, Nicholas A. Bokulich, Christian C. Abnet, Gabriel A. Al-Ghalith, Harriet Alexander, *et al.* 2019. 'Reproducible, Interactive, Scalable and Extensible Microbiome Data Science Using QIIME 2'. *Nature Biotechnology* 37 (8): 852–57. <https://doi.org/10.1038/s41587-019-0209-9>.
- Borin, Sara, Lorenzo Brusetti, Francesca Mapelli, Giuseppe D'Auria, Tullio Brusa, Massimo Marzorati, Aurora Rizzi, *et al.* 2009. 'Sulfur Cycling and Methanogenesis Primarily Drive Microbial Colonization of the Highly Sulfidic Urania Deep Hypersaline Basin'. *Proceedings of the National Academy of Sciences of the United States of America* 106 (23): 9151–56. <https://doi.org/10.1073/pnas.0811984106>.
- Bradley, James A., Jan P. Amend, and Douglas E. LaRowe. 2018. 'Necromass as a Limited Source of Energy for Microorganisms in Marine Sediments'. *Journal of Geophysical Research: Biogeosciences* 123 (2): 577–90. <https://doi.org/10.1002/2017JG004186>.

———. 2019. 'Survival of the Fewest: Microbial Dormancy and Maintenance in Marine Sediments through Deep Time'. *Geobiology* 17 (1): 43–59. <https://doi.org/10.1111/gbi.12313>.

Caporaso, J. G., Lauber, C. L., Walters, W. A., Berg-Lyons, D., Lozupone, C. A., Turnbaugh, P. J., Noah Fierer, N., & Knight, R. (2011). Global patterns of 16S rRNA diversity at a depth of millions of sequences per sample. *Proc Natl Acad Sci USA* 108, 4516–4522. <http://doi.org/10.1073/pnas.1000080107>

Garfunkel, Zvi, and Zvi Ben-Avraham. 1996. 'The Structure of the Dead Sea Basin'. *Tectonophysics, Dynamics of Extensional Basins and Inversion Tectonics*, 266 (1): 155–76. [https://doi.org/10.1016/S0040-1951\(96\)00188-6](https://doi.org/10.1016/S0040-1951(96)00188-6).

Gramain, Audrey, Guillermo Chong Díaz, Cecilia Demergasso, Tim K. Lowenstein, and Terry J. McGenity. 2011. 'Archaeal Diversity along a Subterranean Salt Core from the Salar Grande (Chile)'. *Environmental Microbiology* 13 (8): 2105–21. <https://doi.org/10.1111/j.1462-2920.2011.02435.x>.

Griffiths, Robert, Andrew Whiteley, Anthony O'Donnell, and Mark Bailey. 2001. 'Rapid Method for Coextraction of DNA and RNA from Natural Environments for Analysis of Ribosomal DNA- and rRNA-Based Microbial Community Composition'. *Applied and Environmental Microbiology* 66 (January): 5488–91. <https://doi.org/10.1128/AEM.66.12.5488-5491.2000>.

Ionescu, Danny, Christian Siebert, Lubos Polerecky, Yaniv Y. Munwes, Christian Lott, Stefan Häusler, Mina Bižić-Ionescu, *et al.* 2012. 'Microbial and Chemical Characterization of Underwater Fresh Water Springs in the Dead Sea'. Edited by Stefan Bertilsson. *PLoS ONE* 7 (6): e38319. <https://doi.org/10.1371/journal.pone.0038319>.

Kaplan, I.r., and A. Friedmann. 1970. 'Biological Productivity in the Dead Sea Part I. Microorganisms in the Water Column'. *Israel Journal of Chemistry* 8 (3): 513–28. <https://doi.org/10.1002/ijch.197000058>.

Lensky, N. G., Y. Dvorkin, V. Lyakhovsky, I. Gertman, and I. Gavrieli. 2005. 'Water, Salt, and Energy Balances of the Dead Sea'. *Water Resources Research* 41 (12). <https://doi.org/10.1029/2005WR004084>.

Longmire, Jonathan L., Robert J. Baker, Mary. Maltbie, and Texas Tech University. 1997. *Use of 'Lysis Buffer' in DNA Isolation and Its Implication for Museum Collections* /. Lubbock, TX. : Museum of Texas Tech University,. <https://doi.org/10.5962/bhl.title.143318>.

Mwirichia, Romano, Intikhab Alam, Mamoon Rashid, Manikandan Vinu, Wail Ba-Alawi, Allan Anthony Kamau, David Kamanda Ngugi, *et al.* 2016. 'Metabolic Traits of an Uncultured Archaeal Lineage -MSBL1- from Brine Pools of the Red Sea'. *Scientific Reports* 6 (1): 19181. <https://doi.org/10.1038/srep19181>.

Neev, David, and Kenneth Orris Emery. 1967. *The Dead Sea: Depositional Processes and Environments of Evaporites*. Geological Survey.

Oren, Aharon. 1988. 'The Microbial Ecology of the Dead Sea'. In *Advances in Microbial Ecology*, edited by K. C. Marshall, 193–229. *Advances in Microbial Ecology*. Boston, MA: Springer US.
https://doi.org/10.1007/978-1-4684-5409-3_6.

———. 2011. 'Thermodynamic Limits to Microbial Life at High Salt Concentrations'. *Environmental Microbiology* 13 (8): 1908–23. <https://doi.org/10.1111/j.1462-2920.2010.02365.x>.

Oren, Aharon, and Nina Gunde-cimerman. 2012. 'Fungal Life in the Dead Sea'. *Progress in Molecular and Subcellular Biology* 53 (January): 115–32. https://doi.org/10.1007/978-3-642-23342-5_6.

Oren, Aharon, and Peter Gurevich. 1995. 'Dynamics of a Bloom of Halophilic Archaea in the Dead Sea'. *Hydrobiologia* 315 (2): 149–58. <https://doi.org/10.1007/BF00033627>.

Siam, Rania, Ghada A. Mustafa, Hazem Sharaf, Ahmed Moustafa, Adham R. Ramadan, Andre Antunes, Vladimir B. Bajic, *et al.* 2012. 'Unique Prokaryotic Consortia in Geochemically Distinct Sediments from Red Sea Atlantis II and Discovery Deep Brine Pools'. *PLOS ONE* 7 (8): e42872.
<https://doi.org/10.1371/journal.pone.0042872>.

Sirota, Ido, Yehouda Enzel, and Nadav G. Lensky. 2017. 'Temperature Seasonality Control on Modern Halite Layers in the Dead Sea: In Situ Observations'. *Geological Society of America Bulletin* 129 (9–10): 1181–94. <https://doi.org/10.1130/B31661.1>.

Sirota, Ido, Yehouda enzel, and Nadav G. Lensky. 2017. 'Annual Dynamics of Halite Precipitation in the Dead Sea: In Situ Observations and Their Geological Implications', April, 8848.

Sirota, Ido, Yehouda Enzel, Ziv Mor, Liran Ben Moshe, Haggai Eyal, Tim K. Lowenstein, and Nadav G. Lensky. 2021. 'Sedimentology and Stratigraphy of a Modern Halite Sequence Formed under Dead Sea Level Fall'. *Sedimentology* 68 (3): 1069–90. <https://doi.org/10.1111/sed.12814>.

Sirota, Ido, Raphael Ouillon, Ziv Mor, Eckart Meiburg, Yehouda Enzel, Ali Arnon, and Nadav G. Lensky. 2020. 'Hydroclimatic Controls on Salt Fluxes and Halite Deposition in the Dead Sea and the Shaping of "Salt Giants"'. *Geophysical Research Letters* 47 (22): e2020GL090836.
<https://doi.org/10.1029/2020GL090836>.

Thomas, C., D. Ionescu, and D. Ariztegui. 2014. 'Archaeal Populations in Two Distinct Sedimentary Facies of the Subsurface of the Dead Sea'. *Marine Genomics*, "Omics" at a crossroads - from integrated science to multi-sector implications, 17 (October): 53–62. <https://doi.org/10.1016/j.margen.2014.09.001>.

Thomas, C., D. Ionescu, D. Ariztegui, and DSDDP Scientific Team. 2015. 'Impact of Paleoclimate on the Distribution of Microbial Communities in the Subsurface Sediment of the Dead Sea'. *Geobiology* 13 (6): 546–61. <https://doi.org/10.1111/gbi.12151>.

Torfstein, Adi, Ittai Gavrieli, and Mordechai Stein. 2005. 'The Sources and Evolution of Sulfur in the Hypersaline Lake Lisan (Paleo-Dead Sea)'. *Earth and Planetary Science Letters* 236 (1): 61–77. <https://doi.org/10.1016/j.epsl.2005.04.026>.

Torfstein, Adi, Alexandra Haase-Schramm, Nicolas Waldmann, Yehoshua Kolodny, and Mordechai Stein. 2009. 'U-Series and Oxygen Isotope Chronology of the Mid-Pleistocene Lake Amora (Dead Sea Basin)'. *Geochimica et Cosmochimica Acta* 73 (9): 2603–30. <https://doi.org/10.1016/j.gca.2009.02.010>.

Wielen, Paul W. J. J. van der, Henk Bolhuis, Sara Borin, Daniele Daffonchio, Cesare Corselli, Laura Giuliano, Giuseppe D'Auria, *et al.* 2005. 'The Enigma of Prokaryotic Life in Deep Hypersaline Anoxic Basins'. *Science (New York, N.Y.)* 307 (5706): 121–23. <https://doi.org/10.1126/science.1103569>.

Yakimov, Michail M., Violetta La Cono, Vladlen Z. Slepak, Gina La Spada, Erika Arcadi, Enzo Messina, Mireno Borghini, *et al.* 2013. 'Microbial Life in the Lake Medee, the Largest Deep-Sea Salt-Saturated Formation'. *Scientific Reports* 3 (1): 3554. <https://doi.org/10.1038/srep03554>.

Yang, Yantao, Roberto Verzicco, and Detlef Lohse. 2016. 'From Convection Rolls to Finger Convection in Double-Diffusive Turbulence'. *Proceedings of the National Academy of Sciences* 113 (1): 69–73. <https://doi.org/10.1073/pnas.1518040113>.

5.7 Supplementary info

Table S5.1. Chemical composition of the Longmire buffer preservation (Longmire *et al.* 1997).

Quantity for 1 liter of solution (ml)	Chemical
100	1 M Tris
100	1M EDTA
50	10% SDS
2	5 M NaCl
748	PCR-grade water

Chapter 6: General discussion

Hypersaline environments are dynamic ecosystem with fluctuations between dissolution and precipitation of salt crystals, including halite. Microbial communities living in these environments are also subjected to these fluctuations, and when the halite precipitates they may become entombed in little pockets of brines encased within the salt crystal lattice (Figure 6.1). It has been reported in the literature that Haloarchaea are able to survive inside fluid inclusions of halite over geological time (see Introduction). The question on how they survive over geological time scale is still open, the experiments reported in this thesis are an attempt to begin to answer this question.



Figure 6.1. Detail of a laboratory made halite with entombed cells of *Halobacterium salinarum* NRC-1 (red spots). The photo was taken by Patrick Keith.

In Chapter 2, the results highlight the ability of *Halobacterium* spp. as specialists in long-term survival, as reported by Gramain et al (2011). Although microbes living in hypersaline environment have no choice but to get trapped inside fluid inclusions of halite, the entombment could be an advantage, as the remaining brines after the precipitation of halite are mainly composed of MgCl₂-rich water bodies, which appear to be sterile (Javor, 1989), because of its chaotropicity (Hallsworth *et al.*, 2007). Therefore, the putative role/influence of microbes on the process of precipitation, might result in an advantage for the microbes entombed in the halite. To the best of my knowledge, it is the first time the survival in fluid inclusions of halite of *Dunaliella salina* was tested. It can be concluded that *Dunaliella salina* gets trapped in halite fluid inclusions, but does not survive beyond the initial entombment. Although it appears to not influence the survival of *Halobacterium salinarum* over the short time frame of this experiment, it remains to be tested whether the co-entombment of different species can enhance its survival over the longer term. Another advantage related to the entombment of cells in halite, might be the protection afforded by halite against intense radiation, as discussed in (Chapter 3).

However, the question on how species like *Halobacterium salinarum* are able to survive over geological time scale is still open. In Chapter 4, the setup of the experiment tried to address this question. The pattern arising from the results is that *Halobacterium salinarum* NRC-1, when entombed in fluid inclusions, actively slows down the metabolism. This is clearly indicated by the lower abundance of 20 ribosomal proteins in T-2 compared to T-0, most of them crucial for the interaction with the rRNA, and therefore, for the overall stability and functionality of the ribosome, the site of protein synthesis. Differently, the 50S ribosomal protein L13 was found to be higher abundant after 42 days of entombment. This protein has been reported as a dispensable ribosomal protein, which, when it is released, leads to the silencing of protein synthesis and inhibition of DNA replication in Eukarya (Mazumder *et al.*, 2003). Based on shared similarities between Archaea and Eukarya (Bell and Jackson 1998; Benelli *et al.*, 2017), it is possible to speculate that a similar role L13a has in Eukarya, can be assigned to L13 in Archaea: the 50S ribosomal protein L13 can be phosphorylated either on the ribosomal structure or when it is free in the cytoplasm. This speculation could be supported by the evidence that previous studies have found phosphorylation on proteins in *Halobacterium salinarum* (as post-translational modification) (Spudich and Stoeckenius, 1980) and specifically of ribosomal proteins (Aivaliotis *et al.*, 2009).

Among the main cellular processes, duplication, transcription and translation, Eukarya and Archaea share most similarities in translation, especially at the initiation step. Evolutionary, there might be an advantage resulting from the complexity of this process, as this complexity reflects a major control

over this process. Translation is fundamental for the cell, however, if not finely regulated, might become a sink of energy. In Haloarchaea that have shown the ability to survive over long term, this fine regulation might be at the base of their striking longevity. As evidenced by de Koning *et al.* (2010), “a key element during the flow of genetic information in living systems is fidelity”. With an error rate of 10^4 shown by ribosomes, it becomes crucial to avoid waste of energy, especially in a system where a cell is devoting all the energy to maintenance rather than growth and reproduction. It is the case of *Halobacterium salinarum* in a nutrient-depleted system like the fluid inclusions, where it becomes an advantage to modulate the translation and biosynthesis of new proteins. In the future, a useful experiment could be to quantify RNA:DNA ratios at different time points, which, based on the findings of this study, are expected to decrease through time.

The lower abundance of the protein Translation initiation factor 2 subunit gamma in T-2, able to bind GTP and, together with subunit alpha and beta, responsible for the translation initiation, adds to the interpretation that there might be selective modification of the metabolic activities to survive in fluid inclusions. The down regulation of translation might eventually result in a decreased cell division rate, in fact, the lower abundance of the cell division protein FtsZ1 may suggest this. Interestingly, the cell division protein FtsZ2 increased in abundance, however the values were not statistically significant; a possible interpretation is that it is more effective to regulate FtsZ1 first; on one hand FtsZ1 is fundamental for the cell division (Liao *et al.* 2021; Wang and Lutkenhaus 1996; Bernander and Ettema 2010), but most importantly, it is the one binding, and therefore using, GTP, a high energy molecule that in starvation conditions might be preserved instead of being used to sustain cell division. As a result of the lower abundance found at T-2 of many proteins involved in the transcription and translation processes, the cell might be focussing on the transcription and translation of specific proteins, as indicated by those proteins that were found to be more abundant in T-2. Proteins found to be higher abundant in T-2 might highlight ongoing alternative metabolic activities, confirming that NRC-1 actively responded, adjusting its physiological activities to the new environmental conditions of the fluid inclusions. The latter is supported by the higher abundance of the ribosomal protein L13, that might be involved in the regulation of translation, a similar role found in L13a in Eukarya (Mazumder *et al.*, 2003). Added to that, the higher abundance of some enzymes involved in the fermentation of arginine indicate that NRC-1 is increasing the activity of arginine fermentation to produce energy in form of ATP. The higher abundance of the DMSO reductase found in T-2 compared to T-0, indicates that the levels of oxygen are significantly decreasing, as the operon where this gene is found is sensitive to oxygen levels and is transcribed in the absence of oxygen, as reported by Müller and DasSarma (2005).

What can be the ecological advantages arising from a more regulated translation process? Here I suggest that a more efficient use of energy, might be an advantage from an evolutionary point of view. In extreme environments, archaea have won the competition by displaying unique ecological features, that allowed them to colonize the most extreme environments on Earth (Merino *et al.*, 2019). This in turn has resulted in less competitive pressure, with less need of displaying offensive strategies to win the competition with other life forms, as also suggested by Valentine (2007).

This research could help to design future experiments, and potentially different techniques could also be considered: for instance, there could be advantages in utilizing qRT-PCR or transcriptomics to have a different type of quantification about the active physiology of entombed life in halite over long-term.

The possibility that life could influence the precipitation of halite, has the potential to help us in the search for life on Mars, for instance. When samples from the Mars Sample-return mission will be returning on Earth, it will be crucial to develop methods to study life in fluid inclusions, and most importantly, signs of its presence.

If the presence of life does have a clear and measurable influence on halite precipitation and/or on the structure, abundance and size of fluid inclusions, this could help in identify signs of past life (especially in the case of life based a different chemical composition, which our current methods could potentially fail to identify, e.g., molecular analysis).

Additionally, future studies can see how bio-energetic modelling could be used to ask questions regarding time and energy limits of survival of entombed microbes. To this end, a first step might be to calculate power availability from necromass utilization within halite crystals, as reported in previous studies (Bradley, et al., 2019; 2018). Such an approach could open to the possibility that entombed microbes may reflect depositional settings of salt giants.

Lastly, this study can be part of the effort to understand the limit of life on Earth, as the Haloarchaea are living not only at the extreme of salt, but also of time. To this end, the study of microbial life can help to address the most fundamental questions about life as a phenomenon.

Microbes, that are at the interface between biotic and abiotic processes, are blank pages where the very essence of evolution draws its existence.

6.2 References

- Aivaliotis, M. *et al.* (2009) ‘Ser/Thr/Tyr Protein Phosphorylation in the Archaeon *Halobacterium salinarum*—A Representative of the Third Domain of Life’, *PLoS ONE*. Edited by U. Dobrindt, 4(3), p. e4777. Available at: <https://doi.org/10.1371/journal.pone.0004777>.
- Bell, S.D. and Jackson, S.P. (1998) ‘Transcription and translation in Archaea: a mosaic of eukaryal and bacterial features’, *Trends in Microbiology*, 6(6), pp. 222–228. Available at: [https://doi.org/10.1016/S0966-842X\(98\)01281-5](https://doi.org/10.1016/S0966-842X(98)01281-5).
- Benelli, D., La Teana, A. and Londei, P. (2017) ‘Translation Regulation: The Archaea-Eukaryal Connection’, in B. Clouet-d’Orval (ed.) *RNA Metabolism and Gene Expression in Archaea*. Cham: Springer International Publishing (Nucleic Acids and Molecular Biology), pp. 71–88. Available at: https://doi.org/10.1007/978-3-319-65795-0_3.
- Bernander, R. and Ettema, T.J. (2010) ‘FtsZ-less cell division in archaea and bacteria’, *Current Opinion in Microbiology*, 13(6), pp. 747–752. Available at: <https://doi.org/10.1016/j.mib.2010.10.005>.
- de Boer, P., Crossley, R. and Rothfield, L. (1992) ‘The essential bacterial cell-division protein FtsZ is a GTPase’, *Nature*, 359(6392), pp. 254–256. Available at: <https://doi.org/10.1038/359254a0>.
- Bradley, J.A., Amend, J.P. and LaRowe, D.E. (2018) ‘Necromass as a Limited Source of Energy for Microorganisms in Marine Sediments’, *Journal of Geophysical Research: Biogeosciences*, 123(2), pp. 577–590. Available at: <https://doi.org/10.1002/2017JG004186>.
- Bradley, J.A., Amend, J.P. and LaRowe, D.E. (2019) ‘Survival of the fewest: Microbial dormancy and maintenance in marine sediments through deep time’, *Geobiology*, 17(1), pp. 43–59. Available at: <https://doi.org/10.1111/gbi.12313>.
- Hallsworth, J.E. *et al.* (2007) ‘Limits of life in MgCl₂-containing environments: chaotropicity defines the window’, *Environmental Microbiology*, 9(3), pp. 801–813. Available at: <https://doi.org/10.1111/j.1462-2920.2006.01212.x>.
- Javor, B. (1989) *Hypersaline Environments*. Berlin, Heidelberg: Springer (Brock/Springer Series in Contemporary Bioscience). Available at: <https://doi.org/10.1007/978-3-642-74370-2>.
- Liao, Y. *et al.* (2021) ‘Cell division in the archaeon *Haloferax volcanii* relies on two FtsZ proteins with distinct functions in division ring assembly and constriction’, *Nature Microbiology*, 6(5), pp. 594–605. Available at: <https://doi.org/10.1038/s41564-021-00894-z>.
- Mazumder, B. *et al.* (2003) ‘Regulated Release of L13a from the 60S Ribosomal Subunit as A Mechanism of Transcript-Specific Translational Control’, *Cell*, 115(2), pp. 187–198. Available at: [https://doi.org/10.1016/S0092-8674\(03\)00773-6](https://doi.org/10.1016/S0092-8674(03)00773-6).
- Merino, N. *et al.* (2019) ‘Living at the Extremes: Extremophiles and the Limits of Life in a Planetary Context’, *Frontiers in Microbiology*, 10. Available at: <https://doi.org/10.3389/fmicb.2019.00780>.
- Müller, J.A. and DasSarma, S. (2005) ‘Genomic Analysis of Anaerobic Respiration in the Archaeon *Halobacterium* sp. Strain NRC-1: Dimethyl Sulfoxide and Trimethylamine N-Oxide as Terminal Electron Acceptors’, *Journal of Bacteriology*, 187(5), pp. 1659–1667. Available at: <https://doi.org/10.1128/JB.187.5.1659-1667.2005>.
- Spudich, J.L. and Stoeckenius, W. (1980) ‘Light-regulated retinal-dependent reversible phosphorylation of *Halobacterium* proteins’, *The Journal of Biological Chemistry*, 255(12), pp. 5501–5503.

Valentine, D.L. (2007) 'Adaptations to energy stress dictate the ecology and evolution of the Archaea', *Nature Reviews. Microbiology*, 5(4), pp. 316–323. Available at: <https://doi.org/10.1038/nrmicro1619>.

Wang, X. and Lutkenhaus, J. (1996) 'FtsZ ring: the eubacterial division apparatus conserved in archaeobacteria', *Molecular Microbiology*, 21(2), pp. 313–320. Available at: <https://doi.org/10.1046/j.1365-2958.1996.6421360.x>.